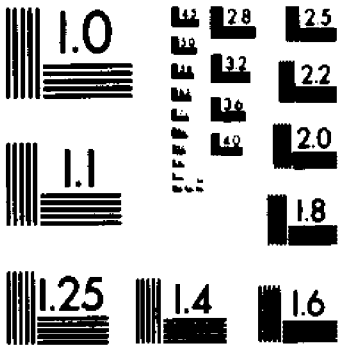

Hsu, Richard Sheng-chuin

HYDRODYNAMIC INTERACTION OF AN ARBITRARY PARTICLE WITH A PLANAR WALL AT LOW REYNOLDS NUMBER

City University of New York PH.D. 1986

PLEASE NOTE:

In all cases this material has been filmed in the best possible way from the available copy. Problems encountered with this document have been identified here with a check mark __✓__.

1. Glossy photographs or pages _____
2. Colored illustrations, paper or print _____
3. Photographs with dark background _____
4. Illustrations are poor copy _____
5. Pages with black marks, not original copy _____
6. Print shows through as there is text on both sides of page _____
7. Indistinct, broken or small print on several pages ✓
8. Print exceeds margin requirements _____
9. Tightly bound copy with print lost in spine _____
10. Computer printout pages with indistinct print _____
11. Page(s) _____ lacking when material received, and not available from school or author.
12. Page(s) _____ seem to be missing in numbering only as text follows.
13. Two pages numbered _____. Text follows.
14. Curling and wrinkled pages _____
15. Dissertation contains pages with print at a slant, filmed as received ✓
16. Other _____

_____

_____

University
Microfilms
International

HYDRODYNAMIC INTERACTION OF AN ARBITRARY PARTICLE WITH A PLANAR WALL AT LOW REYNOLDS NUMBER

by

RICHARD SHENG-CHUIN HSU

A dissertation submitted to the Graduate Faculty in Engineering in partial fulfillment of the requirements for the degree of Doctor of Philosophy, The City University of New York.

1986

This manuscript has been read and accepted for the Graduate Faculty in Engineering in satisfaction of the dissertation requirement for the degree of Doctor of Philosophy.

9/26/85
date

Peter Ganatos
Prof. Peter Ganatos, Chairman of Examining Committee

10/10/85
date

Dean Paul R. Kalmey
Executive Officer

Prof. Zeev Dagan

Prof. Peter Ganatos, Chairman

Prof. Latif M. Jiji

Prof. Ali M. Sadegh

Prof. Richard Skalak, Outside Examiner (Columbia University)

Prof. Sheldon Weinbaum

Supervisory Committee

The City University of New York

Abstract

HYDRODYNAMIC INTERACTION OF AN ARBITRARY PARTICLE WITH A PLANAR WALL AT LOW REYNOLDS NUMBER

by

Richard S.C. Hsu

Adviser : Professor Peter Ganatos

This thesis deals with the creeping motion of an arbitrary body of revolution immersed in a viscous fluid adjacent to a planar wall. The formulation is based on the boundary integral method. The singular solution to the Stokes equations in the presence of a planar wall is used to formulate the integral equations, which are solved numerically by the boundary collocation and weighted residual techniques. The solution for the special case of a spherical particle is compared with the exact solution and found to be in good agreement for sphere-to-wall gap widths as close as one tenth of the sphere radius. The resistance tensor is accurately calculated for oblate and prolate spheroids with varying aspect ratio, a torus and a biconcave shaped body.

The motion of a neutrally buoyant spheroid in shear flow next to a planar wall and the settling motion of a spheroid under gravity adjacent to a inclined plane are examined. The neutrally buoyant spheroid undergoes a

periodical motion toward and away from the wall as it continuously tumbles forward. A spheroid settling under gravity near an inclined plane will reach an equilibrium position for certain inclinations, after which it will translate parallel to the wall without rotation.

ACKNOWLEDGEMENTS

I wish to thank Professor Peter Ganatos for his continuous guidance and many contributions in directing this research. I also wish to thank the staff of the CUNY University Computer Center and the CCNY Computer Center for their technical assistance and the use of their facilities.

This research was supported by a Research Initiation Grant from The National Science Foundation, Grant No. CME81-05914. I also received a one year University Fellowship from New York State. Their support is gratefully acknowledged.

TABLE OF CONTENTS

LIST OF TABLES

CHAPTER 2

CHAPTER 3

LIST OF FIGURES

CHAPTER 2

CHAPTER 3

INTRODUCTION

The motion of a non-spherical particle in three-dimensional Stokes flow in the presence of confining boundaries is of longstanding interest and has important biological and engineering applications. Most existing theories involving the general motion of non-spherical particles in the presence of confining boundaries are based on weak interaction method of reflections techniques. Special cases such as axisymmetric flow past oblate or prolate spheroids at the centerline of an infinitely long circular cylinder or the motion of a slender body near a plane have bean treated by more exact techniques.

This thesis investigates the creeping motion of a body of revolution adjacent to a planar wall using the boundary integral method. The general theory developed is valid for arbitrary motion of a body of arbitrary shape. However, the numerical calculations have been limited to a body of revolution with the motion having planar symmetry since these solutions are of greatest importance and interest. Moreover, for this case it is possible to perform the integration on the particle surface in the azimuthal direction analytically yielding high computational accuracy and efficiency.

This thesis is presented in the form of three independent papers each of which will be submitted for publication to a scientific journal. Each of the chapters, therefore, has its own abstract, introduction and

references. In chapter 1 the theory is formulated. The accuracy and convergence of the solution technique is tested by comparison with exact solutions available in the literature for the force and torque acting on a sphere which is translating parallel or perpendicular to the wall, rotating about an axis parallel to the wall, or in the presence of shear flow. Solutions for the resistance tensor for an oblate and prolate spheroid moving adjacent to the wall are also presented. In chapter 2 the theory presented in chapter 1 is modified to treat a torus and biconcave shaped disc. In chapter 3 solutions for the velocity and trajectory are obtained for a neutrally buoyant spheroid in shear flow and a spheroid settling under gravity adjacent to a inclined plane.

CHAPTER 1

A NUMERICAL SOLUTION TECHNIQUE FOR THE MOTION OF AN ARBITRARY BODY OF REVOLUTION ADJACENT TO A PLANAR WALL AT LOW REYNOLDS NUMBER

Abstract

The boundary integral method is used to calculate the hydrodynamic force and torque on an arbitrary body of revolution near a planar wall at low Reynolds number. The singular solution to the Stokes equations in the presence of a planar wall is used to formulate the integral equations, which are then reduced to a system of linear algebraic equations by satisfying the no-slip boundary conditions on the body surface using the boundary collocation method or weighted residual technique.

Numerical tests for the special case of a sphere moving parallel or perpendicular to a planar wall show that the present theory is accurate to at least three significant digits when compared with the exact solutions for gap widths as close as only one tenth of a particle radius.

The hydrodynamic force and torque on a spheroid with varying aspect ratio and orientation angle relative to the planar wall are obtained and compared with the solutions previously obtained using the method of reflections. It is found that the solutions obtained by reflection theory are good only for particle-wall separations of at least five times of the semi-major axis of the spheroid.

1. Introduction

The motion of a non-spherical particle in three-dimensional Stokes flow in the presence of confining boundaries has important biological and engineering applications. The theory may be used to model the flow of red blood cells in an artery or vein, Wang & Skalak(1969), Chen & Skalak(1970), Leichtberg, Weinbaum & Pfeffer(1976). Specifically, the theory may explain the enhancement in the flux of oxygen and blood platelets near the artery wall, Lightfoot(1974), p.314. Other biological applications include the transport of non-spherical macromolecules or solute particles in intercellular clefts or through porous membranes. In particular, Brenner & Gaydos (1977) have shown how the hydrodynamic resistance coefficients describing the motion of non-spherical particles in the proximity of boundaries can be used in the study of diffusive and convective transport of non-spherical solute particles. Other engineering applications include determination of the motion of a particle passing through an electrostatic precipitator or the trajectory of a foreign particle in a lubricating bearing.

A review of the low Reynolds number flow literature for the motion of a non-spherical particle in the presence of confining boundaries shows that, to date, five different methods of solution have been used to solve such problems. They are the method of reflections, the boundary collocation

truncated series solution technique, the finite element method, the singularity method and the boundary integral method.

The method of reflections which was used by Wakiya (1957,1959) in connection with spheroidal particles in bounded flow is an iterative solution technique which in the present application alternately satisfies the no-slip boundary conditions on the particle surface and on the confining boundary. This series solution gives accurate results using one or two reflected fields only if the particle is far removed from the boundaries. Using this approach Wakiya considered the axisymmetric motion of a spheroid at the centerline of an infinitely long circular cylinder, Wakiya(1957a), and the parallel motion of a spheroid at one-quarter the distance between two plane walls with its semi-major axis parallel to the direction of motion, Wakiya(1957b). In a later study, Wakiya (1959) treated the more difficult problem of the motion of a spheroid parallel to a single plane wall but with the semi-major axis oriented at an arbitrary angle relative to the wall.

The boundary collocation truncated series solution technique was used by Chen and Skalak (1970) to treat the problem of axisymmetric flow past a periodic array of spheroidal particles located at the centerline of an infinitely long circular cylinder. This method is capable

of producing exact results since each particle and boundary is represented by an infinite series or integral of all the simply separable solutions in the appropriate coordinate system and the no-slip boundary conditions on all the surfaces are satisfied simultaneously rather than in an iterative fashion. However, in the present application involving a non-spherical particle inclined at an arbitrary angle relative to a planar wall, the coordinate transformation is complicated by the fact that the orientation angle enters as a parameter. This in turn complicates the inversion integrals which must performed along the planar surface and requires that they be performed numerically which is exceedingly time consuming.

The finite element method was used by Skalak, Chen and Chien (1972) in treating the problem of capillary blood flow consisting of bi-concave disc-shaped solid particles equally spaced and axisymmetrically located in a circular cylinder. However, it is computationally inefficient to use this method in Stokes flow problems where the fluid domain is not periodic and is of infinite extent since a large number of nodal points would be needed to describe the flow domain in which the slowly decaying particle disturbances are felt.

The singularity method is based on the distribution of fundamental singularities along the body axis in such a way that the boundary conditions at the particle surface are satisfied, at least approximately. Liron & Mochon (1976)

studied the problem of fluid transport by cilia, which are periodically arranged along a flat surface in an infinite fluid and beating in a metachronal fashion. In this model the cilia were represented by discrete singularities placed along their central lines. The singularities used identically satisfied the no-slip boundaries on the planar wall. Thus the integrals needed to satisfy the no-slip boundary conditions are performed only along the cilia. Later Liron (1978) extended the solution to the case where the cilia are distributed along two parallel planes. More recently, Yang & Leal (1983,1984) studied the arbitrary motion of a slender body near a planar fluid-fluid interface, which was assumed to remain flat. The flow field was represented by a distribution of appropriate singularities along the centerline of the slender body. The singularities used in this theory also satisfy the no-slip boundary conditions on the flat interface exactly. Applying the no-slip boundary conditions on the surface of the body leads to a system of integral equations for the unknown singularity densities, which are solved numerically.

Ladyzhenskaya (1963) developed a general solution of the Stokes equations, which allows the flow field to be expressed in terms of an integral over the boundary area of a Green's function which is the fundamental solution of the Stokes equations for a point force (stokeslet) multiplied by an unknown density function in each direction which

represents the stress on the boundary surface. The density functions are determined by solving the integral equations which are obtained when the no-slip boundary conditions are applied on the boundary.

Youngren and Acrivos (1975) were the first authors to use Ladyzhenskaya's solution to calculate the creeping motion of an unbounded fluid past an arbitrary isolated three-dimensional body. The flow disturbance produced by the body was formulated as a system of linear integral equations for a distribution of stokeslets over the particle surface. The integral equations were solved numerically using the boundary collocation technique. The body surface was divided into a finite number of discrete elements in each of which the stokeslet strength was assumed to be constant and the no-slip boundary conditions were applied at the center of each element. Thus the integral equations were reduced to a system of linear algebraic equations for the unknown stokeslet densities. Later, Youngren and Acrivos (1976) applied the boundary integral method to determine the steady-state shape for an inviscid gas bubble symmetrically placed in an extensional flow. Rallison and Acrivos (1978) modified the integral formulation to consider the deformation of a bubble of nonzero viscosity in an extensional flow.

Tözeren (1984) considered the problem of axisymmetric creeping flow past a collection of spheroids at the

centerline of an infinitely long circular cylinder using the boundary integral method. A singularity solution in the presence of an infinitely long cylindrical surface for axisymmetric configurations was obtained and applied to formulate the integral equations. Thus the integrals along the infinite cylindrical surface vanish. The integral equations were solved numerically using boundary collocation on the surface of the particle as was done by Youngren and Acrivos (1975).

Lee & Leal (1982) and Leal & Lee (1982) applied the integral technique to obtain a solution for the axisymmetric creeping motion of a sphere translating perpendicular to an initially flat but deformable infinite fluid interface. In this study the integrations were performed over the sphere as well as over the interface. In order to use the boundary collocation technique to satisfy the kinematic and dynamic conditions on the interface the domain of the infinite interface was truncated at a finite distance from the axis of symmetry.

Lewellen (1982) obtained a solution for the creeping motion of a spherical particle in an infinitely long cylindrical tube using the boundary integral method. The densities of the stokeslets were represented by double infinite series, in contrast to discretizating the density functions as done by previous authors. The no-slip boundary conditions on the particle and boundary surfaces were

satisfied by a weighted residual method, in which the coefficients of the series representation were determined by requiring orthogonality of the residual vector to a set of trial functions.

In the next section the boundary integral technique will be used to formulate the solution for the motion of an arbitrary body near a planar wall at low Reynolds number. This general solution will be specialized to obtain the first highly accurate solutions for a body of revolution near a planar wall.

2. Formulation

The creeping motion of an arbitrary particle in a viscous fluid near an infinite planar wall is illustrated in figure 1. The particle has a translational velocity $\vec{U}_0$ and is rotating with an angular velocity $\vec{\omega}$. $\vec{U}_\infty$ represents the undisturbed simple shear flow.

Let $\vec{V}_1$ represent the flow field and define $\vec{V} = \vec{V}_1 - \vec{V}_\infty$. The governing equations for $\vec{V}$ are:

$$\mu \nabla^2 \vec{V} = \nabla P$$
$$\nabla \cdot \vec{V} = 0 \qquad (1)$$

subject to the following boundary conditions:

$$\vec{V} = \vec{U}_p \equiv \vec{U}_0 + \vec{\omega} \times \vec{\rho} - \vec{U}_\infty \qquad \text{at the particle surface} \quad (2)$$
$$\vec{V} = 0 \qquad \text{at the wall} \quad (3)$$
$$\vec{V} = 0 \,, \quad P = 0 \qquad \text{at infinity} \quad (4)$$

where $\vec{\rho}$ is the position vector whose origin is at the particle center.

The boundary value problem posed by equations (1) - (4) will be solved using the boundary integral technique. We now outline the solution procedure.

As mentioned in the introduction, to avoid integration over an infinite domain the singular solution for Stokes flow due to a point force located near a stationary planar wall is used. Consider a semi-infinite fluid domain bounded

by a planar wall as shown in figure 2. Let a unit singular force (stokeslet) pointing in the jth direction be located at a position (y_1, y_2, y_3). The velocity components and the associated pressure field at an arbitrary point (x_1, x_2, x_3) due to this stokeslet are given by Blake (1972) as

$$u_{ij}(\underset{\sim}{x}, \underset{\sim}{y}) = \frac{1}{8\pi\mu}\left\{\left(\frac{1}{r} - \frac{1}{r^*}\right)\delta_{ij} + \frac{r_i r_j}{r^3} - \frac{r_i^* r_j^*}{r^{*3}} + 2y_3\left(\delta_{j\alpha}\delta_{\alpha\ell} - \delta_{j3}\delta_{3\ell}\right)\frac{\partial}{\partial r_\ell^*}\left(\frac{y_3 r_i^*}{r^{*3}} - \frac{\delta_{i3}}{r^*} - \frac{r_i^* r_3^*}{r^{*3}}\right)\right\} \qquad (5)$$

$$p_j(\underset{\sim}{x}, \underset{\sim}{y}) = \frac{1}{4\pi}\left\{\frac{r_j}{r^3} - \frac{r_j^*}{r^{*3}} - 2y_3\left(\delta_{j\alpha}\delta_{\alpha\ell} - \delta_{j3}\delta_{3\ell}\right)\frac{\partial}{\partial r_\ell^*}\left(\frac{r_j^*}{r^{*3}}\right)\right\}$$

where

$$r = \left[(x_1 - y_1)^2 + (x_2 - y_2)^2 + (x_3 - y_3)^2\right]^{1/2}$$

$$r^* = \left[(x_1 - y_1)^2 + (x_2 - y_2)^2 + (x_3 + y_3)^2\right]^{1/2}$$

$i, j, l = 1, 2, 3$, $\alpha = 1, 2$, and the usual summation convention is used. The tensor $\delta_{j\alpha}\delta_{\alpha\ell} - \delta_{j3}\delta_{3\ell}$ is not zero only when $j = 1$, and has the value $+1$ for $j = 1$ or 2 and the value -1 for $j = 3$. The terms in (5) which involve r^* account for the disturbance of the wall in the flow field.

The Green's formula which may be applied to the Stokes problem is given by Ladyzhenskaya (1963) as

$$\iiint_{\Omega}\left\{v_i\left[\mu\nabla^2 u_i - \frac{\partial g}{\partial x_i}\right] - u_i\left[\mu\nabla^2 v_i - \frac{\partial p}{\partial x_i}\right]\right\} d\Omega = \iint_S\left\{v_i T_{ij}(\vec{u})n_j - u_i T_{ij}(\vec{v})n_j\right\} dS \qquad (6)$$

The above formula is a general vector identity, where $\vec{u}$ and $\vec{v}$ are arbitrary smooth solenoidal vectors, p and q

are arbitrary smooth scalar quantities, Ω represents a bounded domain with boundary S, $\vec{n}$ is the outward pointing (with respect to Ω) normal on S and

$$T_{ij}[\vec{u}] = -\delta_{ij} q + \mu \left(\frac{\partial u_i}{\partial x_j} + \frac{\partial u_j}{\partial x_i} \right)$$
$$T_{ij}[\vec{v}] = -\delta_{ij} p + \mu \left(\frac{\partial u_i}{\partial x_j} + \frac{\partial u_j}{\partial x_i} \right) \qquad (7)$$

Here $T_{ij}[\vec{v}]$ represents the local stress tensor corresponding to a flow field $(\vec{v}, p)$, and μ is the dynamic viscosity.

Replacing $(\vec{u}, q)$ in equation (6) with the singular solution $(u_{ij}(\underset{\sim}{x},\underset{\sim}{y}), p(\underset{\sim}{x},\underset{\sim}{y}))$ given by (5), and identifying $(\vec{v}, p)$ to the solution of the boundary value problem posed by (1) - (4), we get

$$v_i(\underset{\sim}{y}) = \iint_{S_p} \left\{ -T_{kj}[\vec{u}^i(\underset{\sim}{x},\underset{\sim}{y})]\, v_k(\underset{\sim}{x})\, n_j(\underset{\sim}{x}) + T_{kj}[\vec{v}(\underset{\sim}{x})]\, n_j(\underset{\sim}{x})\, u_{ki}(\underset{\sim}{x},\underset{\sim}{y}) \right\} dS_{\underset{\sim}{x}} \qquad (8)$$

Here $\vec{u}^i(\underset{\sim}{x},\underset{\sim}{y})$ represents the velocity field due to a stokeslet pointing the ith direction, dS indicates that the integration is performed with respect to the variable $\underset{\sim}{x}$, S_p represents the surface of the particle, $\vec{n}$ is the inward normal to the object. The corresponding pressure is obtained from (1) using (8). The solution can be written as

$$v_i(\underset{\sim}{y}) = v_i^{(1)}(\underset{\sim}{y}) + v_i^{(2)}(\underset{\sim}{y})$$
$$p(\underset{\sim}{y}) = p^{(1)}(\underset{\sim}{y}) + p^{(2)}(\underset{\sim}{y}) \qquad (9)$$

where

$$v_i^{(1)}(\underset{\sim}{y}) = \iint_{S_p} u_{Ki}(\underset{\sim}{x},\underset{\sim}{y})\, T_{kj}[\vec{v}(x)]\, n_j\, dS_{\underset{\sim}{x}}$$

$$= \iint_{S_p} u_{Ki}(\underset{\sim}{x},\underset{\sim}{y})\, f_K(\underset{\sim}{x})\, dS_{\underset{\sim}{x}}$$

$$= \frac{1}{8\pi\mu}\iint_{S_p}\Big\{\Big(\frac{1}{r}-\frac{1}{r^*}\Big)\delta_{iK}+\Big(\frac{r_i r_K}{r^3}-\frac{r_i^* r_K^*}{r^{*3}}\Big)$$

$$+2y_3(\delta_{i\alpha}\delta_{\alpha\beta}-\delta_{i3}\delta_{3\beta})\frac{\partial}{\partial r_\beta^*}\Big(\frac{y_3 r_K^*}{r^{*3}}-\frac{\delta_{K3}}{r^*}-\frac{r_3^* r_K^*}{r^{*3}}\Big)f_K(x)\,dS_{\underset{\sim}{x}} \quad (10)$$

$$v_i^{(2)}(\underset{\sim}{y}) = -\iint_{S_p} T_{kj}[\vec{u}^i(\underset{\sim}{x},\underset{\sim}{y})]\, v_K(\underset{\sim}{x})\, n_j(\underset{\sim}{x})\, dS_{\underset{\sim}{x}}$$

$$= \frac{3}{4\pi\mu}\iint_{S_p}\frac{r_i r_j r_K}{r^5}-\frac{r_i^* r_j^* r_K^*}{r^{*5}}+2y_3(\delta_{i\alpha}\delta_{\alpha\beta}-\delta_{i3}\delta_{3\beta})\cdot$$

$$\cdot\frac{\partial}{\partial r_\beta^*}\Big(\frac{r_\beta^* r_i^* r_K^*}{r^{*5}}-\frac{r_i^* r_K^* y_\beta}{r^{*5}}+\frac{y_3}{r^{*3}}\delta_{jK}\Big)v_K(\underset{\sim}{x})\,n_j(\underset{\sim}{x})\,dS_{\underset{\sim}{x}} \quad (11)$$

$$p^{(1)}(\underset{\sim}{y}) = \frac{1}{4\pi}\iint_{S_p}\Big\{\frac{r_K}{r^3}-\frac{r_K^*}{r^{*3}}-2y_3(\delta_{k\beta}\delta_{\alpha 3}-\delta_{k3}\delta_{3\beta})\frac{\partial}{\partial r_\beta^*}\Big(\frac{r_\alpha^*}{r^{*3}}\Big)f_K(\underset{\sim}{x})\,dS_{\underset{\sim}{x}} \quad (12)$$

$$p^{(2)}(\underset{\sim}{y}) = \frac{1}{4\pi}\iint_{S_p}\Big\{\Big(\frac{1}{r}-\frac{1}{r^*}\Big)\delta_{Kj}-3\Big(\frac{\delta_K\delta_j}{r^5}-\frac{\delta_K^*\delta_j^*}{r^{*5}}\Big)$$

$$+(\delta_{j\alpha}\delta_{\alpha\beta}-\delta_{j3}\delta_{3\beta})\frac{\partial}{\partial r_\beta^*}\Big(\frac{x_3}{r^{*3}}\delta_{K3}+\frac{3r_K r_j y_3}{r^{*5}}\Big)$$

$$+(\delta_{i\alpha}\delta_{\alpha\beta}-\delta_{k3}\delta_{3\beta})\frac{\partial}{\partial r_\beta^*}\Big(\frac{x^3}{r^{*3}}\delta_{j3}-\frac{3r_K r_j y_3}{r^{*5}}\Big)\Big\}v_k(\underset{\sim}{x})n_j(\underset{\sim}{x})\,dS_{\underset{\sim}{x}} \quad (13)$$

The quantities ($v_i^{(1)}$, $p^{(1)}$) and ($v_i^{(2)}$, $p^{(2)}$) are termed single and double layer potentials with densities f_K and v_K respectively. The quantity $f_K = T_{kj}\cdot n_j$ is the density of the stokeslets, identical to the local surface stress force in the kth direction.

The solution for v_i and p, given by (9), satisfies the governing equations (1), the no-slip boundary conditions on the infinite wall and tends zero at infinity. Therefore

it only remains to satisfy the no-slip boundary conditions on the surface of the particle.

The single-layer potentials $v_i^{(1)}$ are continuous in the entire space if S_p is a Lyapunov surface (Günter, 1967). This requires the surface to have a well-defined tangent plane at all points for surfaces of practical interest. However, the double-layer potentials $v_i^{(2)}$ are not continuous at S_p. According to Adqvist (1930) and Ladyzhenskaya (1965):

$$\lim_{\underline{y}\to\underline{y}_0} v_i^{(1)}(\underline{y}) = v_i^{(1)}(\underline{y}_0) + \frac{1}{2} v_i(\underline{y}_0) \qquad (14)$$
$$\underline{y} \in \Omega\ ,\ \underline{y}_0 \in S_p$$

Therefore using (14) and applying the no-slip boundary conditions on the surface of the particle leads to the following linear integral equations of the first kind to be solved for the unknown density functions f_K:

$$\begin{aligned} v_i(\underline{y}) = \frac{1}{4\pi\mu} \iint_{S_p} \Big\{ & \Big(\frac{1}{r} - \frac{1}{r^*} \Big) \delta_{iK} + \frac{r_i r_K}{r^3} - \frac{r_i^* r_K^*}{r^{*3}} \\ & + 2\gamma_3 \left(\delta_{i\alpha}\delta_{\alpha\beta} - \delta_{i3}\delta_{3\beta} \right) \Big(\frac{3 x_3 r_i^* r_K^*}{r^{*5}} - \frac{x_3}{r^{*3}} \delta_{iK} + \frac{r_i^*}{r^{*3}} \delta_{K3} \\ & - \frac{r_K^*}{r^{*3}} \delta_{i3} \Big) \Big\} f_K(\underline{x})\, dS_{\underline{x}} - \frac{3}{2\pi\mu} \iint_{S_p} \Big\{ \frac{r_i r_j r_K}{r^5} \\ & - \frac{r_i^* r_j^* r_K^*}{r^{*5}} - 2\gamma_3 \left(\delta_{i\alpha}\delta_{\alpha\beta} - \delta_{i3}\delta_{3\beta} \right) \Big(\frac{-5 x_3 r_i^* r_j^* r_K^*}{r^{*7}} \\ & + \frac{r_j^* r_K^*}{r^{*5}} \delta_{i3} + \frac{x_3 r_j^*}{r^{*5}} \delta_{iK} + \frac{x_3 r_K^*}{r^{*5}} \delta_{ij} - \frac{\gamma_3 r_i^*}{r^{*3}} \delta_{jK} \Big) \Big\} \cdot \\ & \cdot v_K(\underline{x})\, n_j(\underline{x})\, dS_{\underline{x}} \end{aligned} \qquad (15)$$

The solution of the velocity and pressure field (9) with the density distribution given by (15) is valid for arbitrary motion of a particle of arbitrary shape adjacent to a planar wall at low Reynolds number. The system of integral equations (15) can only be solved numerically. This requires discretization of the unknown density functions and double numerical integration over the surface of the particle. An important special case of problems may be solved much more accurately and efficiently by considering only bodies of revolution with the motion having planar symmetry.

In this special case a cylindrical coordinate system (R, θ, Z) is used, as shown in figure 3. The Z axis lies along the particle axis of symmetry and the radius of the body surface, R, can be represented by a single-valued function

$$R = R_S(Z) \tag{16}$$

The transformation of coordinates (R, θ, Z) to (x_1, x_2, x_3) is given by

$$\begin{aligned} x_1 &= Z\cos\alpha - R\sin\alpha\cos\theta \\ x_2 &= -R\sin\theta \\ x_3 &= Z\cos\alpha + R\cos\alpha\cos\theta + H \end{aligned} \tag{17}$$

Using (16) and (17) and denoting the coordinates of the

points $\underset{\sim}{x}$ and $\underset{\sim}{y}$ by $(R(Z), \theta, z)$ and $(R(Z^*), \theta^*, z^*)$ in the cylindrical coordinate system respectively, all variables in equations (15) can be expressed as functions of z, θ, z^* and θ^* and are listed in Appendix A. The unknown density functions for the motion having planar symmetry can be represented by double infinite series

$$
\begin{aligned}
f_1 &= \sum_{m=0}^{\infty} \sum_{n=0}^{\infty} A_{1,m,n} P_n\left(\frac{z}{a}\right) \cos m\theta \\
f_2 &= \sum_{m=1}^{\infty} \sum_{n=0}^{\infty} A_{2,m,n} P_n\left(\frac{z}{a}\right) \sin m\theta \\
f_3 &= \sum_{m=0}^{\infty} \sum_{n=0}^{\infty} A_{3,m,n} P_n\left(\frac{z}{a}\right) \cos m\theta
\end{aligned}
\tag{18}
$$

where P_n are the Legendre function of order n, $A_{K,m,n}$ are coefficients to be determined.

To solve the integral equation (15) we define a residual vector $v_i^R(\underset{\sim}{y})$ as follows:

$$
v_i^R(\underset{\sim}{y}) = v_i(\underset{\sim}{y}) - v_i^*(\underset{\sim}{y}) \tag{19}
$$

where $v_i(\underset{\sim}{y})$ represents the true solution and $v_i^*(\underset{\sim}{y})$ is the right side of the integral equation (15). If the stokeslet density function $f_K(\underset{\sim}{x})$ in equation (15) is exact, the residual vector $v_i^R(\underset{\sim}{y})$ will be identically zero. To find an approximate solution of $f_K(\underset{\sim}{x})$ we will use two different methods.

A. The boundary collocation method: In this method we let the residual vector $v_i^R(\underset{\sim}{y})$ vanish at discrete points on the

surface of the body.

Substituting the series representations of f_K into (15), truncating the series of f_K after M terms in m and N terms in n and choosing M x N collocation points on the surface of the particle on which the no-slip boundary conditions are satisfied, leads to 3 x M x N linear algebraic equations for the 3 x M x N unknown $A_{K,m,n}$ coefficients. The integrals in (15) are performed analytically in θ direction and numerically in ζ direction. The evaluation of the integrals in θ direction is outlined in Appendix A.

B. Weighted residual method: In this method we multiply the residual vector by trial functions $F_i(\theta^*, z^*)$ which are equal to $Cos m\theta^* P_n(z^*)$ for i=1 or 3 and $Sin m\theta^* P_n(z^*)$ for i=2 and let the weighted residual vanish, i.e.

$$\iint_{S_p} v_i(\underline{y}) F_i(\theta^*, z^*) dS_{\underline{y}} = 0 \qquad (20)$$

Taking n=0,1,2,....,N-1, m=0,1,2,....,M-1 for i=1 and 3 and m=1,2,3....,M for i=2, we also get 3 x M xN linear algebraic equations for the 3 x M x N unknown coefficients A .

After the A coefficients are obtained the total force and torque acting on the particle may be obtained from

$$F_K = \sum_{m=0}^{M-1} \sum_{n=0}^{N-1} A_{K,m,n} \int_{-a}^{a} \int_{0}^{2\pi} P_n\left(\frac{\zeta}{a}\right) Cos m\theta \, R_s(\zeta) \sqrt{1+\left(\frac{dR_s}{d\zeta}\right)^2} \, d\theta \, d\zeta$$

$$(K = 1 \text{ and } 3) \qquad (21)$$

$$T_2 = \sum_{m=0}^{M-1} \sum_{n=0}^{N-1} \{ A_{1,m,n} \int_{-a}^{a} \int_{0}^{2\pi} [R_s(z) \cos\theta \cos\alpha + z \sin\alpha] \cdot \cos m\theta \, P_n(\tfrac{z}{a}) \, R_s(z) \sqrt{1+(\tfrac{dR_s}{dz})^2} \, d\theta \, dz + A_{3,m,n} \int_{-a}^{a} \int_{0}^{2\pi} [R_s(z) \cos\theta \sin\alpha - z \cos\alpha] \cos m\theta \, P_n(\tfrac{z}{a}) \sqrt{1+(\tfrac{dR_s}{dz})^2} \, d\theta \, dz \quad (22)$$

3. Numerical tests for a spherical particle

To test the accuracy and convergence characteristics of the solution technique we first consider the special case for the motion of a spherical body adjacent to a planar wall where exact solutions are available for comparison. Due to the linearity of the governing equations and the boundary conditions the planar motion of a particle can be decomposed into four simpler problems:

(1) pure translation of the particle perpendicular to the wall.

(2) Pure translation of the particle parallel to the wall.

(3) Pure rotation of the particle about an axis parallel to the wall.

(4) Shear flow past a rigidly held particle near the wall.

The Z axis in the cylindrical coordinate system is set to be perpendicular to the wall. In the first case the flow is axisymmetric. The stress forces in the R and z directions must be independent of the azimuthal angle θ and the stress forces in the azimuthal direction are identically zero, so we set

$$
\begin{aligned}
f_1 &= \sum_{n=0}^{\infty} A_n P_n\left(\frac{z}{a}\right) \cos\theta \\
f_2 &= \sum_{n=1}^{\infty} B_n P_n\left(\frac{z}{a}\right) \sin\theta \\
f_3 &= \sum_{n=0}^{\infty} C_n P_n\left(\frac{z}{a}\right)
\end{aligned}
\qquad (23)
$$

Substituting (21) into (15) and applying the no-slip

boundary conditions on the surface of the body at discrete values of z , we get a system of linear algebraic equations, whose coefficient matrix is independent of the θ coordinate of the collocation points. Therefore only one dimensional collocation is needed.

It is found that when the gap between the sphere and the wall is greater than half the radius of the sphere the choice of the collocation points is not critical if they are evenly spaced. When the sphere is located closer to the wall, some special points are important to achieve fast convergence. One important point is Z = 0 since it satisfies the no-slip conditions on the ring covering the largest surface area on the particle and defining the maximum radius of the particle. The two end points Z=±a, the radius of the sphere, are also important. Due to numerical difficulty the two end points are replaced by points as close to them as possible. The remaining collocation points are then evenly spaced along the circular arc.

Table 1a shows the results of convergence tests of the dimensionless force coefficient $F_3^{t_3}$ as a function of particle-to-wall spacing H for perpendicular motion using the boundary collocation method. $F_3^{t_3}$ is related to the hydrodynamic force by

$$F_3 = 6\pi\mu a U_3 F_3^{t_3} \tag{24}$$

where U_3 is the velocity of the particle perpendicular to the wall. The numerical results are compared to the exact solution given by Brenner (1961). Convergence to at least three significant digits is obtained using 15 collocation points for gap widths as small as one-tenth of the sphere radius. When the gap width is larger than half the sphere radius only seven collocation points are needed to give four significant digit accuracy.

Table 1b shows the results of convergence tests of the dimensionless force coefficient $F_3^{t_3}$ for the perpendicular motion using the weighted residual method. The convergence characteristics are surprisingly similar to those of the boundary collocation method shown in table 1a. Because of the similarity of the convergence characteristics of both methods and the fact that the computation time using the weighted residual method is somewhat greater than that of the boundary collocation method, we will only use the boundary collocation method in the computations which follow.

We now consider the non-axisymmetric motions, cases (2)-(4). For these motions we set

$$\begin{aligned} f_1 &= \sum_{n=0}^{\infty} \left(A_n + B_n \cos 2\theta \right) P_n\left(\frac{\gamma}{a}\right) \\ f_2 &= \sum_{n=1}^{\infty} B_n \sin 2\theta \, P_n\left(\frac{\gamma}{a}\right) \\ f_3 &= \sum_{n=0}^{\infty} C_n \cos 2\theta \, P_n\left(\frac{\gamma}{a}\right) \end{aligned} \qquad (25)$$

Again the coefficient matrix of the linear algebraic equations is independent of the θ coordinate of the collocation points, and only one-dimensional collocation is needed even though the fluid motion is now three-dimensional. For these cases, however, using the point $Z = 0$ leads to a nearly singular matrix. Therefore the point $Z = 0$ is replaced by two closely spaced points $Z = \pm\epsilon$ as done by Gluckman et al (1970). The remaining points are equally spaced along the circular arc as done in the axisymmetric case.

Tables 2 - 4 show the results of convergence tests for the dimensionless force and torque coefficients as a function of particle-to-wall spacing. These coefficients are related to the hydrodynamic force and torque acting on the sphere as follows. For a sphere translating with velocity U_1 parallel to the wall, the force and torque exerted by the fluid on the sphere are given by

$$F_1 = 6\pi\mu a U_1 F_1^{t_1} \tag{26a}$$

$$T_2 = 8\pi\mu a^2 U_1 T_2^{t_1} \tag{26b}$$

For a sphere rotating with angular velocity ω about the x_2 axis the force and torque exerted on the sphere is

$$F_1 = 6\pi\mu a^2 \omega F_1^{r} \tag{27a}$$

$$T_2 = 8\pi\mu a^3 \omega T_2^{r} \tag{27b}$$

while for a shear flow with strength S past a rigidly held sphere the force and torque is

$$F_1 = 6\pi\mu a H S F_1^S \tag{28a}$$

$$T_2 = 8\pi\mu a^3 S T_2^S \tag{28b}$$

Comparing with the exact solutions given by Goldman et al (1967A,B), convergence to at least three significant digits is obtained for all coefficients for sphere-to-wall gap widths as small as only one tenth of the sphere radius using a maximum of 12 collocation points.

In order to check the convergence characteristics for the general case when the particle is inclined at an arbitrary angle relative to the wall, the general double series representation of stokeslet strength (18) and general two-dimensional collocation over the body surface are required. Of course for the special case of a sphere, the drag and torque should be independent of the orientation angle.

Numerous convergence tests for the general two-dimensional collocation have been performed to find the number of collocation points in both z and θ directions needed to achieve convergence to a desired accuracy. The two dimensional collocation points used in the following runs are arranged such that the rings, which are represented by constant values of z, are evenly spaced along the

spherical arc. At each ring the collocation points are evenly spaced along the θ direction. The number of collocation points used at each ring is equal to the number of terms retained in the Fourier series representation of the density functions (18), while the number of rings used is equal to the number of terms retained in the Legendre series.

Tables 5 and 6 show numerical results of the dimensionless force and torque coefficients for a sphere with a fluid gap width of about one-half and one-tenth of the sphere radius respectively using the general two-dimensional collocation procedure. When the fluid gap width is one-half the sphere radius the same arrangement of collocation points (given values of z) and four points at each ring (given values of θ) are used for all orientation angles as shown in table 5. Comparing with the exact solution the maximum error of all coefficients in any orientation is less than 0.5%. When the separation gap is only one-tenth of the sphere radius, two different arrangements of the collocation points are used as shown in tables 6a and 6b. We find that although both sets of results exhibit good accuracy, the arrangement used in table 6a (10 rings and six points at each ring) is better than the arrangement used in table 6b (eight rings and eight points at each ring) when the orientation angle is larger

than 45 degrees, and vice versa when the orientation angle is smaller. This behavior is to be expected since as $\alpha \rightarrow 90^{\circ}$ fewer terms in the Fourier series and thus fewer collocation points on each ring are needed. In fact, as already demonstrated, in the limit of $\alpha = 90^{\circ}$ only one term of the Fourier series and one-dimensional collocation in the Z-direction is required.

It should be noted that the coefficients on the left hand side of the integral equations (15) depend only on the geometry and the form of the series representation of the stokeslet densities but not on the boundary conditions satisfied on the particle surface or $\vec{v}_{\infty}$. Since the bulk of the computation time is used to evaluate the coefficient matrix for a given configuration, the force and torque coefficients may be determined in a single run for a given geometry for all four of the problems outlined at the beginning of this section with a negligible increase in the computation time which would be required for a single problem. The computation time required for one configuration is approximately proportional to the square of the number of collocation points and can be estimated by the formula $T = 0.0015 \cdot N^2$, where T is the CPU time in minutes on an IBM 3081 computer and N is the total number of collocation points.

4. Solution for the motion of a spheroid near a planar wall

In this section the theory derived in section 2 is used to obtain the solution for the motion of a spheroid near a planar wall. The surface of a spheroid is represented in the cylindrical coordinate system (see figure 3) by

$$R_s(z) = b\left[1 - \left(\frac{z}{a}\right)^2\right]^{1/2} \tag{29}$$

where it is oblate for a<b and prolate for a>b.

Let a spheroid translate with velocity components U_1 and U_3 in the directions parallel and perpendicular to the wall respectively, and rotate with angular velocity ω about axis x_2. The undisturbed shear flow has a gradient S. The force and torque on the spheroid may be related to the particle velocity and shear strength using 12 dimensionless resistance coefficients as follows:

$$\begin{pmatrix} F_1 \\ F_3 \\ T_2 \end{pmatrix} = 6\pi\mu C \begin{pmatrix} F_1^{t_1} & F_1^{t_3} & F_1^{r} & HF_1^{S} \\ F_3^{t_1} & F_3^{t_3} & F_3^{r} & HF_3^{S} \\ \frac{4}{3}bT_2^{t_1} & \frac{4}{3}bT_2^{t_3} & \frac{4}{3}bT_2^{r} & \frac{2}{3}bT_2^{S} \end{pmatrix} \begin{pmatrix} U_1 \\ U_3 \\ b\omega \\ S \end{pmatrix} \tag{30}$$

Here c=b for an oblate spheroid and c=a for a prolate spheroid. H is distance between the center of the spheroid and the wall. F_1 and F_3 are the force components in the x_1 and x_3 directions respectively and T_2 is the torque acting on the spheroid.

All the dimensionless resistance coefficients are

functions of the separation distance of the spheroid from the wall, the orientation angle of the spheroid relative to the wall and the aspect ratio of the spheroid. The separation distance will be expressed by the dimensionless parameter H/c. The aspect ratio ϵ is defined as a/b for an oblate spheroid and b/a for a prolate spheroid, so that it varies between zero and unity in both cases.

It is worth noting that only nine of the twelve resistance coefficients are independent. From reciprocity theorems three pairs of the resistance coefficients are related as follows :

$$F_1^{t_3} = F_3^{t_1} \tag{31}$$

$$F_1^{r} = \frac{4}{3} T_2^{t_1} \tag{32}$$

$$F_3^{r} = \frac{4}{3} T_2^{t_3} \tag{33}$$

These relations are used as a further check of the consistency of the numerical results.

Tables 7a - 7f show convergence tests of the force and torque coefficients for an oblate spheroid having aspect ratio a/b = 0.5 with its axis of symmetry oriented perpendicular to the wall (i.e. $\alpha = 90^{\circ}$). For this particular case only one dimensional collocation is required. Note that the convergence for H/b = 0.55, which is equivalent to H/a = 1.1, is somewhat slower than for a sphere with H/a = 1.1 . When the particle is oriented at an

arbitrary angle relative to the wall two-dimensional collocation is required. The rate of convergence is found to be similar to the case of a sphere if we replace H/a by H/c. Tables 8 - 10 show the convergence of the coefficients $F_3^{t_3}$, T_2^{r} and $T_2^{t_1}$ for an oblate spheroid having aspect ratio ϵ = 0.5 and 0.1 inclined at $\alpha = 15^{\circ}$ relative to the wall. The remaining resistance coefficients exhibited similar convergence characteristics and are not shown.

Figures 4 to 12 show the converged values of the dimensionless hydrodynamic force and torque coefficients for an oblate and prolate spheroid as a function of the orientation angle α at constant separation distance H/b and aspect ratio ϵ. The coefficients are presented as the ratios of their values in the presence of the wall to the corresponding values in an unbounded fluid domain, except for the torque coefficients $T_2^{t_1}$ and $T_2^{t_3}$ for translation parallel and perpendicular to the wall which are identically zero in the absence of the wall. The hydrodynamic force coefficients of a spheroid moving parallel or perpendicular to its axis of symmetry in an unbounded fluid domain were obtained by Oberbeck(1876) and are presented by Happe and Brenner (1965,table 5-11). The torque coefficients of a spheroid which is rotating in an otherwise quiescent unbounded fluid or rigidly held in an unbounded shear flow $u = S\,z$ were obtained by Jeffery (1932). A summary of these formulas is presented in Appendix B for reference.

Figures 4 and 5 show $F_1^{t_1}/F_{1,\infty}^{t_1}$ and $F_3^{t_3}/F_{3,\infty}^{t_3}$, the ratios of the drag force for the motion parallel and perpendicular to the wall, respectively, to the corresponding force when $H \to \infty$. The curves of $F_1^{t_1}/F_{1,\infty}^{t_1}$ are similar in shape for both ϵ =0.5 and 0.1 with the values for ϵ =0.1 somewhat smaller than for ϵ =0.5. But the behavior of $F_3^{t_3}/F_{3,\infty}^{t_3}$ is radically different for ϵ =0.1 and 0.5, especially at close spacings. At H/b=1.1 the ratio $F_3^{t_3}/F_{3,\infty}^{t_3}$ decreases with increasing α for ϵ =0.5 while it increases for ϵ =0.1.

Figure 6 shows $F_3^{t_1}/F_{3,\infty}^{t_1}$, the ratio of the force component perpendicular to the wall due to the motion parallel to the wall to the same force in the absence of the wall. Although the values of $F_3^{t_1}$ are zero for the orientation angle α equal to 0° and 90°, the ratio $F_3^{t_1}/F_{3,\infty}^{t_1}$ has a finite limiting value for each particle-to-wall spacing at the two extreme points. The ratio $F_3^{t_1}/F_{3,\infty}^{t_1}$ is a weak function of α up to H/c=1.5 but becomes strongly dependent on α when the spheroid is closer to the wall.

Figures 7 and 8 show the variation of ratios $F_1^s/F_{1,\infty}^s$ and $F_3^s/F_{3,\infty}^s$ respectively. It is interesting to note that $F_1^s = -F_1^{t_1}$ and $F_3^s = -F_3^{t_1}$. Comparing with figures 4 and 5, the absolute value of F_1^s is always less than $F_1^{t_1}$ and the absolute value of F_3^s is always less than $F_3^{t_1}$ and their difference increases as the particle is brought closer to the wall.

Figure 9 shows $T_2^r/T_{2,\infty}^r$, the ratio of the torque experienced by a rotating spheroid to the value in an

unbounded fluid domain. The ratio is almost unity for H/c greater than 5. When the separation distance is decreased, the orientation angle α at which $T_2^r / T_{2,\infty}^r$ becomes maximum gradually shifts from $\alpha = 0^\circ$ toward 90° for an oblate spheroid and vice versa for a prolate spheroid.

All the ratios shown above are greater than unity for any orientation angle α ,so these force and torque coefficients are always larger than the corresponding values in an unbounded fluid domain. But for the ratio $T_2^s / T_{2,\infty}^s$ this is not the case, as shown in figure 10. For an oblate spheroid the ratio is less than unity for small α and is greater than unity for large α . When α approaches 90° the ratio of $T_2^s / T_{2,\infty}^s$ increases very rapidly. When the aspect ratio is very small ($\epsilon = 0.1$) and α is very close to 90°, $T_2^s / T_{2,\infty}^s$ becomes very large although the actual value of T_2^s at $\alpha = 90^\circ$ is much less than the value at $\alpha = 0^\circ$. For a prolate spheroid the ratio $T_2^s / T_{2,\infty}^s$ has its maximum value at $\alpha = 0^\circ$ for a given spacing.

The dimensionless torque coefficients for parallel and perpendicular motion are shown in figures 11 and 12, respectively. As expected both coefficients vanish when $H/c \to \infty$. It is interesting to note that the torque due to the parallel motion changes sign as function of the orientation angle. Therefore for each particle-to-wall spacing and aspect ratio, there is a critical orientation angle for which a spheroid can translate parallel to the

wall without experiencing any torque.

Comparing the corresponding curves for a prolate and oblate spheroid having the same aspect ratio we find that the quantitative variation of all the coefficients with is similar to that for an oblate spheroid having the same aspect ratio at an orientation of $90^{\circ}-\alpha$. This is because while the angle between the long axis and the wall is α for a prolate spheroid, it is $90^{\circ}-\alpha$ for an oblate spheroid.

In order to more clearly see the effect of body shape, figure 13 shows the force coefficients $F_1^{t_1}$, $F_3^{t_3}$ and $F_3^{t_1}$ as a function of the aspect ratio ϵ at $\alpha = 45^{\circ}$ and several constant values of H/c. All three ratios have their maximum values for a sphere ($\epsilon = 1$). The coefficient $F_3^{t_1}$ is zero for a sphere. When ϵ approaches unity the ratio $F_3^{t_1}/F_{3,\infty}^{t_1}$ increases with ϵ very rapidly but has limiting values. For a spheroid with ϵ close to unity the absolute value of $F_3^{t_1}$ is very small and converges much slower than other coefficients. Limited by computer time, the values of $F_3^{t_1}$ have not been calculated accurately for ϵ very close to unity at H/c = 1.1 and, therefore, are not shown in figure 15.

The force and torque coefficients of a spheroid moving parallel to a wall have been obtained by the method of reflections in Wakiya (1957). The results achieved by the method of reflections are compared to the solutions of the

present boundary integral method in table 11. At large spacings the results of Wakiya are in good agreement with the values achieved by the boundary integral method. At close spacings the discrepancy increases, but agreement is still good for the coefficient $F_1^{t_1}$ up to H/b = 1.5 . For the coefficients $F_3^{t_1}$ and $T_2^{t_1}$ the results obtained by the method of reflections have substantial error at close spacings. For example, at H/b=1.5 and 1.1 the value of $F_3^{t_1}$ calculated by the method of reflections is 25% and four times less respectively than the strong-interaction solutions obtained by the present theory. Even at H/b=5 the error of the values of $T_1^{t_1}$ computed by the method of reflections is close to 10% .

Appendix A

A key step in keeping computation time at a minimum while maintaining high accuracy is to evaluate the integrals in (15) analytically in the θ direction. Let $R = R_S(z)$ represent the body shape in the (R, θ, z) cylindrical coordinate system. The coordinates $(R(z), \theta, z)$ and $(R(z^*), \theta^*, z^*)$ represent two distinct points $\underset{\sim}{x}$ and $\underset{\sim}{y}$ on the particle surface respectively. The inclination angle of the axis of symmetry of the body with respect to the wall is α and the particle-to-wall separation distance is H (see figure 3). Then the various quantities appearing in (15) can be expressed in terms of the coordinates of these two points as follows:

$$r^2 = C_1 + D_1 \cos(\theta - \theta^*) \tag{A-1}$$

$$r^{*2} = C_2 + D_2 \cos(\theta - \theta_*) \tag{A-2}$$

$$r_1 = r_1^* = C_3 + D_3 \cos\theta \tag{A-3}$$

$$r_2 = r_2^* = C_4 + D_4 \sin\theta \tag{A-4}$$

$$r_3 = C_5 + D_5 \cos\theta \tag{A-5}$$

$$r_3^* = C_6 + D_6 \cos\theta \tag{A-6}$$

$$\chi_3 = C_7 + D_7 \cos\theta \tag{A-7}$$

$$n_1 = C_8 + D_8 \cos\theta \tag{A-8}$$

$$n_2 = C_9 + D_9 \sin\theta \tag{A-9}$$

$$\eta_3 = C_{10} + D_{10}\cos\theta \qquad \text{(A-10)}$$

$$\vartheta_1 = C_{11} + D_{11}\cos\theta \qquad \text{(A-11)}$$

$$\vartheta_2 = 0 \qquad \text{(A-12)}$$

$$\vartheta_3 = C_{12} + D_{12}\cos\theta \qquad \text{(A-13)}$$

where, in the order of appearance in (A-1) - (A-13)

$$C_1 = (Z - Z^*)^2 + R^2 + R''^2 \qquad \text{(A-14)}$$

$$C_2 = -2RR'' \qquad \text{(A-15)}$$

$$C_3 = 4H\,(H + Z^*\sin\alpha + R^*\cos\theta^*\cos\alpha + Z\sin\alpha + Z''^2 + Z^2 + R''^2 + R^2 - 2Z^*Z\cos 2\alpha + 2ZR^*\sin 2\alpha\cos\theta'') \qquad \text{(A-16)}$$

$$D_2 = -2R\left[R''^2\sin^2\theta'' + (R^*\cos 2\alpha\sin\theta'' + Z\sin 2\alpha + 2H\cos\alpha)^2\right]^{1/2} \qquad \text{(A-17)}$$

$$\theta_1 = \tan^{-1}\left[R''\sin\theta''/(R^*\cos 2\alpha\sin\theta'' + Z\sin 2\alpha + 2H\cos\alpha)\right] \qquad \text{(A-18)}$$

$$C_3 = (Z - Z^*)\cos\alpha + R''\sin\alpha\cos\theta'' \qquad \text{(A-19)}$$

$$D_3 = -R\sin\alpha \qquad \text{(A-20)}$$

$$C_4 = -R''\sin\theta'' \qquad \text{(A-21)}$$

$$D_4 = R \qquad \text{(A-22)}$$

$$C_5 = (Z - Z^*)\sin\alpha - R''\cos\theta''\cos\alpha \qquad \text{(A-23)}$$

$$D_5 = R\cos\alpha \qquad \text{(A-24)}$$

$$C_6 = (Z + Z^*)\sin\alpha + R^*\cos\theta^*\cos\alpha + 2H \qquad \text{(A-25)}$$

$$\mathcal{D}_6 = R\cos\alpha \qquad \text{(A-26)}$$

$$C_7 = H + \ell\sin\alpha \qquad \text{(A-27)}$$

$$\mathcal{D}_7 = R\cos\alpha \qquad \text{(A-28)}$$

$$C_8 = R'\cos\alpha \,/\, (1+R'^2)^{1/2} \qquad \text{(A-29)}$$

$$\mathcal{D}_8 = \sin\alpha \,/\, (1+R'^2)^{1/2} \qquad \text{(A-30)}$$

$$\mathcal{D}_9 = -1 \,/\, (1+R'^2)^{1/2} \qquad \text{(A-31)}$$

$$C_{10} = R'\sin\theta^* \,/\, (1+R'^2)^{1/2} \qquad \text{(A-32)}$$

$$\mathcal{D}_{10} = -\cos\theta^* \,/\, (1+R'^2)^{1/2} \qquad \text{(A-33)}$$

In the above expressions $R = R(z)$, $R^* = R(z^*)$ and $R' = dR/dz$. The quantities C_{11}, C_{12}, D_{11} and D_{12} depend on the velocity field. For motion parallel to the wall with unit velocity:

$$C_{11} = 1 \;, \quad C_{12} = \mathcal{D}_{11} = \mathcal{D}_{12} = 0 \qquad \text{(A-34)}$$

For motion perpendicular to the wall with unity velocity:

$$C_{12} = 1 \;, \quad C_{11} = \mathcal{D}_{11} = \mathcal{D}_{12} = 0 \qquad \text{(A-35)}$$

For a shear flow having unit strength:

$$C_{11} = -H - \ell\sin\alpha \;, \quad \mathcal{D}_{11} = R\cos\alpha \;, \quad C_{12} = \mathcal{D}_{12} = 0 \qquad \text{(A-36)}$$

For rotation with angular velocity of unity:

$$C_{11} = \ell\sin\alpha \;, \quad \mathcal{D}_{11} = R\cos\alpha \;, \quad C_{12} = -\ell\cos\alpha \;, \quad \mathcal{D}_{12} = R\sin\alpha \qquad \text{(A-37)}$$

We now substitute A-1 to A-37 into integral equation (15). After a lengthy algebraic operations the integrals in

the direction can be expressed in the following form :

$$I = \int_0^{2\pi} \frac{\cos m\theta \, d\theta}{[A^2 + B^2 \cos(\theta - \theta_0)]^{p/2}} \qquad \text{(A-38)}$$

where p = 1, 3, 5 and 7. This integral can be written as

$$I = \frac{A \cos 2m\theta_0}{(A^2 + B^2)^{p/2}} \cdot Q(K, m, P, \pi/2) \qquad \text{(A-39)}$$

where

$$Q(K, m, P, \theta) = \int_0^{\theta} \frac{\cos mt \, dt}{[1 - K^2 \sin^2 t]^{p/2}} \qquad \text{(A-40)}$$

$$K^2 = \frac{2B^2}{A^2 + B^2} \leq 1 \qquad \text{(A-41)}$$

To evaluate the integral Q(k, m, p,) we discuss three cases.

(a) 0.8 < K < 1

This integral can be represented by the series

$$Q(K, m, P, \theta) = \sum_{i=0}^{m} \alpha_{mi} \, G(K, P, i, \theta) \qquad \text{(A-42)}$$

where

$$\alpha_{mi} = \begin{cases} 1 & i = m = 1 \\ m \dfrac{(-1)^i 2^{2i} (m+i-1)!}{(2i)! \; (m-i)!} & \text{otherwise} \end{cases} \qquad \text{(A-43)}$$

$$G(K, P, i, \theta) = \int_0^{\theta} \frac{\cos^{2i} t \, dt}{(1 - K^2 \sin^2 t)^{p/2}} \qquad \text{(A-44)}$$

The function G(k, p, i, θ) can be expressed in terms of the elliptic functions of the first and second kind as follows:

$$G(K, -1, 0, \theta) = E(\theta, K) \qquad \text{(A-45)}$$

$$G(K,1,0,\theta) = F(\theta,K) \qquad \text{(A-46)}$$

$$G(K,P,0,\theta) = -\frac{K^2 \sin\theta\cos\theta}{(P-1)K'^2\Delta^{P-1}} + \frac{(P-2)(2-K^2)}{(P-1)K'^2} G(K,P-2,0,\theta) - \frac{P-4}{(P-2)K'^2} \cdot G(K,P-4,0,\theta) \qquad \text{(A-47)}$$

$$G(K,P,i,\theta) = \frac{1}{K^2} G(K,P-2,i-1,\theta) - \frac{K'^2}{K^2} G(K,P,i-1,\theta) \qquad \text{(A-48)}$$

where E and F are the elliptic functions of the first and second kind, respectively. $K'^2 = 1-K^2$ and $\Delta = (1-K^2\sin^2\theta)^{1/2}$

Unfortunately the results given by (A-37) produce large round off error for small k and large m. Therefore (A-37) can be used only for K close to 1.

(b) $0 < K < 0.8$

When K is not close to unity we use the infinite series

$$(1-K^2\sin^2\theta)^{-n/2} = 1 + \frac{n}{2}K^2\sin^2\theta + \frac{\frac{n}{2}\cdot(\frac{n}{2}+1)}{2}K^4\sin^2\theta + \cdots - \frac{(\frac{n}{2})(\frac{n}{2}+1)\cdots(\frac{n}{2}+J-1)}{J!}K^{2J}\sin^{2J}\theta + \cdots \qquad \text{(A-49)}$$

then using the known result:

$$\int_0^{\frac{\pi}{2}} \sin^{2J}\chi \cos 2m\chi \, d\chi = \begin{cases} \frac{(-1)^m\pi}{2^{2m-1}}\binom{2J}{J-m} & J \geq m \\ 0 & J < m \end{cases} \qquad \text{(A-50)}$$

We get

$$Q(K,m,P,\tfrac{\pi}{2}) = \frac{(-1)^m\pi}{2^{2m-1}} \sum_{J=m}^{\infty} \binom{2J}{J-m} \frac{\frac{P}{2}(\frac{P}{2}+1)\cdots(\frac{P}{2}+J-1)K^{2J}}{J!} \qquad \text{(A-51)}$$

The infinite series (A-51) converges very fast for K not close to unity.

The applicable regions for K of equations (A-42) and (A-51) overlap. Numerical tests show that K = 0.8 is a

reasonable value for matching the two solutions.

(c) When $z = z^*$ and $\theta = \theta^*$ the following integrals become singular:

$$\iint_{S_p} \left(\frac{1}{r} - \frac{r_i r_k}{r^3} \right) f_k(\underset{\sim}{x})\, dS_{\underset{\sim}{x}} \qquad \text{(A-52)}$$

and

$$\iint_{S_p} \frac{r_i r_j r_k}{r^5}\, v_k(\underset{\sim}{x})\, n_j(\underset{\sim}{x})\, dS_{\underset{\sim}{x}} \qquad \text{(A-53)}$$

To evaluate these integrals we divide the region of integration into four subregions as follows:

$$\int_{-1}^{+1}\int_{0}^{2\pi} \varphi\, d\theta\, d\zeta = \left(\int_{-1}^{\zeta^*-\epsilon}\int_{0}^{2\pi} + \int_{\zeta^*+\epsilon}^{+1}\int_{0}^{2\pi} + \int_{\zeta^*-\epsilon}^{\zeta^*+\epsilon}\int_{\epsilon_1}^{2\pi-\epsilon_1} + \int_{\zeta^*-\epsilon}^{\zeta^*+\epsilon}\int_{-\epsilon_1}^{\epsilon_1} \right) \varphi\, d\theta\, d\zeta \qquad \text{(A-54)}$$

where $0 < \epsilon \ll 1$, $\epsilon_1 = \epsilon / R$. The first three integrals on the right side of A-53 are regular, while the fourth is singular. The first two integrals in the θ direction can be evaluated using (A-42) or (A-51). The third one can be represented by

$$\int_{0}^{2\pi-\epsilon_1} \frac{\cos 2m\theta\, d\theta}{[1 - K^2 \sin^2\theta]^{3/2}} = A \sum_{i=0}^{m} \alpha_{mi}\, G\left(K, P, i, \frac{\pi-\epsilon_1}{2}\right) \qquad \text{(A-55)}$$

where the function G(K, p, i, $(\pi-\epsilon_1)/2$) can be expressed in terms of the incomplete elliptic functions by equations (A-45) - (A-48). The last one can be evaluated analytically by treating the small region around the singularity as a flat plane as was done by Youngren & Acrivos (1975).

Appendix B

In this appendix we list formulas for calculating the force and torque coefficients of a spheroid in an unbounded fluid. In the following a is the half-length, b is the radius and $\phi = a/b$ for both oblate and prolate spheroids. Table B-1 and B-2 list some values of these coefficients.

When a spheroid is translating in an unbounded fluid it does not experience any torque. The drag coefficient for the translating motion is defined as

$$F_{1,\infty}^{t_1} = F_1 / 6\pi\mu C U_1 \qquad (B-1)$$

where c=b for an oblate spheroid and c=a for a prolate spheroid.

The drag coefficient for translating motion with arbitrary angle α toward the symmetry axis can be expressed as follows:

$$F_{1,\infty}^{t_1} = F_{1,\infty}^{t_1,*} \cos^2\alpha + F_{1,\infty}^{t_1,**} \sin^2\alpha \qquad (B-2)$$

where $F_{1,\infty}^{t_1,*}$ and $F_{1,\infty}^{t_1,**}$ represent the drag coefficients for translating motion parallel and perpendicular to the axis of symmetry respectively. The coefficients $F_{1,\infty}^{t_1,*}$ and $F_{1,\infty}^{t_1,**}$ are given by Happel & Brenner (1965) and listed below for reference. For an oblate spheroid:

$$F_{1,\infty}^{t_1,*} = -\frac{8}{3}\left\{ \frac{2\phi}{1-\phi^2} - \frac{2(1-2\phi^2)}{(1-\phi^2)^{3/2}} \tan^{-1}\left[\frac{(1-\phi^2)^{1/2}}{\phi} \right] \right\}^{-1} \qquad (B-3)$$

$$= \frac{8}{3}\left\{ \frac{\phi}{1-\phi^2} - \frac{2\phi^2-3}{(1-\phi^2)^{3/2}} \sin^{-1}(1-\phi^2)^{1/2} \right\}^{-1} \qquad (B-4)$$

For a prolate spheroid:

$$F^{\dagger,*}_{1,\infty} = \frac{8}{3}\left\{\frac{2\phi^2}{\phi^2-1} - \frac{(2\phi^2-1)\phi}{(\phi^2-1)^{3/2}} ln\left[\frac{\phi+(\phi^2-1)^{1/2}}{\phi-(\phi^2-1)^{1/2}}\right]\right\}^{-1} \qquad (B-5)$$

$$F^{\dagger,**}_{1,\infty} = -\frac{8}{3}\left\{\frac{\phi^2}{\phi^2-1} - \frac{(2\phi^2-3)\phi}{(\phi^2-3)^{3/2}} ln\left[\phi+(\phi^2-1)^{1/2}\right]\right\}^{-1} \qquad (B-6)$$

When a spheroid is rotating in an unbounded fluid it only experiences a torque. The torque coefficient is defined as

$$T^{r}_{2,\infty} = T_2 / 8\pi\mu b^2 c\omega \qquad (B-7)$$

The force experienced by a spheroid in an unbound shear flow is equal to that it would have if it is translating in an otherwise unbounded quiescent fluid with a velocity equal to the incoming fluid velocity at the spheroid center. The torque coefficient for a spheroid rigidly held in a shear flow at an arbitrary angle α is defined as:

$$T^{S}_{2,\infty} = T_2 / 4\pi\mu b^2 c S \qquad (B-8)$$

The torque coefficients can be expressed as

$$T^{S}_{2,\infty} = T^{S*}_{2,\infty} Cos^2\alpha + T^{S**}_{2,\infty} Sin^2\alpha \qquad (B-9)$$

where $T^{S*}_{2,\infty}$ and $T^{S**}_{2,\infty}$ represent the coefficients for shear flow whose direction is parallel and perpendicular to the axis of symmetry of the spheroid, respectively. The torque coefficients $T^{r}_{2,\infty}$, $T^{S*}_{2,\infty}$ and $T^{S**}_{2,\infty}$ has been solved by Jeffery (1922) and listed below for reference. For an oblate spheroid:

$$T_{2,\infty}^{r} = -\frac{2}{3}\cdot\frac{1+\phi^2}{\gamma_1+\phi^2\gamma_2} \tag{B-10}$$

$$T_{2,\infty}^{s\perp} = -\frac{4}{3}\cdot\frac{1}{\gamma_1+\phi^2\gamma_2} \tag{B-11}$$

$$T_{2,\infty}^{s\parallel} = -\frac{4}{3}\,\frac{\phi^2}{\gamma_1+\phi^2\gamma_2} \tag{B-12}$$

For a prolate spheroid:

$$T_{2,\infty}^{r} = -\frac{2}{3}\cdot\frac{1+\phi^2}{\phi(\gamma_1+\phi^2\gamma_2)} \tag{B-13}$$

$$= -\frac{4}{3}\,\frac{1}{\phi(\gamma_1+\phi^2\gamma_2)} \tag{B-14}$$

$$= -\frac{4}{3}\,\frac{\phi}{\gamma_1+\phi^2\gamma_2} \tag{B-15}$$

where

$$\gamma_1 = \int_0^\infty \frac{d\lambda}{(1+\lambda)\cdot\Delta} \tag{B-16a}$$

$$\gamma_2 = \int_0^\infty \frac{d\lambda}{(\phi^2+\lambda)\cdot\Delta} \tag{B-16b}$$

$$\Delta = (\phi^2+\lambda)(1+\lambda) \tag{B-16c}$$

REFERENCES

Brenner, H. 1964 Chem. Eng. Sci. 19 , 519

Brenner, H. & Gaydos, L.J. 1977 Colloid Interface Sci. 58 , 312.

Chen, T.C. & Skalak, R. 1970 Appl. Sci. Res. 22 , 403.

Chwang, A.T. 1975 J. Fluid Mech. 72, 17

Chwang, A.T. & Wu, T.Y. 1974 J. Fluid Mech. 63, 607.

Chwang, A.T. & Wu, T.Y. 1975 J. Fluid Mech. 67, 787.

Goldman, A.J., Cox, R.G. & Brenner, H. 1967A Chem. Eng. Sci. 22, 637

Goldman, A.J., Cox, R.G. & Brenner, H. 1967B Chem. Eng. Sci. 22, 653

Gunter, N.M. 1967 Potential Theory , Frederch Unger, New York.

Hyman, M.A. & Skalak, R. 1972 Appl. Sci. Res. 26 , 27.

Jeffery, G.B. 1922 Proc. Roy. Soc. A102 , 161.

Ladyzhenskaya, U.A. 1963 The Mathematical Theory of Viscous Incompressible Flow, Gordon and Breach, New York.

Leal D.G. & Lee, S.H. 1982 Advances in Colloid and interface Sci. 17 , 61

Lee, S.H. & Leal, L.G. 1982 J. colloid Interface Sci. 87, 81.

Lewellen, P. 1982 Hydrodynamic Analysis of Microporous Mass Transport Ph.D. Thesis, Univer. of Winsconsin-Madison.

Lightfoot, E.N. 1974 Transport Phenomena and Living Systems, John Wiley & Sons, New York.

Liron, N. 1978 J. Fluid Mech. 86 , 705.

Liron, N & Mochon, S. 1976 J. Fluid Mech. 75 , 593.

O'Brien, V. 1968 A.I.CH.E J. 14 , 870

Rallison, J.M. & Acrivos, A. 1978 J.Fluid Mech. 89 , 91.

Skalak, R., Chen, P.H. Chien, S. 1972 Biorheol 9 , 67.

Tözeren, H. 1984 Inter. J. Num. Meth. in Fluids 4, N 2. 159

Wakiya, S. 1957A J. Phys. Soc. Japan 12 , 1130

Wakiya, S. 1959 Res. Rep. Fac. Eng. NIigate Univ. (Japan)
8, 17.

Wang, H. & Skalak, R. 1969 J. Fluid Mech. 38 , 75.

Youngren, G.K. & Acrivos, A. 1975 J Fluid Mech. 69 , 377

Youngren, G.K. & Acrivos, A. 1976 J Fluid Mech. 76 , 433

N	H/a			
	1.1276	1.5431	2.3524	3.7622
5	-32.13	-3.039	-1.839	-1.222
7	-12.09	-3.036	-1.838	-1.222
9	-9.45	-3.036	-1.838	-1.222
11	-9.25	-3.036		
13	-9.25			
exact	-9.25	-3.036	-1.838	-1.222

(a) boundary collocation method

N	H/a			
	1.1276	1.5431	2.3524	3.7622
5	-8.38	-3.035	-1.837	-1.222
7	-9.05	-3.036	-1.838	-1.222
9	-9.21	-3.036	-1.838	-1.222
11	-9.24	-3.036		
13	-9.25			
exact	-9.25	-3.036	-1.838	-1.222

(b) weighted residual method

Table 1 Convergence of dimensionless resistance coefficient F_3^t for a sphere moving perpendicular to a wall at various sphere-to-wall spacings.

N	H/a			
	1.1276	1.5431	2.3524	3.7622
4	-2.016	-1.462	-1.283	-1.168
6	-2.116	-1.567	-1.308	-1.174
8	-2.144	-1.567	-1.308	-1.174
10	-2.152			
12	-2.151			
14	-2.151			
exact	-2.151	-1.567	-1.308	-1.174

(a) Tests of $F_1^{t_1}$

N	H/a			
	1.1276	1.5431	2.3524	3.7622
4	-0.1126	-0.0323	-0.00242	-0.000415
6	-0.0985	-0.0298	-0.00253	-0.000418
8	-0.0760	-0.0145	-0.00263	-0.000419
10	-0.0723	-0.0146	-0.00264	-0.000422
12	-0.0737	-0.0147	-0.00264	-0.000422
14	-0.0737	-0.0147		
exact	-0.0737	-0.0147	-0.00264	-0.000422

(b) tests of $T_2^{t_1}$

Table 2 Convergence of dimensionless resistance coefficients for a sphere moving parallel to a wall at various sphere-to-wall spacings.

N	H/a			
	1.1276	1.5431	2.3524	3.7622
4	-0.173	-0.0226	-0.00375	-0.00549
6	-0.149	-0.0202	-0.00351	-0.00553
8	-0.106	-0.0188	-0.00351	-0.00558
10	-0.0983	-0.0195	-0.00352	-0.00562
12	-0.0983	-0.0195	-0.00352	-0.00562
exact	-0.0983	-0.0195	-0.00352	-0.00562

(a) Tests of F_1^r

N	H/a			
	1.1276	1.5431	2.3524	3.7622
4	-1.334	-1.097	-1.023	-1.006
6	-1.374	-1.100	-1.025	-1.006
8	-1.382	-1.100	-1.025	-1.006
10	-1.388	-1.100	-1.025	
12	-1.388			
exact	-1.388	-1.100	-1.025	-1.006

(b) tests of T_2^r

Table 3 Convergence of dimensionless resistance coefficients for a sphere rotating along a wall at various sphere-to-wall spacings.

N	H/a			
	1.1276	1.5431	2.3524	3.7622
4	1.610	1.437	1.277	1.167
6	1.614	1.439	1.278	1.167
8	1.616	1.439	1.278	
10	1.616			
12	1.616			
exact	1.616	1.439	1.278	1.167

(a) Tests of F_1^A

N	H/a			
	1.1276	1.5431	2.3524	3.7622
4	-0.9508	-0.9737	-0.9923	-0.9973
6	-0.9526	-0.9746	-0.9911	-0.9971
8	-0.9533	-0.9744	-0.9903	-0.9971
10	-0.9538	-0.9742	-0.9901	
12	-0.9537	-0.9742	-0.9901	
14	-0.9537			
exact	-0.9537	-0.9742	-0.9901	-0.9971

(b) tests of I_1^S

Table 4 Convergence of dimensionless resistance coefficients for a sphere rigidly held in a shear flow near a wall at various sphere-to-wall spacings.

α	$F_1^{t_1}$	F_1^r	F_1^s	$F_3^{t_1}$	$T_2^{t_1}$	T_2^r	T_2^s
15°	-1.566	-0.01955	1.439	-3.032	-0.01470	-1.100	-0.9742
30°	-1.567	-0.01955	1.439	-3.032	-0.01470	-1.100	-0.9742
45°	-1.567	-0.01957	1.439	-3.035	-0.01462	-1.100	-0.9742
60°	-1.567	-0.01956	1.439	-3.037	-0.01467	-1.100	-0.9743
75°	-1.567	-0.01950	1.439	-3.036	-0.01468	-1.100	-0.9742
exact	-1.567	-0.01953	1.439	-3.036	-0.01465	-1.100	-0.9745

Table 5 Numerical Tests of two-dimensional collocation for a sphere at H/a = 1.5431 (α is the orientation angle of the sphere axis, 24 collocation points were used).

(a)

α	$F_1^{t_1}$	F_1^r	F_1^s	$F_3^{t_3}$	$T_2^{t_1}$	T_2^r	T_2^s
15°	-2.149	-0.09866	1.616	-8.91	-0.07467	-1.386	-0.9537
30°	-2.150	-0.09886	1.616	-9.04	-0.07416	-1.387	-0.9537
45°	-2.151	-0.09839	1.616	-9.24	-0.07408	-1.387	-0.9537
60°	-2.151	-0.09815	1.616	-9.25	-0.07411	-1.387	-0.9537
75°	-2.151	-0.09813	1.616	-9.26	-0.07412	-1.387	-0.9537
exact	-2.151	-0.09829	1.616	-9.252	-0.07372	-1.387	-0.9537

(b)

α	$F_1^{t_1}$	F_1^r	F_1^s	$F_3^{t_3}$	$T_2^{t_1}$	T_2^r	T_2^s
15°	-2.151	-0.09836	1.616	-9.23	-0.07352	-1.388	-0.9537
30°	-2.150	-0.09838	1.616	-9.27	-0.07340	-1.387	-0.9537
45°	-2.152	-0.09810	1.616	-9.26	-0.07387	-1.387	-0.9537
60°	-2.151	-0.09859	1.616	-9.20	-0.07484	-1.387	-0.9537
75°	-2.148	-0.1029	1.616	-9.31	-0.07605	-1.385	-0.9537
exact	-2.151	-0.09829	1.616	-9.252	-0.07372	-1.387	-0.9537

Table 6 Numerical tests of two dimensional collocation for a sphere at H/a=1.1276.
(a) Using 10 rings and 6 points at each ring.
(b) using 8 rings and 8 points at each rings.

N	H/b			
	0.5	0.8	1.1	1.5
2	8.9	5.326	3.407	2.393
4	23.7	6.918	3.567	2.379
6	40.3	7.226	3.589	2.385
8	53.1	7.257	3.589	2.385
10	57.5	7.263	3.589	2.385
12	60.4	7.264		
14	61.4	7.262		
16	61.7	7.262		
18	62.6	7.262		
20	62.9			
22	62.9			

Table 7a Convergence of resistance coefficient $F_3^{t_1}/F_{3,\infty}^{t_1}$ for an oblate spheroid having a/b=0.5 with its symmetry axis perpendicular to the wall.

N	H/b			
	0.55	0.8	1.1	1.5
2	4.732	1.850	1.460	1.267
4	3.218	1.917	1.564	1.376
6	3.355	1.923	1.568	1.380
8	3.374	1.923	1.568	1.380
10	3.378	1.923	1.568	1.380
12	3.381			
14	3.384			
16	3.386			
18	3.388			
20	3.389			
22	3.389			
24	3.390			
26	3.390			

Table 7b Convergence of resistance coefficient $F_1^{t_1}/F_{1,\infty}^{t_1}$ for an oblate spheroid having a/b=0.5 with its symmetry axis perpendicular to the wall.

N	H/b			
	0.55	0.8	1.1	1.5
2	-0.168	0.0134	0.01057	0.00647
4	0.475	0.1233	0.05913	0.03243
6	0.580	0.1217	0.05921	0.03251
8	0.588	0.1211	0.05916	0.03251
10	0.576	0.1211	0.05916	0.03251
12	0.567	0.1211		
14	0.561			
16	0.557			
18	0.556			
20	0.555			
22	0.555			
24	0.555			

Table 7c Convergence of resistance coefficient $T_z^{t_1}$ for an oblate spheroid having a/b=0.5 with its symmetry axis perpendicular to the wall.

N	H/b			
	0.55	0.8	1.1	1.5
2	12.05	0.843	0.672	0.625
4	4.47	1.670	1.242	1.100
6	5.19	1.656	1.245	1.102
8	4.90	1.655	1.245	1.102
10	4.80	1.654	1.245	1.102
12	5.12	1.654		
14	4.90			
16	4.80			
18	4.91			
20	5.03			
22	5.04			
24	5.03			
26	4.97			
28	4.97			

Table 7d Convergence of resistance coefficient $T_1^r / T_{1,\infty}^r$ for an oblate spheroid having a/b=0.5 with its symmetry axis perpendicular to the wall.

N	H/b			
	0.55	0.8	1.1	1.5
2	1.421	1.516	1.354	1.230
4	1.991	1.664	1.478	1.342
6	1.985	1.671	1.481	1.346
8	1.994	1.670	1.480	1.346
10	1.990	1.670	1.480	1.346
12	1.984			
14	1.988			
16	1.990			
18	1.992			
20	1.990			
24	1.988			
26	1.988			

Table 7e Convergence of resistance coefficient $F_1^s/F_{1,\infty}^s$ for an oblate spheroid having a/b=0.5 with its symmetry axis perpendicular to the wall.

N	H/b			
	0.55	0.8	1.1	1.5
2	-1.23	0.780	0.915	0.955
4	1.36	1.363	1.354	1.324
6	1.32	1.370	1.362	1.331
8	1.43	1.369	1.361	1.331
10	1.31	1.369	1.361	1.331
12	1.28	1.369		
14	1.34			
16	1.41			
18	1.43			
20	1.37			
24	1.35			
26	1.35			

Table 7f Convergence of resistance coefficient $T_2^S / T_{2,\infty}^S$ for an oblate spheroid having a/b=0.5 with its symmetry axis perpendicular to the wall.

(A) a/b = 0.5, H/c = 1.5

N \ M	4	6	8
4	2.363	2.364	2.365
6	2.368	2.370	2.370
8	2.369	2.370	2.370

(b) a/b = 0.5, H/c = 1.1

N \ M	4	6	8	10
4	4.80	5.02	5.21	5.21
6	4.96	5.08	5.16	5.16
8	5.03	5.15	5.20	5.20
10	5.04	5.15	5.20	5.20

Table 8 Convergence tests of $F_3^{t_3}/F_{3,\infty}^{t_3}$ for an oblate spheroid inclined at 15° with respect to the planar wall.
N ___ Number of rings (constant values of ξ)
M ___ Number of points at each ring (constant values of θ)

(c) a/b = 0.1, H/c = 1.5

N \ M	4	6	8
4	1.741	1.741	1.742
6	1.833	1.837	1.838
8	1.834	1.840	1.840
10	1.835	1.840	1.840

(d) a/b = 0.1, H/C = 1.1

N \ M	4	6	8	10
4	2.50	2.53	2.55	2.57
6	2.51	2.59	2.61	2.61
8	2.53	2.71	2.72	2.72
10	2.54	2.71	2.72	2.72

Table 8 Convergence tests of $F_3^{t_1}/F_{3,\infty}^{t_1}$ for an oblate spheroid inclined at 15° with respect to the planar wall.
N ___ Number of rings (constant values of ξ)
M ___ Number of points at each ring (constant values of θ)

(A) a/b = 0.5, H/c = 1.5

N \ M	4	6	8
4	1.070	1.070	1.071
6	1.071	1.071	1.071
8	1.071	1.071	1.071

(b) a/b = 0.5, H/c = 1.1

N \ M	4	6	8	10
4	1.294	1.303	1.324	1.322
6	1.296	1.307	1.310	1.310
8	1.297	1.309	1.313	1.313
10	1.298	1.309	1.313	1.313

Table 9 Convergence tests of $T_2^r / T_{1,\infty}^r$ for an oblate spheroid inclined at 15° with respect to the planar wall.
N ___ Number of rings (constant values of Z)
M ___ Number of points at each ring (constant values of θ)

(C) a/b = 0.1, H/c = 1.5

N \ M	4	6	8
4	1.081	1.081	1.081
6	1.087	1.087	1.087
8	1.087	1.087	1.087

(d) a/b = 0.1, H/C = 1.1

N \ M	4	6	8	10
4	1.314	1.320	1.328	1.330
6	1.317	1.324	1.330	1.331
8	1.318	1.338	1.339	1.339
10	1.321	1.338	1.339	1.339

Table 9 Convergence tests of $T_2^r / T_{2,\infty}^r$ for an oblate spheroid inclined at 15° with respect to the planar wall.
N ___ Number of rings (constant values of Z)
M ___ Number of points at each ring (constant values of θ)

(a) a/b = 0.5, H/c = 1.5

N \ M	4	6	8
4	-0.0591	-0.0591	-0.0591
6	-0.0588	-0.0589	-0.0589
8	-0.0588	-0.0589	-0.0589

(b) a/b = 0.5, H/c = 1.1

N \ M	4	6	8	10
4	-0.193	-0.198	-0.202	-0.201
6	-0.193	-0.194	-0.195	-0.195
8	-0.193	-0.194	-0.195	-0.195
10	-0.193	-0.194	-0.195	-0.195

Table 10 Convergence tests of $T_2^{t_1}$ for an oblate spheroid inclined at 15° with respect to the planar wall.
N ___ Number of rings (constant values of Z)
M ___ Number of points at each ring (constant values of θ)

(c) a/b = 0.1, H/C = 1.5

N \ M	4	6	8
4	-0.0660	-0.0660	-0.0660
6	-0.0662	-0.0666	-0.0667
8	-0.0663	-0.0667	-0.0667

(d) a/b = 0.1, H/C = 1.1

N \ M	4	6	8	10
4	-0.187	-0.189	-0.192	-0.192
6	-0.187	-0.190	-0.192	-0.193
8	-0.189	-0.194	-0.194	-0.194
10	-0.190	-0.194	-0.194	-0.194

Table 10 Convergence tests of $I_2^{t_1}$ for an oblate spheroid inclined at 15° with respect to the planar wall.
N ___ Number of rings (constant values of Z)
M ___ Number of points at each ring (constant values of θ)

	boundary integral method			method of reflections		
H/b	$\alpha=0°$	$\alpha=45°$	$\alpha=90°$	$\alpha=0°$	$\alpha=45°$	$\alpha=90°$
1.1	2.08	1.75	1.574	1.77	1.57	1.345
1.5	1.530	1.455	1.380	1.488	1.415	1.346
2.0	1.343	1.309	1.269	1.333	1.298	1.259
2.5	1.256	1.234	1.209	1.252	1.230	1.204
5.0	1.113	1.106	1.097	1.113	1.106	1.097
10.0	1.054	1.051	1.047	1.054	1.051	1.047

Table 11a Comparison of values of the force coefficient $F_1^{t)}/F_{1,\infty}^{t)}$ obtained by the present boundary integral method to values obtained by method of reflections for an oblate spheroid with a/b=0.5 moving parallel to the wall.

	boundary integral method			method of reflections		
H/b	$\alpha=0°$	$\alpha=45°$	$\alpha=90°$	$\alpha=0°$	$\alpha=45°$	$\alpha=90°$
1.1	7.18	5.23	4.59	1.54	1.31	1.13
1.5	3.21	3.096	2.86	2.282	2.222	2.172
2.0	2.269	2.265	2.265	2.023	2.031	2.043
2.5	1.886	1.899	1.911	1.790	1.807	1.826
5.0	1.349	1.358	1.367	1.342	1.351	1.361
10.0	1.156	1.160	1.164	1.156	1.160	1.164

Table 11b Comparison of values of the force coefficient $F_3^{t)}/F_{3,\infty}^{t)}$ obtained by the present boundary integral method to values obtained by method of reflections for an oblate spheroid with a/b=0.5 moving parallel to the wall.

	boundary integral method			method of reflections		
H/b	$\alpha=0^\circ$	$\alpha=45^\circ$	$\alpha=90^\circ$	$\alpha=0^\circ$	$\alpha=45^\circ$	$\alpha=90^\circ$
			(X 0.01)			
1.1	-22.8	-5.14	5.91	-12.6	-0.870	8.97
1.5	-6.56	-1.55	3.25	-5.72	-0.796	4.53
2.0	-3.02	-0.603	1.89	-2.88	-4.09	2.38
2.5	-1.77	-0.307	1.24	-1.73	-0.233	1.46
5.0	-0.385	-0.0481	0.316	-0.385	-0.0436	0.332
10.0	-0.0910	-0.00963	0.0781	-0.0911	-0.00935	0.0792

Table 11c Comparison of values of the force coefficient $T_2^{t_1}$ obtained by the present boundary integral method to values obtained by method of reflections for an oblate spheroid with a/b=0.5 moving parallel to the wall.

	F_∞^t	
	motion parallel to symmetry axis	motion perpendicular to symmetry axis
oblate a/b		
0.1	-0.8525	-0.6133
0.2	-0.8615	-0.6596
0.5	-0.9053	-0.7927
0.8	-0.9606	-0.9189
prolate b/a		
0.8	-0.8408	-0.8784
0.5	-0.6020	-0.6895
0.2	-0.3570	-0.4742
0.1	-0.2647	-0.3812

Table B-1 Force coefficients for a spheroid in an infinite fluid.

	$T^{s}_{2,\infty}$		$T^{r}_{2,\infty}$
	flow parallel to symmetry axis	flow perpendicular to symmetry axis	
oblate a/b			
0.1	-0.8525	-0.008525	-0.4305
0.2	-0.8615	-0.03446	-0.4480
0.5	-0.9053	-0.2263	-0.5658
0.8	-0.9606	-0.6148	-0.7877
prolate b/a			
0.8	-0.8408	-1.313	-1.077
0.5	-0.6020	-2.408	-1.505
0.2	-0.3570	-8.924	-4.640
0.1	-0.2647	-26.47	-13.37

Table 8-2 Torque coefficients for a spheroid in an infinite fluid.

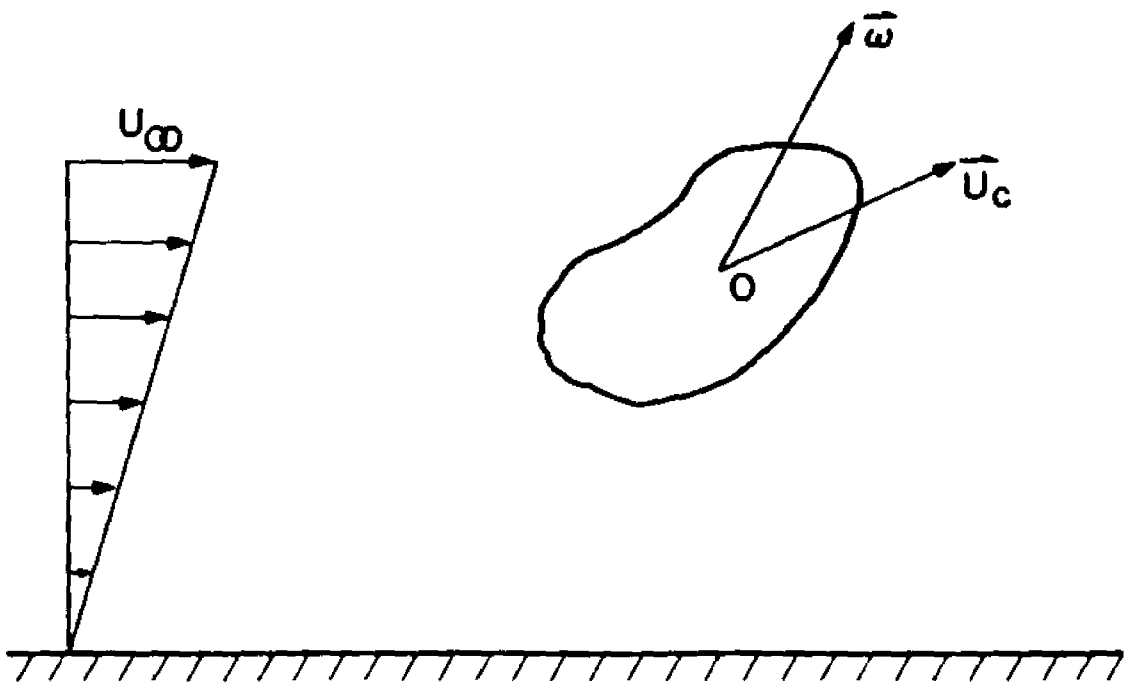

Figure 1. Arbitrary motion of an object of any shape in a shear flow near a planar wall.

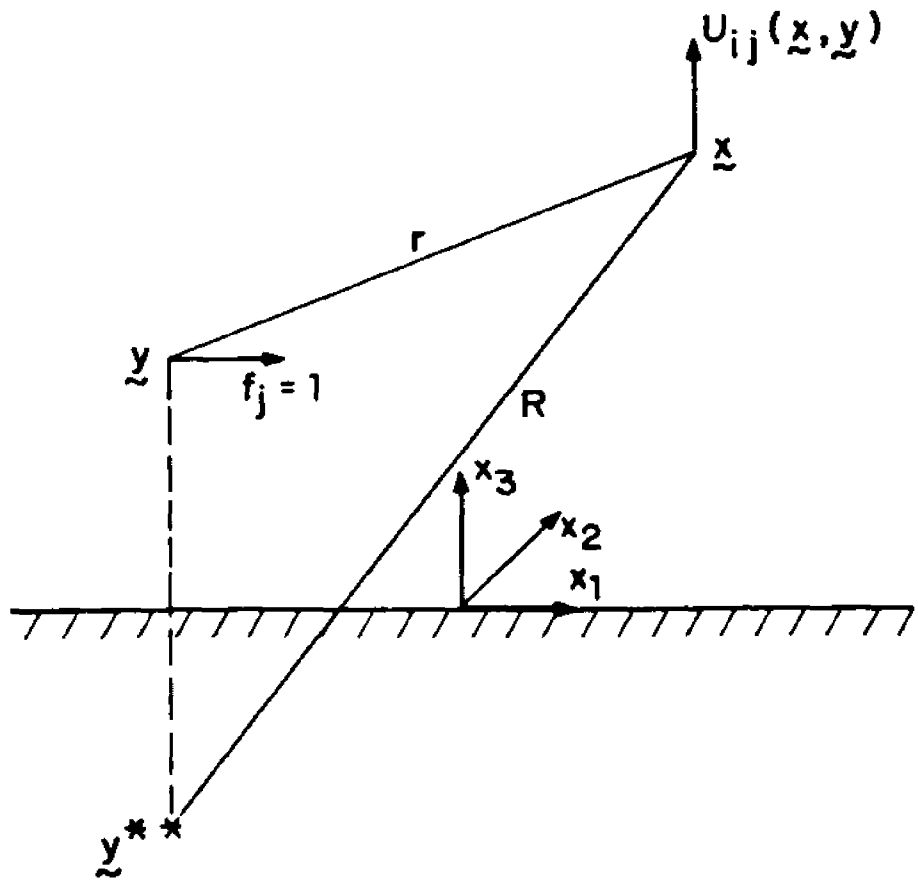

Figure 2. The flow field produced by a stokeslet in the vicinity of a planar wall.

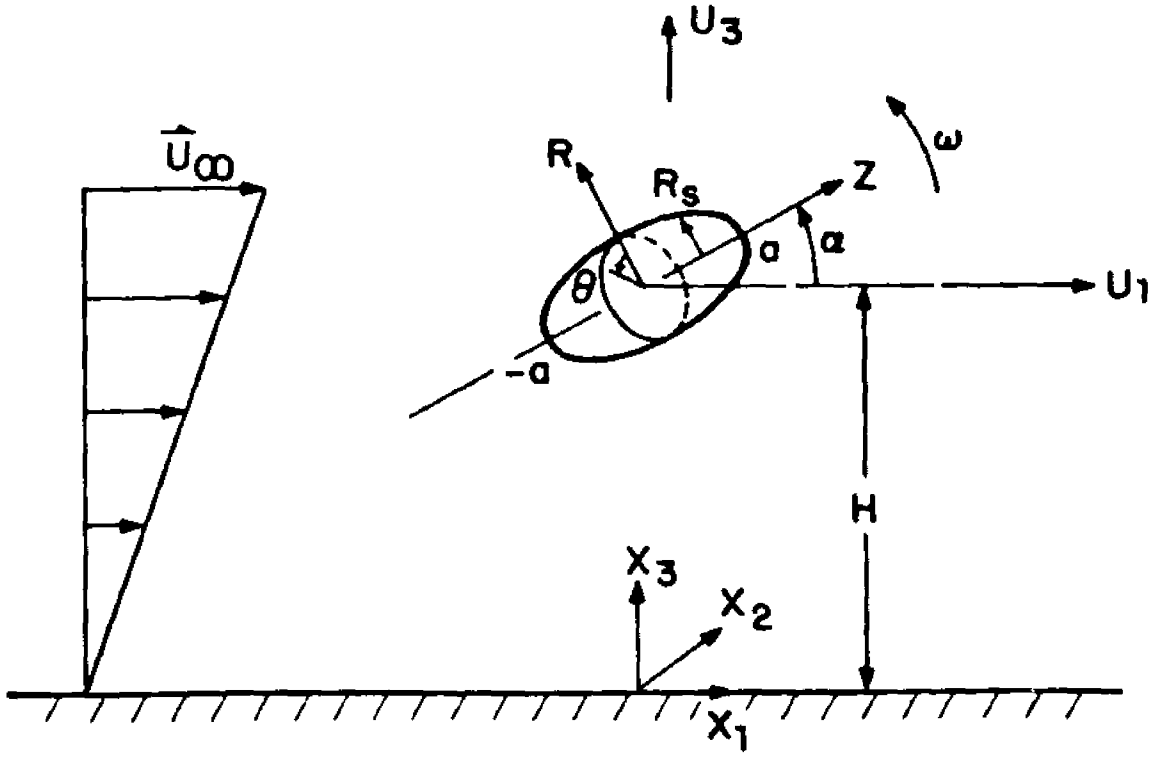

Figure 3. The planar motion of a body of revolution in a shear flow near a planar wall.

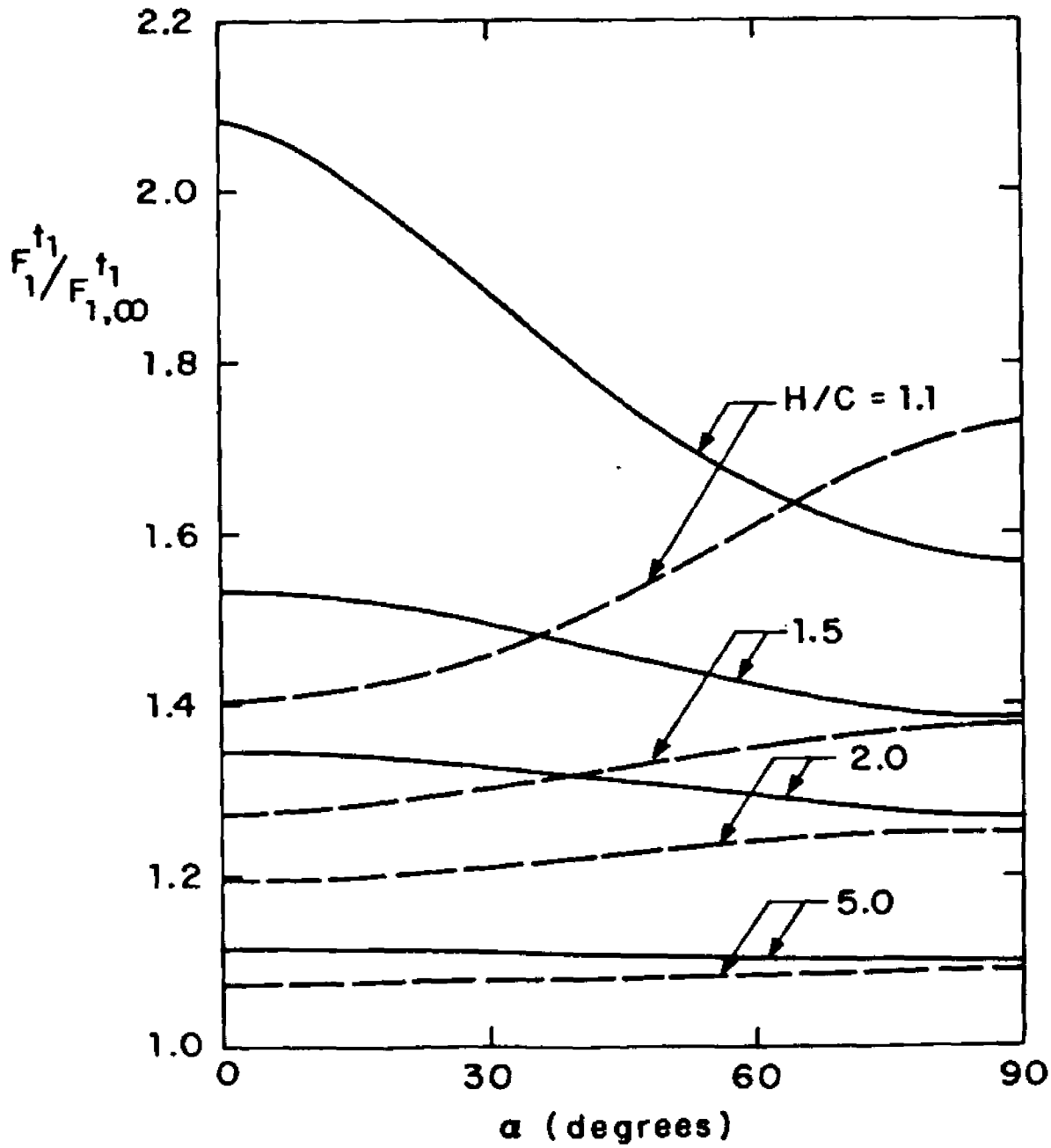

Figure 4a The drag coefficient of an oblate or prolate spheroid having aspect ratio ϵ = 0.5 moving parallel to a wall normalized by the value in an infinite fluid.
(_____ oblate , _ _ _ _ prolate)

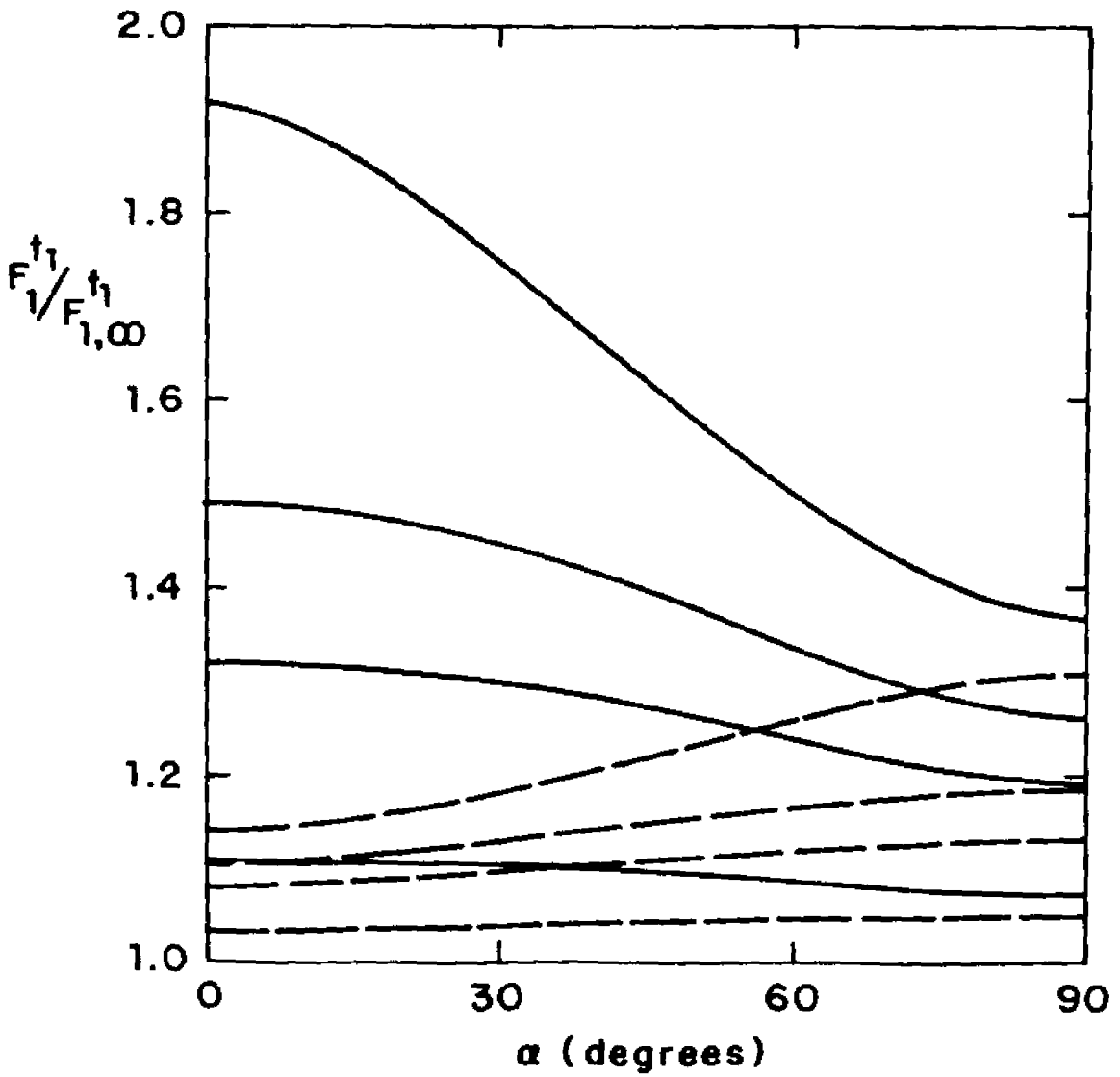

Figure 4b The drag coefficient of an oblate or prolate spheroid having aspect ratio ϵ = 0.1 moving parallel to a wall normalized by the value in an infinite fluid.
(_____ oblate • _ _ _ _ prolate)

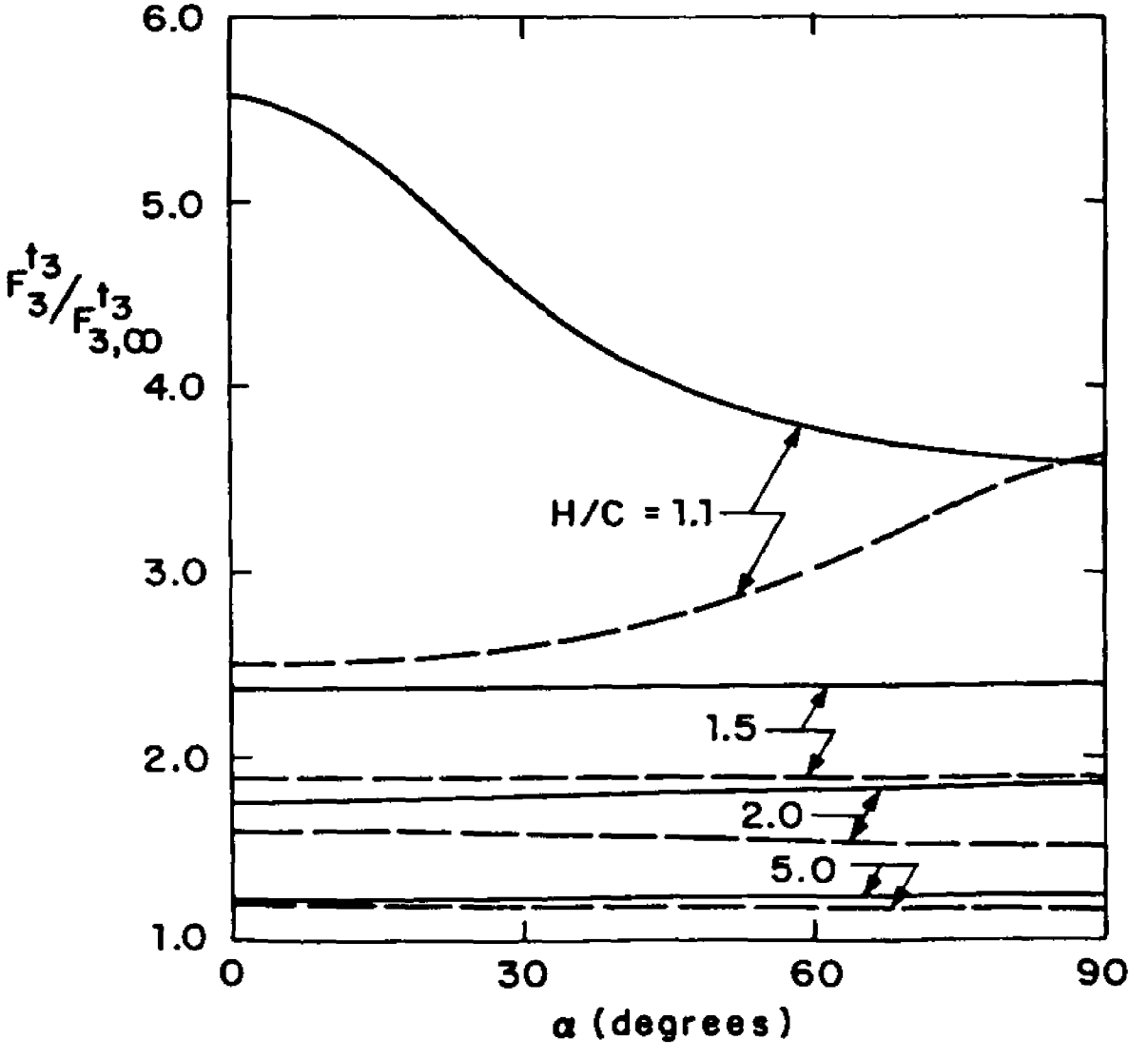

Figure 5a The drag coefficient of an oblate or prolate spheroid having aspect ratio $\epsilon = 0.5$ moving perpendicular to a wall normalized by the value in an infinite fluid.
(_____ oblate , _ _ _ _ prolate)

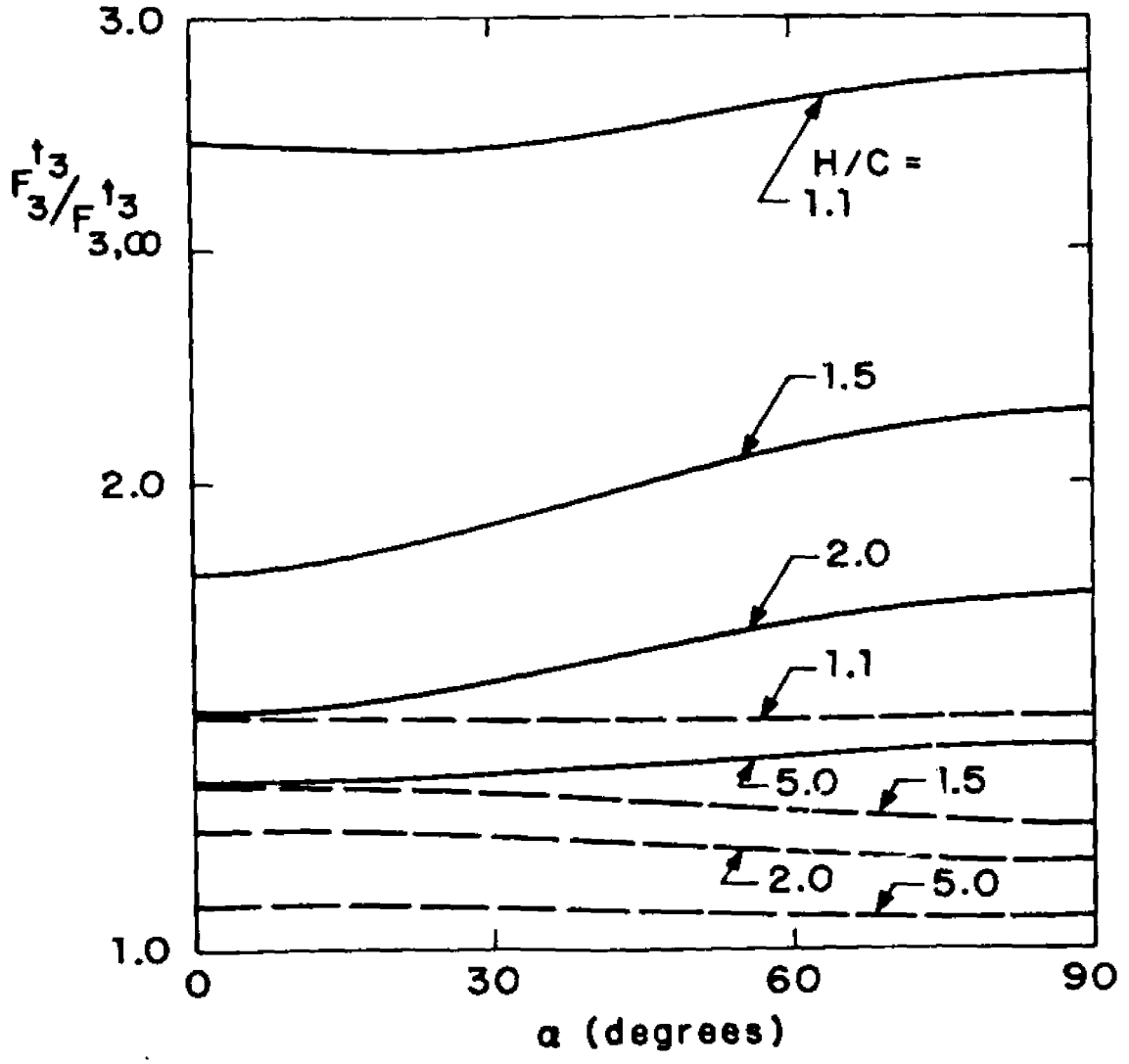

Figure 5b The drag coefficient of an oblate or prolate spheroid having aspect ratio $\epsilon = 0.1$ moving perpendicular to a wall normalized by the value in an infinite fluid.
(_____ oblate , _ _ _ _ prolate)

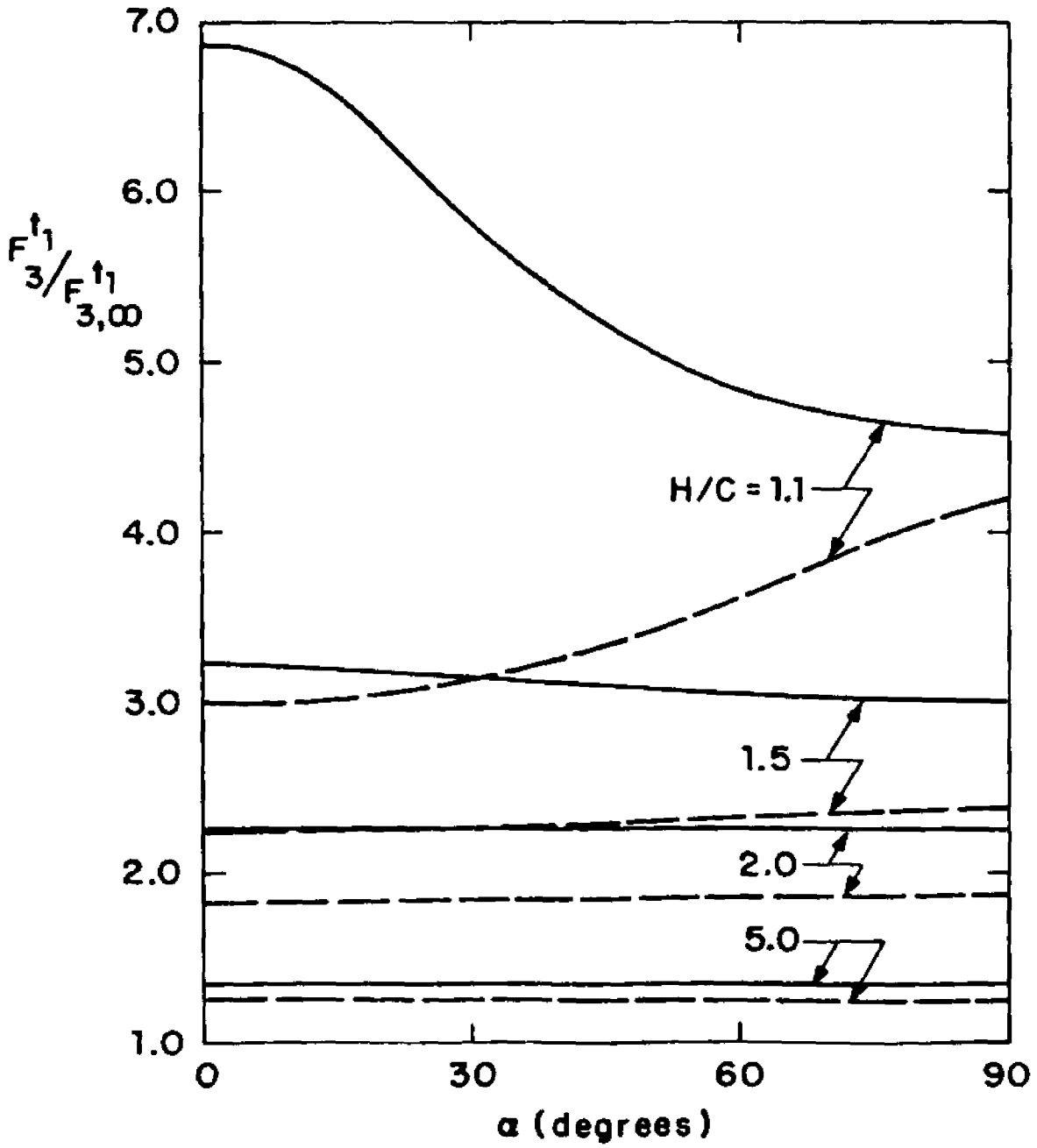

Figure 6a The force perpendicular to the wall on an oblate or prolate spheroid having aspect ratio ϵ =0.5 due to the motion parallel to the wall normalized by the value in an infinite fluid. (_____ oblate • _ _ _ _ prolate)

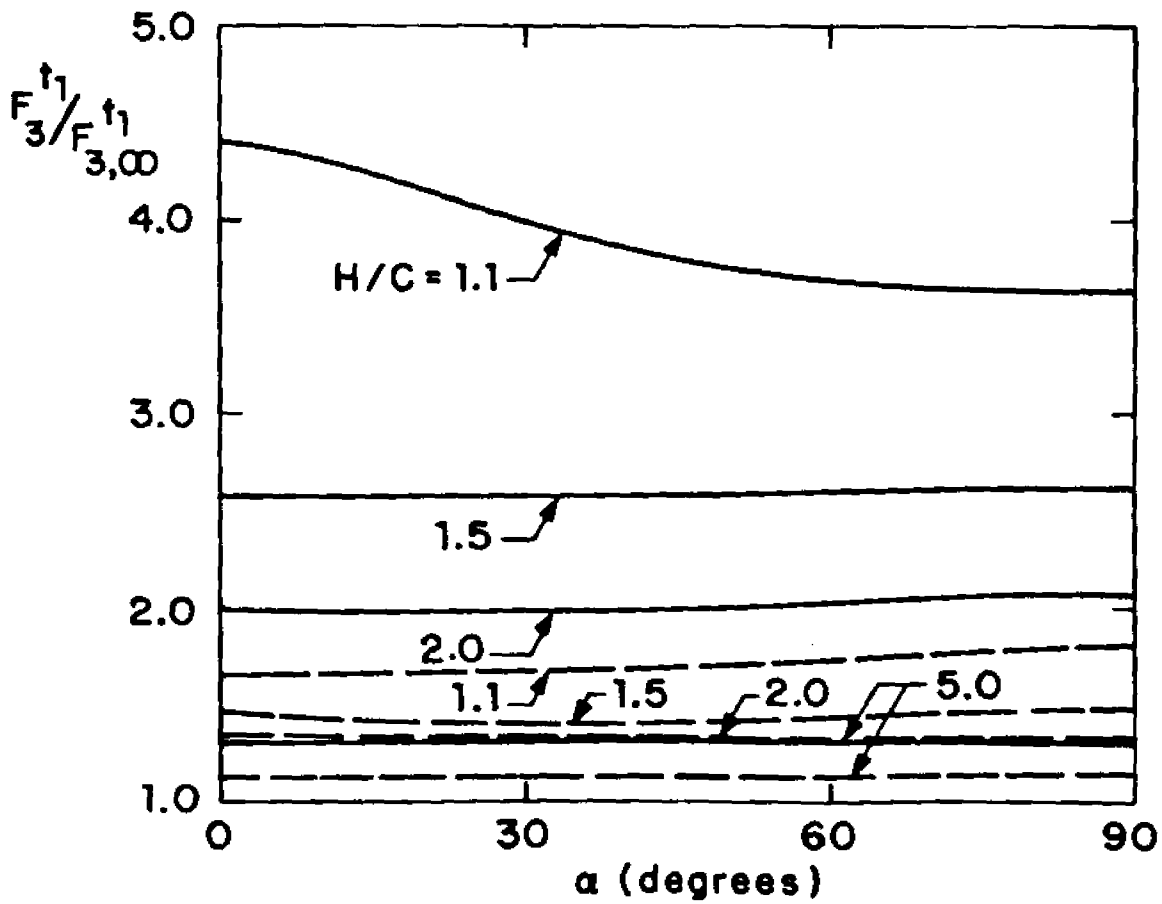

Figure 6b The force perpendicular to the wall on an oblate or prolate spheroid having aspect ratio ϵ =0.1 due to the motion parallel to the wall normalized by the value in an infinite fluid. (_____ oblate , _ _ _ _ prolate)

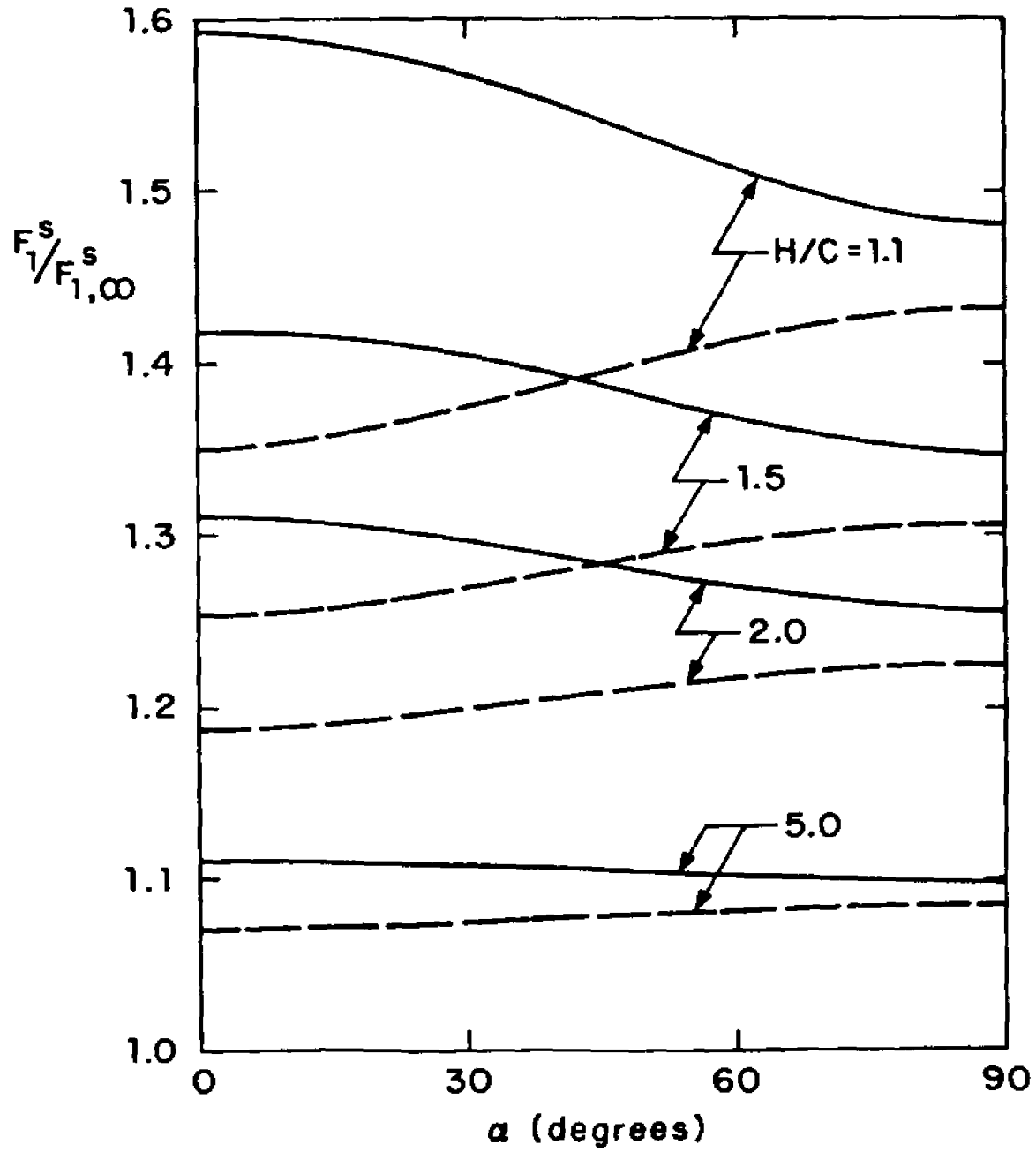

Figure 7a The force coefficient (parallel to the wall) of an oblate or prolate spheroid having aspect ratio $\epsilon = 0.5$, which is rigidly held in a shear flow normalized by the force coefficient of parallel motion in an infinite fluid. (_____ oblate , _ _ _ _ prolate)

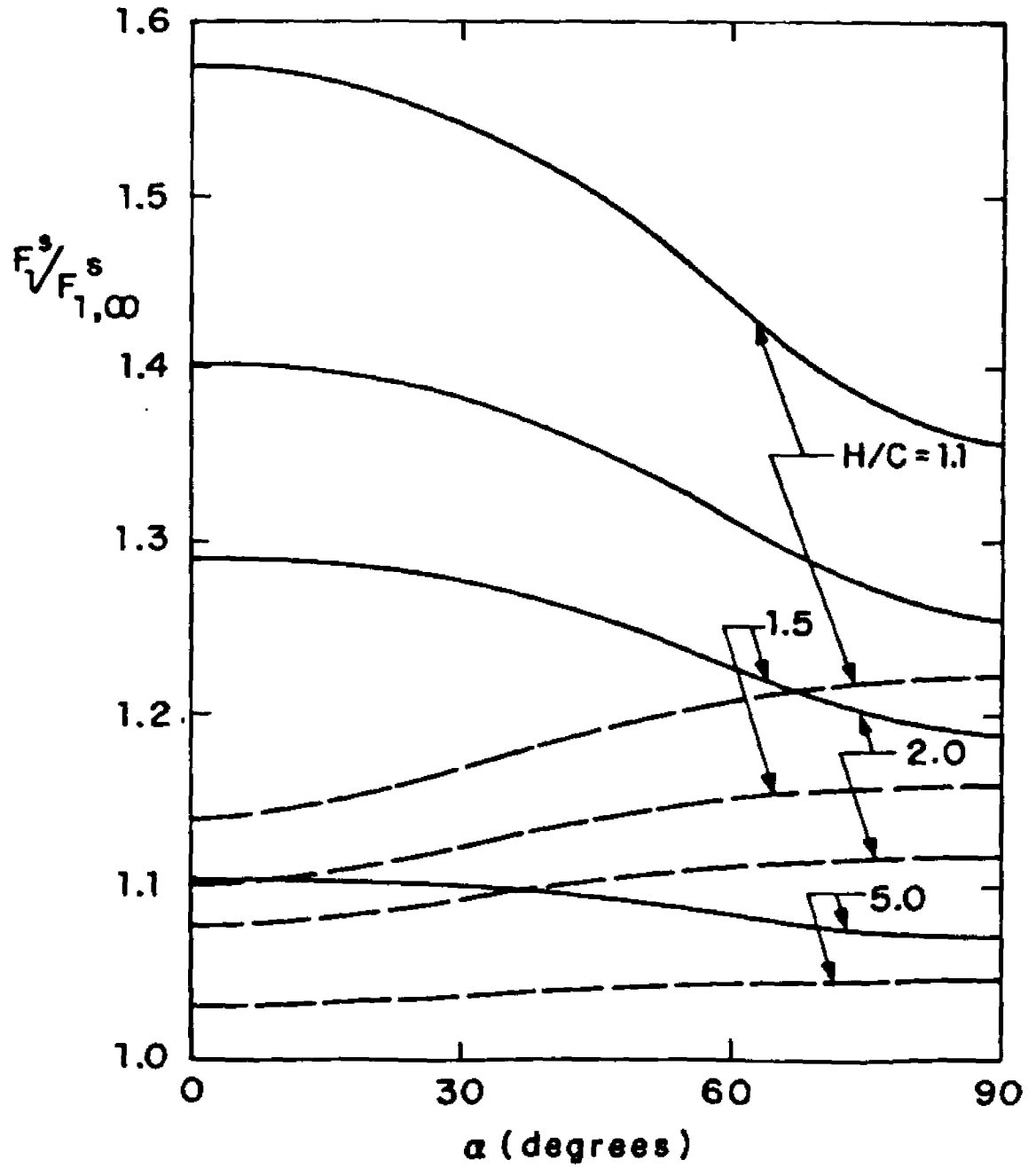

Figure 7b The force coefficient (parallel to the wall) of an oblate or prolate spheroid having aspect ratio $\epsilon = 0.1$, which is rigidly held in a shear flow normalized by the force coefficient of parallel motion in an infinite fluid. (_____ oblate, _ _ _ _ prolate)

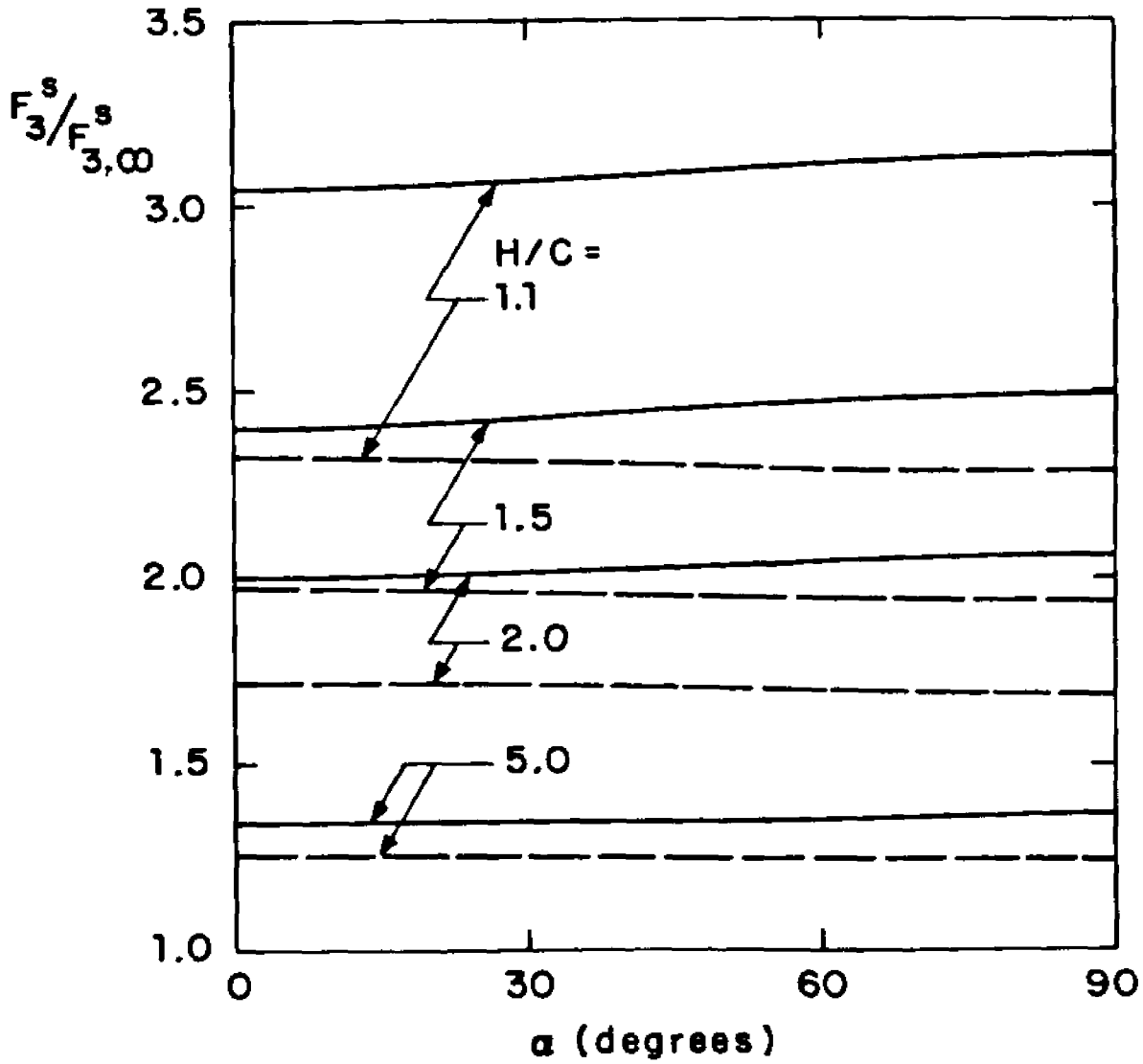

Figure 8a The force coefficient (perpendicular to the wall of an oblate or prolate spheroid having aspect ratio $\epsilon = 0.5$, which is rigidly held in a shear flow normalized by the force coefficient of perpendicular motion in an infinite fluid.
(_____ oblate, _ _ _ _ prolate)

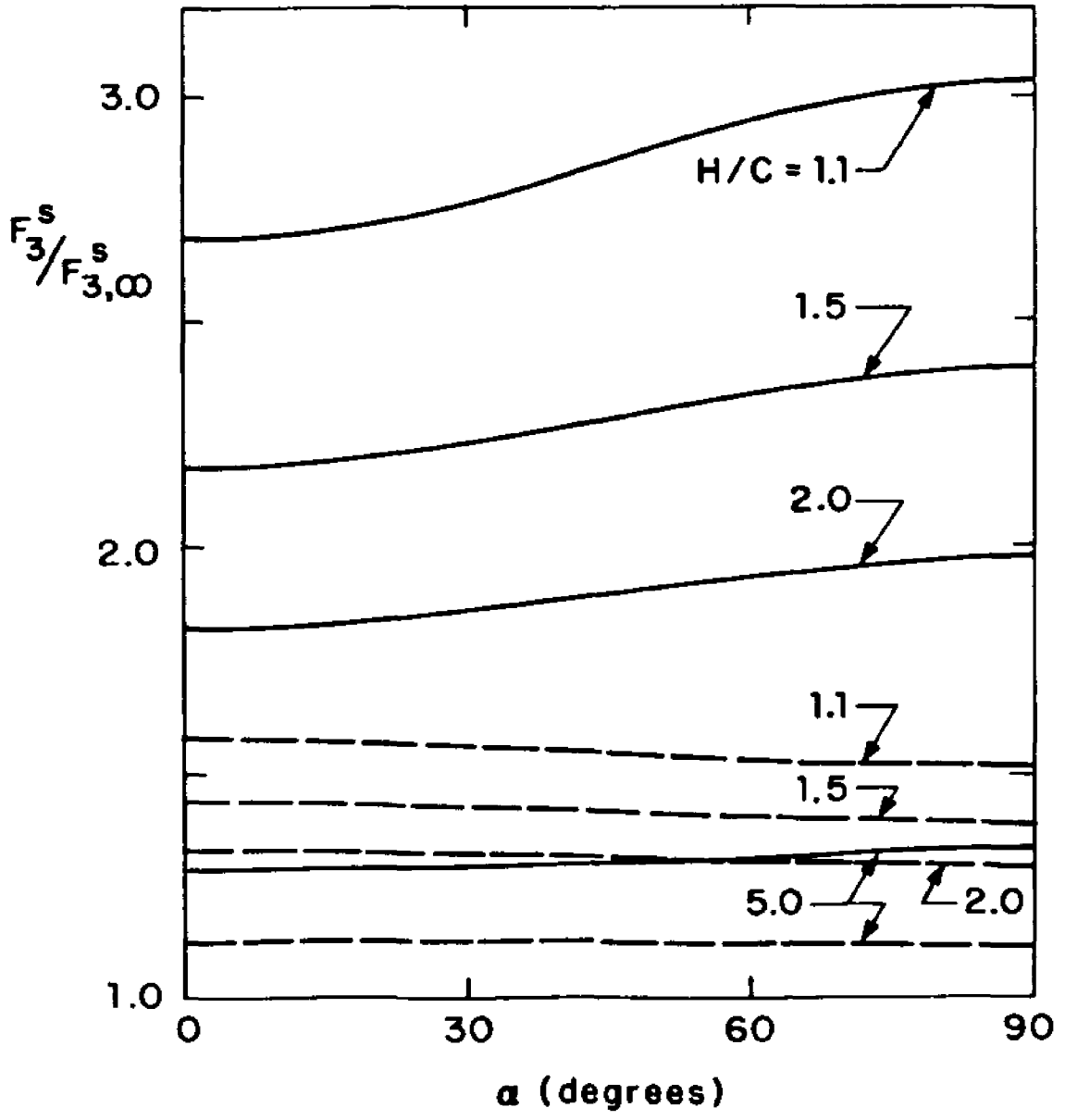

Figure 8b The force coefficient (perpendicular to the wall of an oblate or prolate spheroid having aspect ratio $\epsilon = 0.1$, which is rigidly held in a shear flow normalized by the force coefficient of perpendicular motion in an infinite fluid.
(_____ oblate , _ _ _ _ prolate)

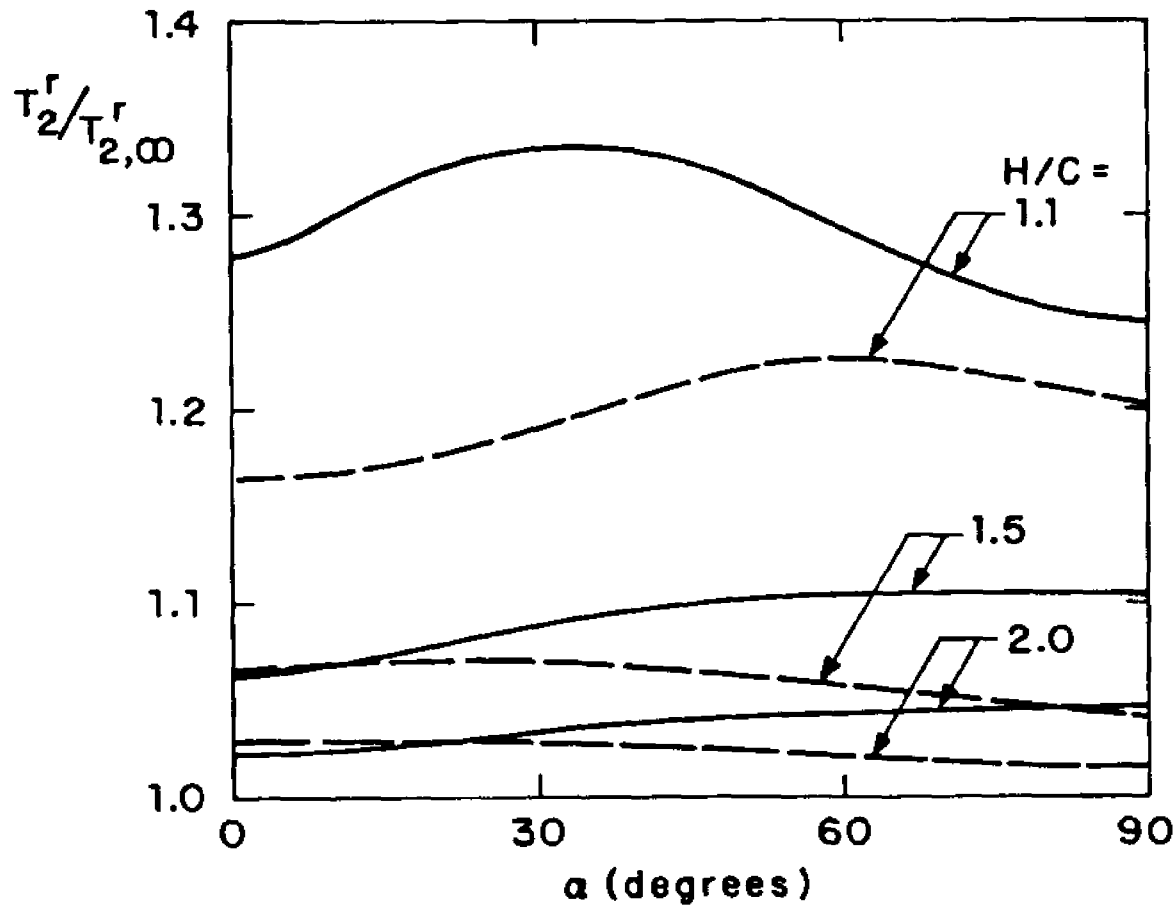

Figure 9a The torque coefficient due to rotation of an oblate or prolate spheroid having aspect ratio ϵ = 0.5 normalized by the value in an infinite fluid.
(_____ oblate , _ _ _ _ prolate)

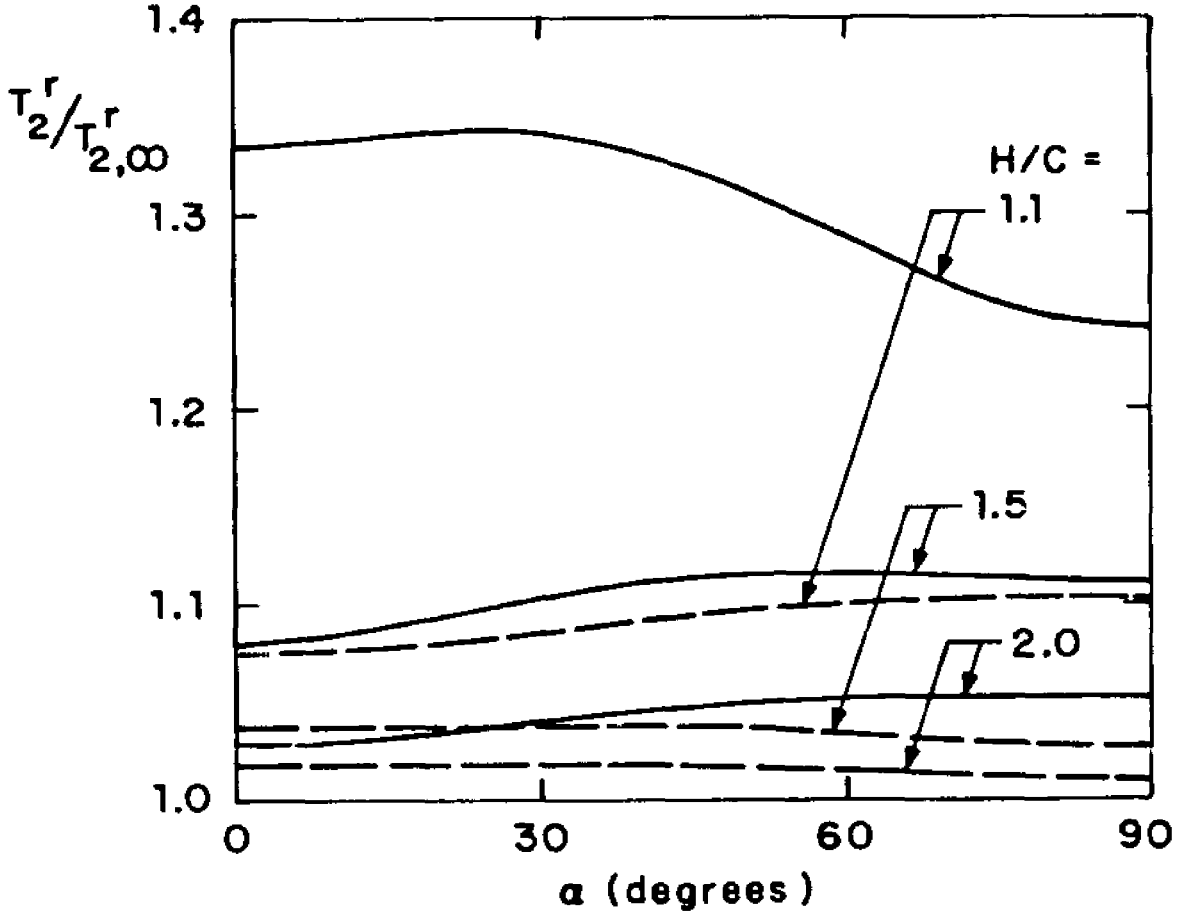

Figure 9b The torque coefficient due to rotation of an oblate or prolate spheroid having aspect ratio ϵ = 0.1 normalized by the value in an infinite fluid.
(_____ oblate , _ _ _ _ prolate)

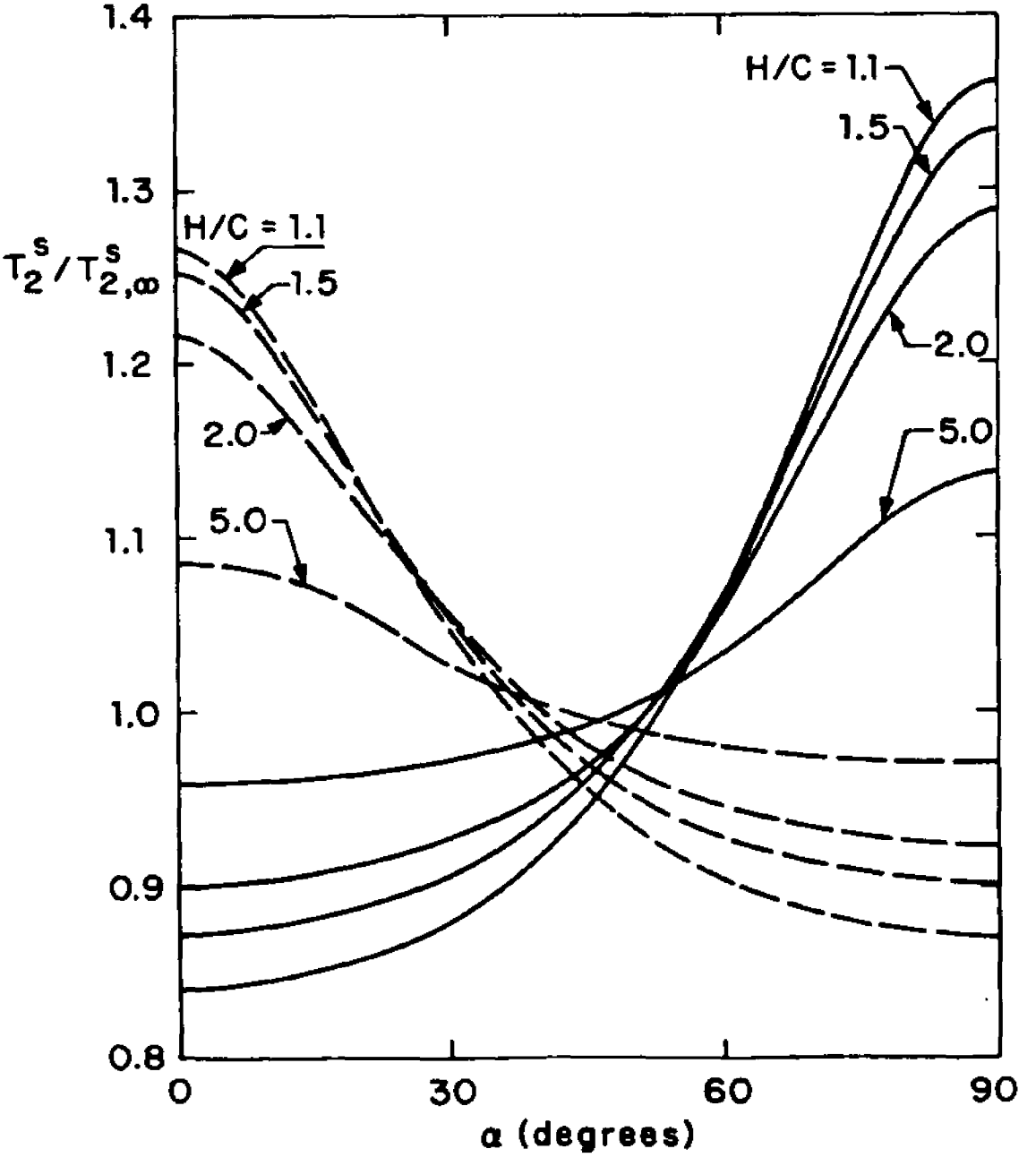

Figure 10a The torque coefficient of an oblate or prolate spheroid having aspect ratio $\epsilon = 0.5$ which is rigidly held in a shear flow normalized by the value in an unbounded shear flow
(_____ oblate, _ _ _ _ prolate)

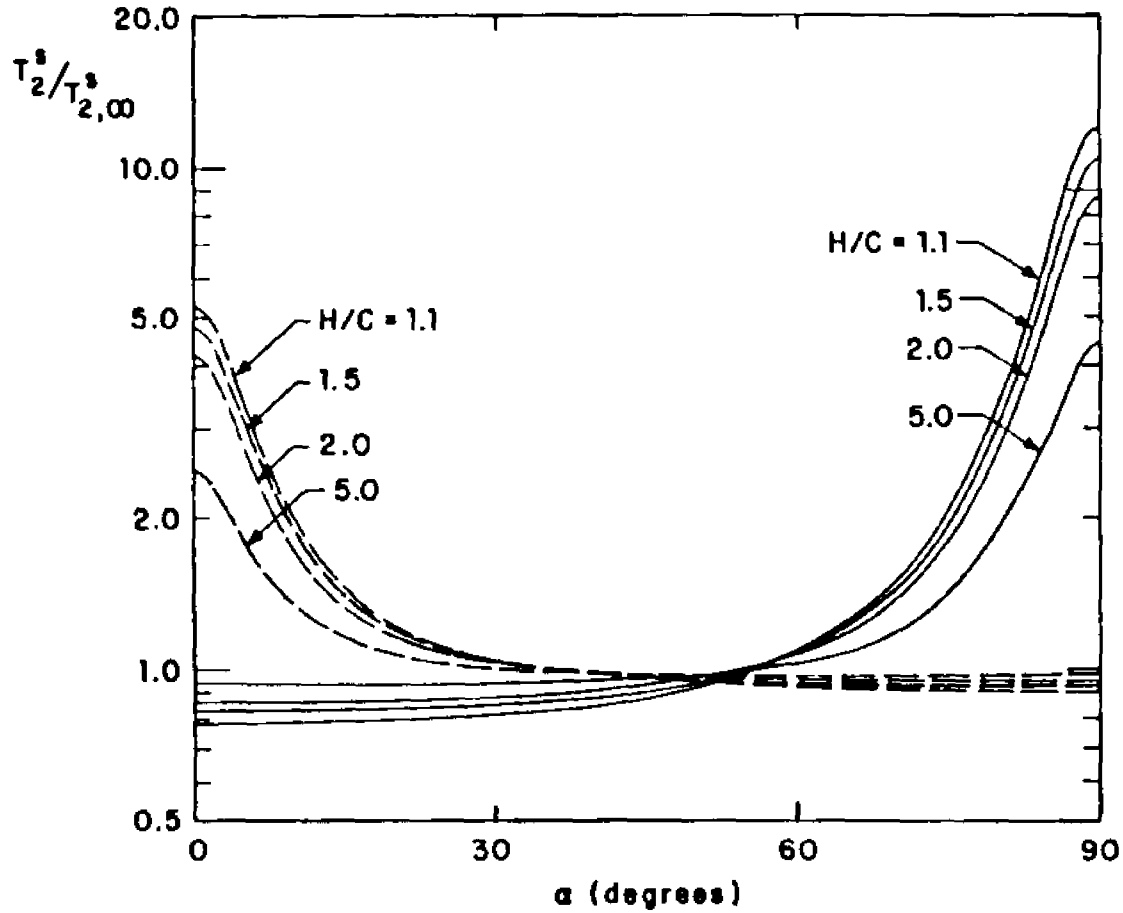

Figure 10b The torque coefficient of an oblate or prolate spheroid having aspect ratio = 0.1 which is rigidly held in a shear flow normalized by the value in an unbounded shear flow
(_____ oblate , _ _ _ _ prolate)

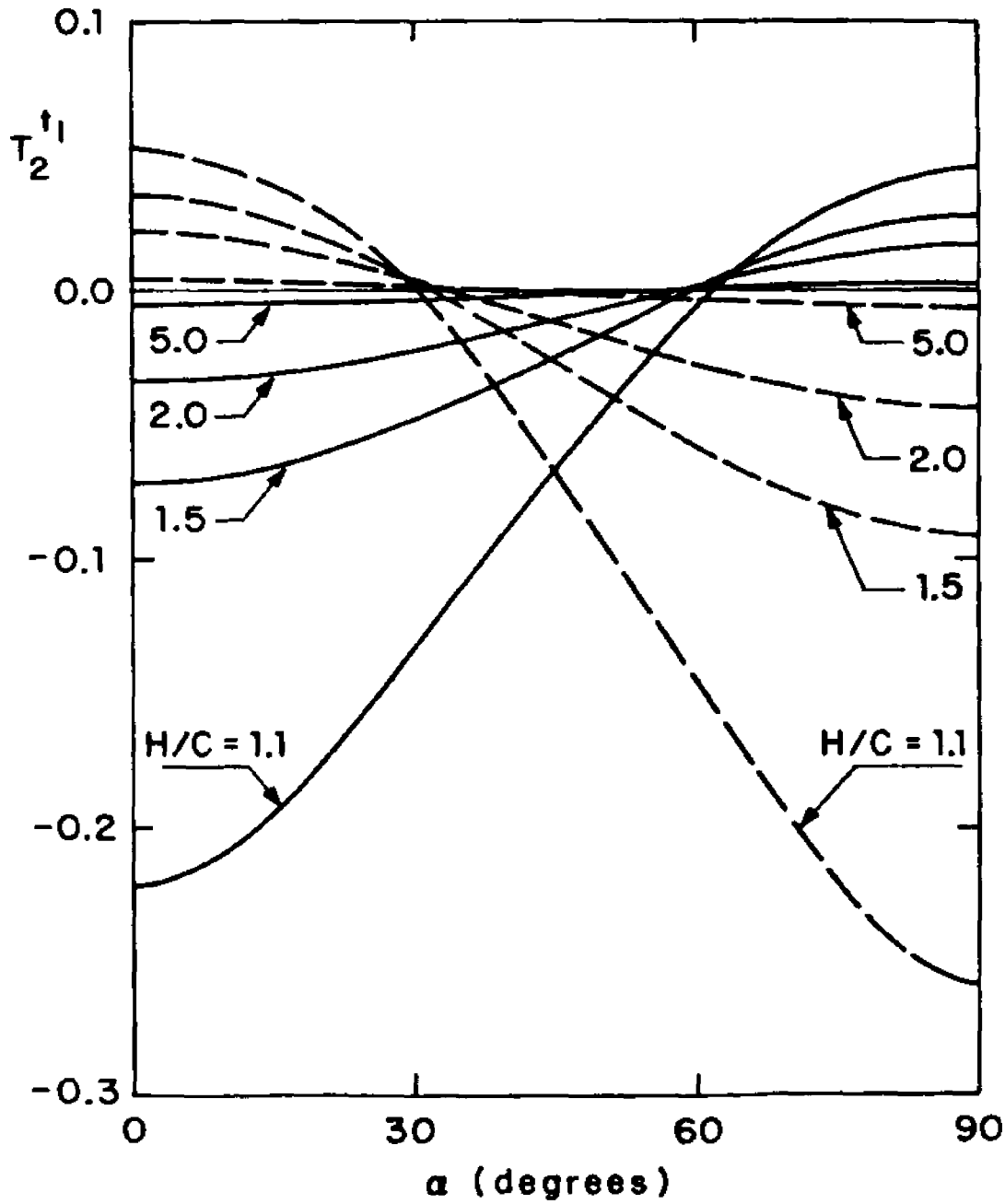

Figure 11a The torque coefficient of an oblate or prolate spheroid having aspect ratio $\epsilon = 0.5$ for motion parallel to the wall.
(_____ oblate • _ _ _ _ prolate)

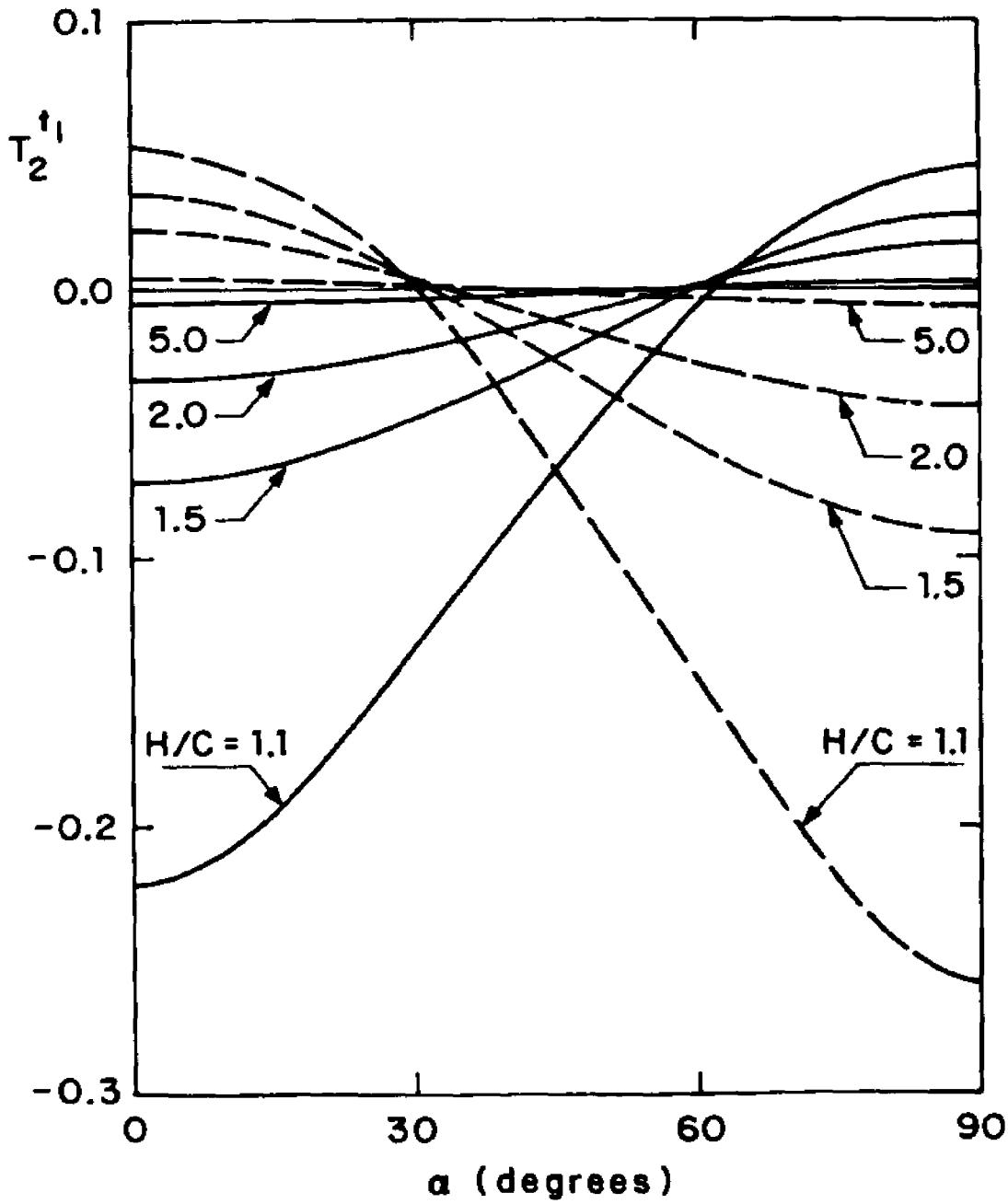

Figure 11b The torque coefficient of an oblate or prolate spheroid having aspect ratio $\epsilon = 0.1$ for motion parallel to the wall.
(_____ oblate , _ _ _ _ prolate)

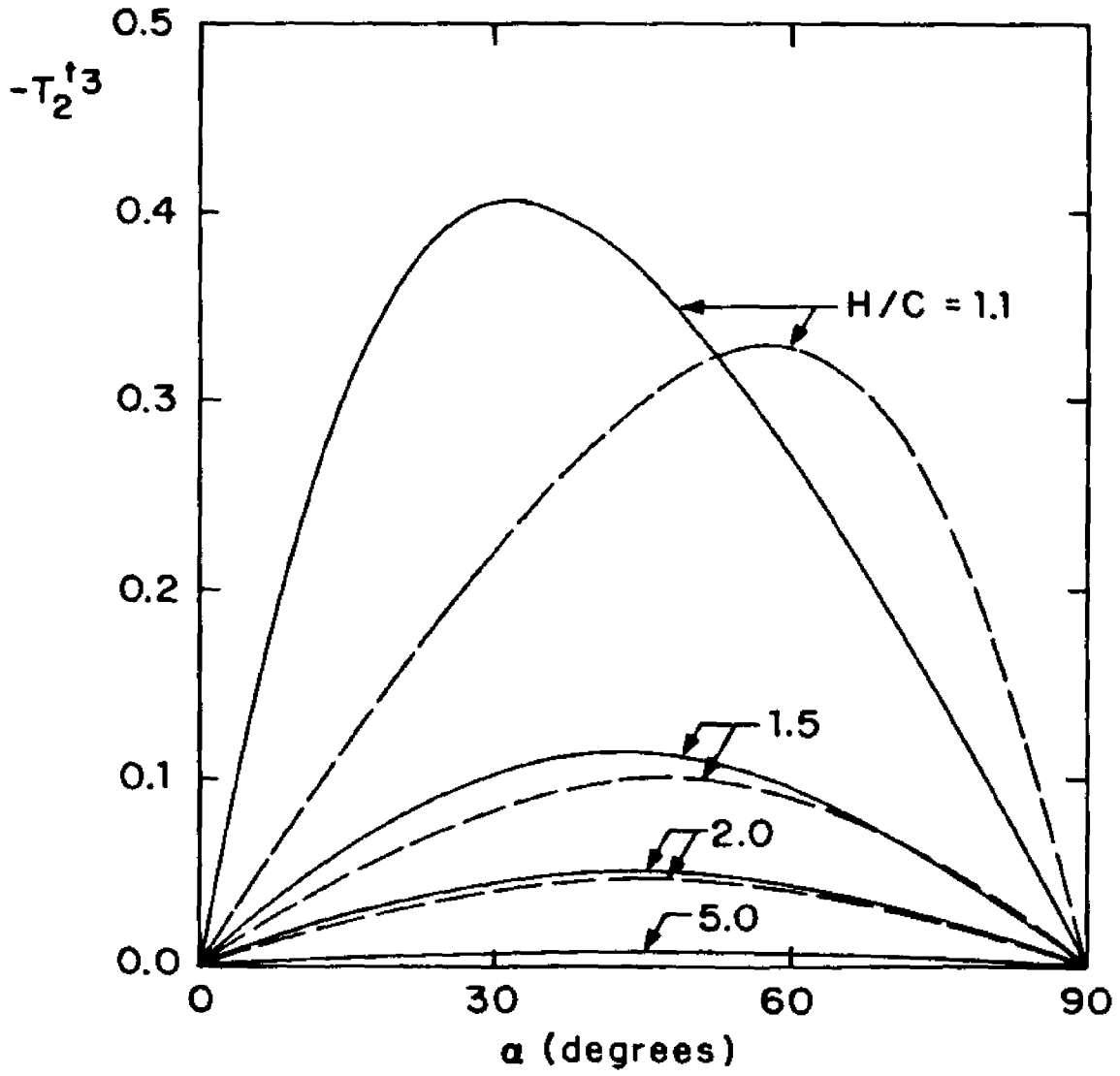

Figure 12a The torque coefficient of an oblate or prolate spheroid having aspect ratio $\epsilon = 0.5$ for motion perpendicular to the wall.
(_____ oblate , _ _ _ _ prolate)

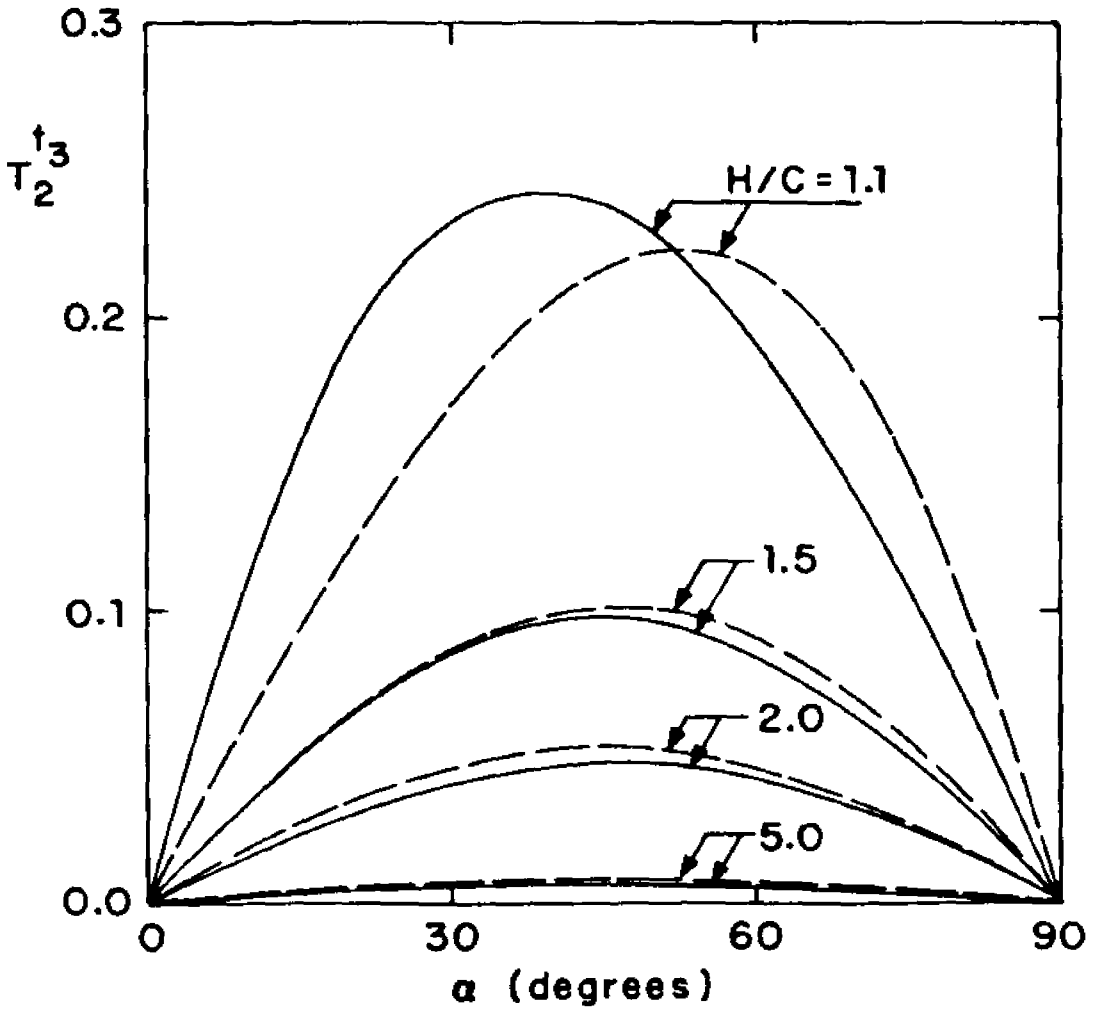

Figure 12b The torque coefficient of an oblate or prolate spheroid having aspect ratio $\epsilon = 0.1$ for motion perpendicular to the wall.
(_____ oblate , _ _ _ _ prolate)

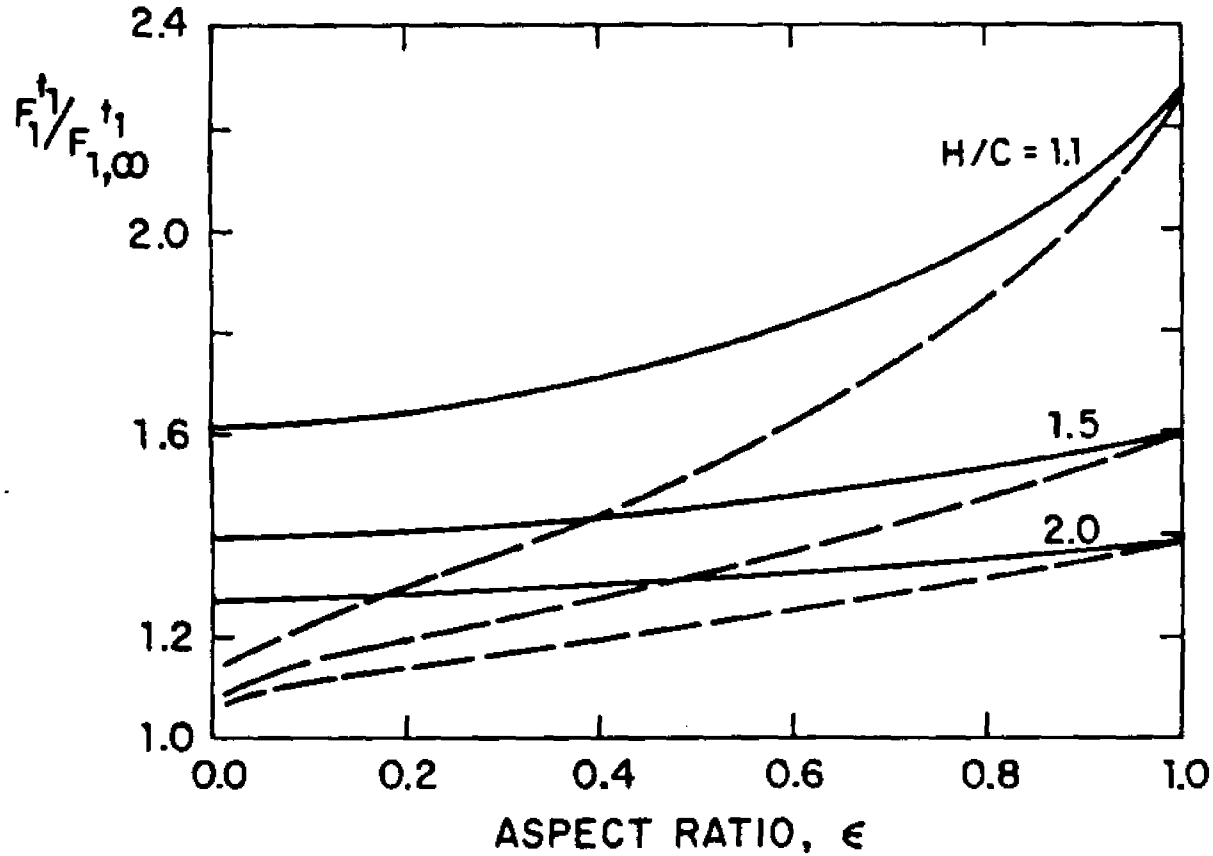

Figure 13a The ratio of resistance coefficients $F_1^{t_1}/F_{1,\infty}^{t_1}$ as a function of aspect ratio ϵ for various of values of H/c .
(_____ oblate , _ _ _ _ prolate)

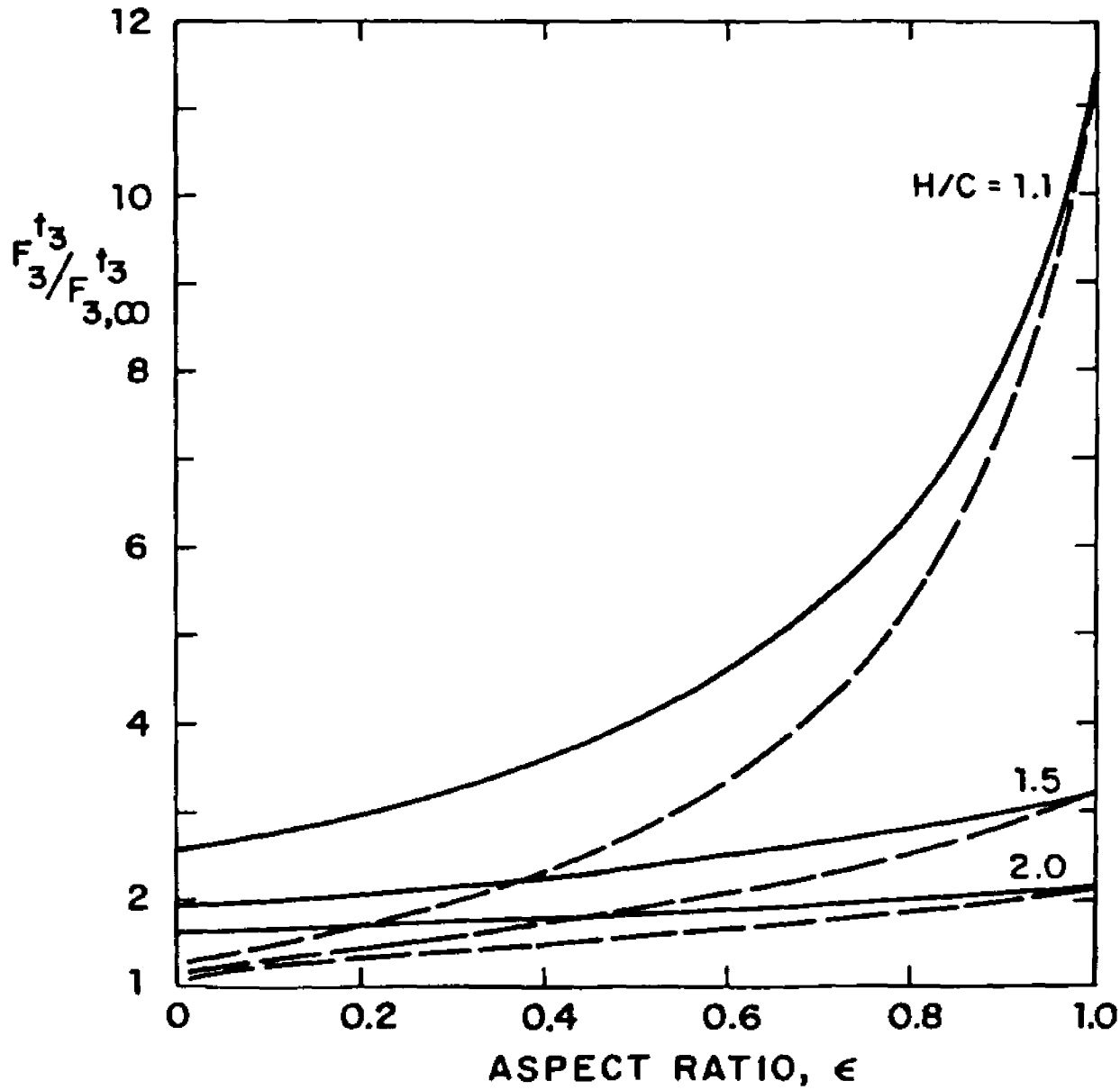

Figure 13b The ratio of resistance coefficients $F_3^{t_3}/F_3^{t_3}$ as a function of aspect ratio ϵ for various of values of H/c .
(_____ oblate , _ _ _ _ prolate)

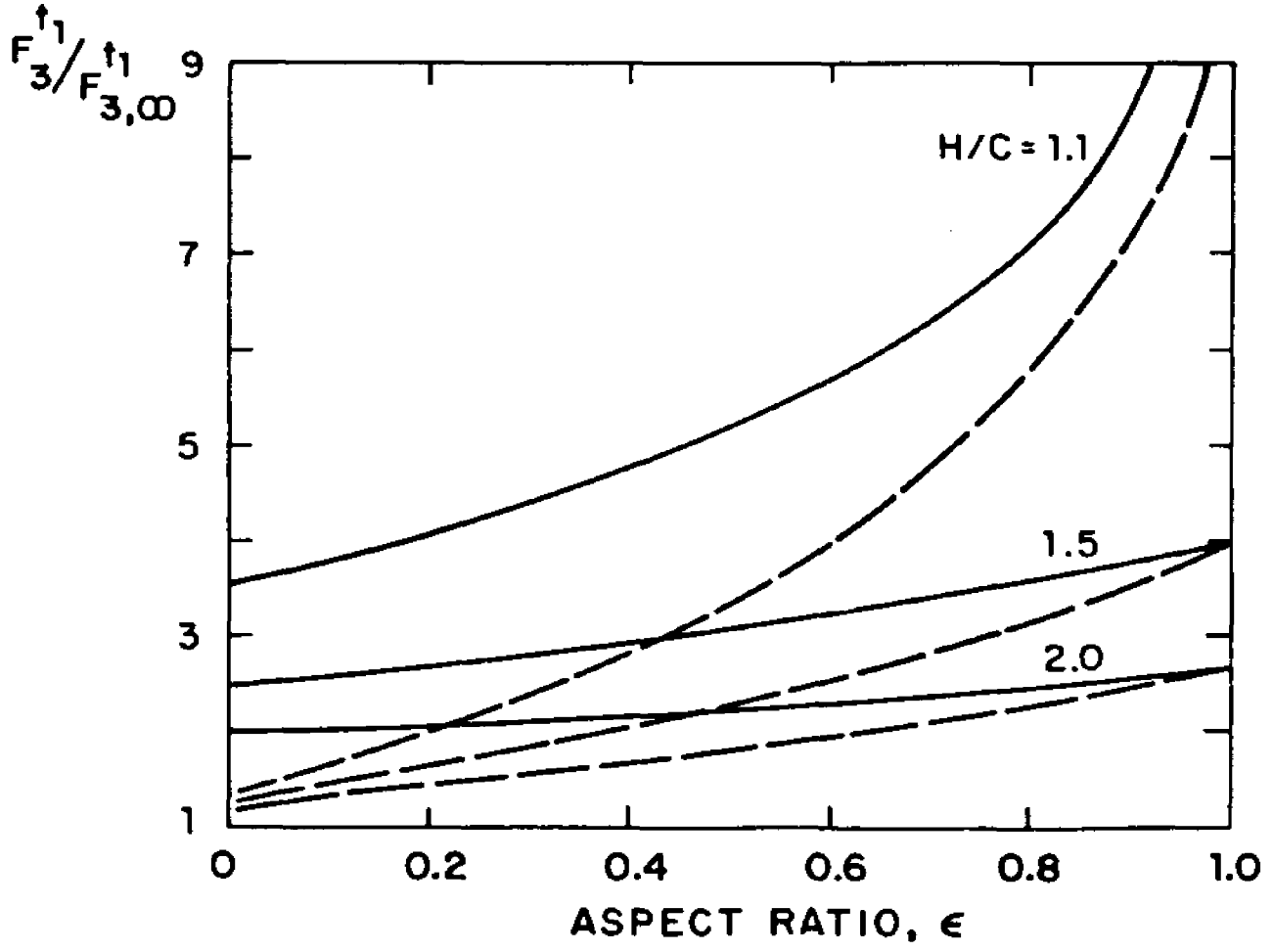

Figure 13c The ratio of resistance coefficients $F_3^{\dagger_1}/F_{3,\infty}^{\dagger_1}$ as a function of aspect ratio ϵ for various of values of H/c .
(_____ oblate , _ _ _ _ prolate)

CHAPTER 2

THE MOTION OF A TORUS AND BICONCAVE SHAPED DISC ADJACENT TO A PLANAR WALL AT LOW REYNOLDS NUMBER

Abstract

The boundary integral method presented in chapter 1 is modified to obtain solutions for the motion of a toroidal particle or a biconcave shaped disc adjacent to a planar wall at low Reynolds number. The coincidence of the drag and torque of a biconcave shaped body and a torus having aspect ratio b/a=2 with the same surface area shows that in this case the hole of a torus has little influence on the flow field. On the other hand, for an aspect ratio b/a=10, the effect of the hole is significant. It is also shown that when the body is not very close to the wall, an oblate spheroid can be used as a good approximation of a biconcave shaped disc.

1. Introduction

In chapter 1 the boundary integral method has been applied to the motion of a body of revolution adjacent to a planar wall at low Reynolds number. The singular solution of the Stokes equation in the presence of a planar wall was used to formulate the integral equations. The shape of the body of revolution was represented by a single-valued function $R = R_s(Z)$, where z is the coordinate along the body axis. The densities of the stokeslets were represented by a double series and the surface integrals were reduced to double integrals in the z direction and the azimuthal direction. The integration in the azimuthal direction was performed analytically and that in the z direction was performed numerically. The no-slip boundary conditions were applied at discrete collocation points on the surface of the body and the integral equations were reduced to a system of linear equations for the unknown coefficients of the double series representation of the stokeslet density.

In this chapter the theory developed in chapter 1 is modified to deal with another kind of body of revolution, for which the shape $R = R_s(z)$ is a double-valued function such as with biconcave shaped bodies and toroidal particles.

The biconcave shaped disc is a good approximation of the shape of an undeformed red blood cell. Despite the importance of red blood cells in microcirculatory flow, very little work involving biconcave shaped discs has been done.

Skalak, Chen and Chien (1977) solved the problem of an infinite periodic array of biconcave shaped bodies in a circular tube using the finite element method.

The interest in studying the motion of a toroidal particle partly lies in that some important biological macromolecules, such as low molecular weight circular DNA and acetylcholine receptor, are approximately toroidal in shape.

The creeping motion of a toroidal particle has previously been solved only in an unbounded flow field. Kanwal (1961) solved for rotation about the symmetry axis, Payne & Pell (1960) and Majumdar & O'Neill (1977) solved for translation along the symmetry axis, Goren & O'Neill obtained solutions for translation normal to the symmetry axis and rotation about an axis normal to the symmetry axis. All of the above solutions are exact.

2. Solution for the motion of a torus near a planar wall

The creeping motion of a torus in a viscous fluid near an infinite planar wall is illustrated in figure 1. The particle has a translational velocity $\vec{U}_o$ and is rotating with an angular velocity ω. $\vec{U}_\infty$ represents the undisturbed simple shear flow.

Let $\vec{V}_1$ represent the flow field and define $\vec{V} = \vec{V}_1 - \vec{V}_\infty$. The governing equations for $\vec{V}$ are:

$$\mu \nabla^2 \vec{V} = \nabla P \tag{1a}$$

$$\nabla \cdot \vec{V} = 0 \tag{1b}$$

subject to the following boundary conditions:

$$\vec{V} = \vec{U}_p \equiv \vec{U}_o + \vec{\omega} \times \vec{\rho} - \vec{U}_\infty \quad \text{at the particle surface} \tag{2a}$$

$$\vec{V} = 0 \quad \text{at the wall} \tag{2b}$$

$$\vec{V} = 0 \ , \ P = 0 \quad \text{at infinity} \tag{2c}$$

where $\vec{\rho}$ is the position vector whose origin is at the particle center.

The boundary value problem posed by equations (1)-(2) has been formulated in chapter 1 by the following integral equation:

$$\begin{aligned} v_i(\underline{y}) = \frac{1}{4\pi\mu} \iint_{S_p} \Big\{ &\left(\frac{1}{r} - \frac{1}{r^*}\right) - \left(\frac{r_i r_k}{r^3} - \frac{r_i^* r_k^*}{r^{*3}}\right) \\ &+ 2y_3 \left(\delta_{i\alpha}\delta_{\alpha\ell} - \delta_{i3}\delta_{3\ell}\right)\left(\frac{3x_3 r_i^* r_k^*}{r^{*5}} - \frac{x_3}{r^{*3}}\delta_{ik} + \frac{r_i^*}{r^{*3}}\delta_{k3} - \frac{r_k^*}{r^{*3}}\delta_{i3}\right)\Big\} \cdot \\ &\cdot f_k(\underline{x})\, dS_{\underline{x}} - \frac{3}{2\pi\mu} \iint_{S_p} \Big\{ \frac{r_i r_j r_k}{r^5} - \frac{r_i^* r_j^* r_k^*}{r^{*5}} - 2y_3\left(\delta_{i\alpha}\delta_{\alpha\ell} - \delta_{i3}\delta_{3\ell}\right) \cdot \\ &\cdot \left(\frac{-5x_3 r_i^* r_j^* r_k^*}{r^{*7}} + \frac{r_j^* r_k^*}{r^{*5}}\delta_{i3} + \frac{x_3 r_i^*}{r^{*5}}\delta_{ik} + \frac{x_3 r_k^*}{r^{*5}}\delta_{ij} - \frac{y_3 r_i^*}{r^{*5}}\delta_{jk}\right)\Big\} u_k(\underline{x}) n_j(\underline{x})\, dS_{\underline{x}} \end{aligned} \tag{3}$$

where $\underset{\sim}{x} = (x_1, x_2, x_3)$, $\underset{\sim}{y} = (y_1, y_2, y_3)$, $\underset{\sim}{r} = (x_1 - y_1, x_2 - y_2, x_3 - y_3)$, $\underset{\sim}{r}^* = (x_1 - y_1, x_2 - y_2, x_3 + y_3)$, f_K is the unknown stokeslet density function, v_K is the flow velocity, S_p is the subject surface and n_j is its inward normal. The integral equation (3) will be solved by the boundary collocation method for the unknown stokeslet density function f_K as done in chapter 1 for a spheroid.

As in chapter 1 a cylindrical coordinate system (R, θ, Z) is used to treat a body of revolution, where the Z axis lies along the particle axis of symmetry. In this chapter we consider a body of revolution whose shape R_S is a multivalued function of Z. We choose a suitable parameter η so that both R_S and Z are related to it by a single-valued function. For the case of a torus:

$$R_S = b + a \sin \eta \qquad (5a)$$

$$0 \le \eta < 2\pi$$

$$Z = a \cdot \cos \eta \qquad (5b)$$

The outside portion of the torus is represented by varying η from 0° to 180° while the inside portion by varying η from 180° to 360°. The stokeslet density functions for motion having planar symmetry are represented by the double Fourier series:

$$\begin{aligned} f_1 &= \sum_{m=0}^{\infty} \left\{ A_{1,m,0} + \sum_{n=1}^{\infty} (A_{1,m,n} \cos n\eta + B_{1,m,n} \sin n\eta) \right\} \cos m\theta \\ f_2 &= \sum_{m=1}^{\infty} \left\{ A_{2,m,0} + \sum_{n=1}^{\infty} (A_{2,m,n} \cos n\eta + B_{2,m,n} \sin n\eta) \right\} \sin m\theta \\ f_3 &= \sum_{m=0}^{\infty} \left\{ A_{3,m,0} + \sum_{n=1}^{\infty} (A_{3,m,n} \cos n\eta + B_{3,m,n} \sin n\eta) \right\} \cos m\theta \end{aligned} \qquad (6)$$

Substituting (5a,b) and (6) into the integral equation (3), all integrals can be performed with respect to the variables θ and γ. The integration along θ direction is performed analytically in the same way as in chapter 1 for a sphere. The integral in the γ direction is performed numerically. After the coefficients $A_{K,m,n}$ and $B_{K,m,n}$ are solved the drag and torque on the particle can be found to be:

$$F_K = 2\pi^2 a\,(2b A_{K,0,0} + a B_{K,0,1}) \qquad K = 1 \text{ and } 3 \tag{7}$$

$$\begin{aligned} T_2 = \pi^2 \{ & -(a^2+2b^2)(A_{1,1,0}\cos\alpha + A_{3,1,0}\sin\alpha) \\ & + 2ab[(A_{3,0,1} - B_{1,1,1})\cos\alpha - (A_{1,0,1} + B_{3,1,1})\sin\alpha] \\ & + a^2[(\tfrac{1}{2}A_{1,1,2} + B_{3,0,2})\cos\alpha + (\tfrac{1}{2}A_{3,1,2} + B_{3,0,2})\sin\alpha]\} \end{aligned} \tag{8}$$

The hydrodynamic force coefficients are defined as follows:

$$\begin{pmatrix} F_1 \\ F_3 \\ T_2 \end{pmatrix} = 6\pi\mu c \begin{pmatrix} F_1^{t_1} & F_1^{t_3} & F_1^{r} & HF_1^{s} \\ F_3^{t_1} & F_3^{t_3} & F_3^{r} & HF_3^{s} \\ \frac{4}{3}cT_2^{t_1} & \frac{4}{3}cT_2^{t_3} & \frac{4}{3}cT_2^{r} & \frac{4}{3}c^2T_2^{s} \end{pmatrix} \begin{pmatrix} U_1 \\ U_3 \\ c\omega \\ S \end{pmatrix} \tag{9}$$

where $c=a+b$ is the outer radius of the torus.

The force and torque coefficients for the translational and rotational motion of a torus in an otherwise unbounded quiescent fluid are listed in Goren & O'Neill (1980). For reference the force and torque coefficients for a torus with b/a = 2 and 10 are listed in table 1. These values are also calculated using the present boundary integral method and

are found to be in full agreement with the exact solution. To the best of the author's knowledge the torque coefficient for a torus in an unbounded shear flow has not previously been computed. The values of this coefficient presented in table 1 have been calculated using the present theory.

When the axis of symmetry is perpendicular to the wall the coefficient matrix in equation (3) is independent of β and only one-dimensional collocation is needed as illustrated in chapter I for a sphere. The collocation points, each of which represents a ring on the particle surface on which the no-slip boundary conditions are exactly satisfied, are chosen by specifying equally spaced values of γ in the range between the range 0° and 360°. Tables 2 - 4 show convergence tests for the coefficients $F_3^{t_3}$, $F_1^{t_1}$ and T_2^r for a torus having b/a = 2 and 10. The values of the coefficients in an infinite fluid rapidly converge to the exact solutions using only 8 collocation points. As expected more collocation points are needed to get the same accuracy when the particle is close to the wall. Convergence is somewhat slower for b/a=2 than for b/a=10. In the worst case tested (b/a=2, H/c=0.5) only 14 collocation points are required to achieve four digit accuracy for all the force and torque coefficients.

When the torus is arbitrarily oriented relative to the wall, the general two-dimensional collocation is needed. The collocation points are placed at equally spaced values

of γ between 0° and 360°. A constant value of γ represents a ring on the particle surface. At each ring the points are equally spaced between $\beta = 0^\circ$ and 180°. Convergence tests of the coefficients $F_3^{t_3}$, T_2^r and $T_2^{t_1}$ for a torus inclined at 30° with respect to the wall are shown in tables 5 - 7. The remaining force and torque coefficients exhibited similar convergence characteristic and have not been tabulated. Inspection of these tables shows that convergence to three to four significant figures can be achieved for spacings H/c as close as 1.1 using a maximum of 10 rings with 10 points on each ring. Larger spacings (H/c>1.5) require only 4-6 rings and points to achieve the same accuracy.

Figures 2 - 10 show converged values of the nine independent coefficients for a torus with b/a = 2 and 10 as a function of orientation angle α and the separation distance H/c.

Comparing the curves for a torus of b/a = 2 with those for an oblate spheroid having aspect ratio $\epsilon = 0.5$ presented in chapter 1, most of the curves having the same value of H/c exhibit similar behavior qualitatively and quantitatively especially for small values of the orientation angle α. The only exception is the ratio $F_3^{t_1}/F_{3,\infty}^{t_1}$, which increases with increasing α for a torus while it decreases with increasing α for an oblate spheroid. Although the ratio of $F_3^{t_1}/F_{3,\infty}^{t_1}$ is substantially

different for the torus and the oblate spheroid at H/c=1.1, the ratio becomes relatively insensitive to orientation angle for H/c>2 and for a given value of H/c, the two ratios are approximately equal. In an unbounded fluid the difference between the corresponding values of the actual resistance coefficients for both shapes is less than 1%. Therefore an oblate spheroid having aspect ratio ϵ = 0.5 can be used as a good approximation of the motion of a torus with b/a=2 when the torus is not very close to the wall. It is worth noting that an oblate spheroid with ϵ = 0.5 and a torus with b/a=2 having the same outer radius have approximately same surface area. On another hand the motion of a torus having b/a = 10 would not be similar to the motion of an oblate spheroid even in unbounded fluid.

Finally figure 11 shows the variation of $F_1^{t_1}/F_{1,\infty}^{t_1}$ and $F_3^{t_1}/F_{3,\infty}^{t_1}$ as functions of b/a for a torus with its axis of symmetry oriented perpendicular to the wall. Both ratios decrease with increasing aspect ratio. As expected, the ratio $F_3^{t_1}/F_{3,\infty}^{t_1}$ is a much stronger function of the aspect ratio than the ratio $F_1^{t_1}/F_{1,\infty}^{t_1}$ is.

3. Solution for the motion of a biconcave shaped body

The typical shape of an undeformed red blood cell is shown in figure 12. The shape can be expressed as

$$B = R_0 (1 - R_s^2)^{1/2} (C_0 + C_1 R_s^2 + C_2 R_s^4) \qquad (10)$$

where B is the width. R_s is the radius of the blood cell. R_0 C_1 C_2 and C_3 are constants. and R_0 represents the largest radius . Representative values of these constants are listed in Fung (1981). In this section we solve for the motion of a blood cell adjacent to a planar wall using the values

$$R_0 = 3.91\,\mu \;,\; C_0 = 0.81\,\mu,\; C_1 = 7.83\,\mu,\; C_2 = 4.39\,\mu \qquad (11)$$

As in the case of a torus the shape R = R(z) is not a single-valued function. To describe the biconcave shape we introduce a new parameter η and let

$$R_s = R_0 \cos\eta \qquad (12a)$$

$$z = \frac{R_0}{2} (1 - R_s^2)^{1/2} (C_0 + C_1 R_s^2 + C_2 R_s^4) \, \mathrm{Sign}(\eta) \qquad (12b)$$

where sign(x) = |x|/x. Then both R and z are single-valued functions of η . The stokeslet density functions are represented by the double Fourier-Legendre series:

$$\begin{aligned} f_1 &= \sum_{m=0}^{\infty} \sum_{n=0}^{\infty} A_{1,m,n} P_n (\sin\eta) \cos m\theta \\ f_2 &= \sum_{m=1}^{\infty} \sum_{n=0}^{\infty} A_{2,m,n} P_n (\sin\eta) \sin m\theta \\ f_3 &= \sum_{m=0}^{\infty} \sum_{n=0}^{\infty} A_{3,m,n} P_n (\sin\eta) \cos m\theta \end{aligned} \qquad (13)$$

where $P_n(x)$ is the Legendre function of order n. Substituting (12a,b) and (13) into integral equation (3) all integrals in equation (3) can be performed with respect to variable θ and γ as was done for the torus. The collocation points are arranged such that the rings, which are represented by constant values of γ, are nearly equally spaced along the arc length of the body shown in figure 13 and somewhat more concentrated in the vicinity of maximum radius. At each ring the collocation points are equally spaced between $\theta = 0^\circ$ and 180°. The convergence behavior of the force and torque coefficients is similar to the case of a torus having $b/a = 2$.

The hydrodynamic force and torque coefficients of the biconcave shaped disc are defined as follows:

$$\begin{pmatrix} F_1 \\ F_3 \\ T_2 \end{pmatrix} = 6\pi\mu R_0 \begin{pmatrix} F_1^{t_1} & F_1^{t_3} & F_1^{r} & HF_1^{s} \\ F_3^{t_1} & F_3^{t_3} & F_3^{r} & HF_3^{s} \\ \frac{4}{3}R_0 T_2^{t_1} & \frac{4}{3}R_0 T_2^{t_3} & \frac{a}{3}R_0 T_2^{r} & \frac{2}{5}R_0^2 T_2^{s} \end{pmatrix} \begin{pmatrix} U_1 \\ U_3 \\ R_0\omega \\ S \end{pmatrix} \qquad (14)$$

The values of the force and torque coefficients for the biconcave shaped disc described by equations (10) and (11) in an infinite fluid, obtained using the present theory, are listed in table 8. All the coefficients are remarkably close to the corresponding values for a torus with $b/a = 2$. When a planer wall is present the numerical solutions show that the force and torque coefficients are still quite close

for the two bodies having the same H/c and α. The difference between them is less than 1% for all nine force and torque coefficients for the separation distances as close as H/c=1.1. Therefore figures 2 - 10 can also be used to predict the force and torque of a biconcave shape body described by equations (8) and (9) to a high degree of accuracy. It is worth noting that the biconcave shaped body and a torus with b/a = 2 have the same surface area if their outer radii are the same. The coincidence of the force and torque shows that the hole of a torus of b/a = 2 has little influence on the flow field. As mentioned in section 2 an oblate spheroid having aspect ratio ϵ = 0.5 can also serve as a good approximation for the motion of a torus of b/a = 2 when it is not very close to the wall.

REFERENCES

Fung, Y.C. 1981 Biomechanics: Mechanical Properties of Living Tissues. Spring-Verlag New York Inc.

Kanyal, R.P. 1961 J. Fluid Mech. 10 , 17.

Majumdar, S.R. & O'Neill, M.E. 1977 Z. angew Math. Phys. 28 , 541.

Payne, L.E. & Pell, W.M. 1960 Mathematics 7 , 78.

Skalak, R., Chen, P.H. Chien, S. 1972 Biorheol 9 , 67.

Simon,L.G. & O'Neill, M.E. 1980 J.Fluid Mech. 13 , 97.

	b/a=2	b/a=10
force coefficient $F^{\parallel}_{1,\infty}$ for motion parallel to symmetry axis	-0.9072	-0.7843
force coefficient $F^{\perp}_{1,\infty}$ for motion perpendicular to symmetry axis	-0.7733	-0.6174
torque coefficient $T^{s}_{2,\infty}$ for a torus rigidly held in a shear flow parallel to the symmetry axis	-0.9477	-0.8440
torque coefficient $T^{s}_{2,\infty}$ for a torus rigidly held in a shear flow perpendicular the symmetry axis	-0.1703	-0.01678
torque coefficient for rotation	-0.5590	-0.4304

Table 1 Force and torque coefficients for a torus in an infinite fluid.

(a) b/a = 2

N	H/c 0.5	0.8	1.1	1.5	∞
4	-25.15	-5.921	-3.677	-2.150	-0.9174
6	-19.60	-5.500	-3.111	-2.136	-0.9072
8	-18.30	-5.499	-3.121	-2.140	-0.9072
10	-18.42	-5.500	-3.122	-2.141	-0.9072
12	-18.52	-5.500	-3.122	-2.141	
14	-18.51	-5.500			
16	-18.51				

(b) b/a = 10

N	H/c 0.2	0.5	0.8	1.1	1.5	∞
4	-9.122	-3.120	-2.167	-1.741	-1.348	-0.7823
6	-7.547	-2.858	-2.142	-1.764	-1.471	-0.7843
8	-7.232	-2.859	-2.140	-1.764	-1.471	-0.7843
10	-2.233	-2.859	-2.140			
12	-2.233					

Table 2 Convergence of the coefficient $F_s^{(1)}$ for a torus with its symmetry axis perpendicular to the wall.

(a) b/a = 2

N	H/c 0.5	0.8	1.1	1.5	∞
4	-3.124	-1.542	-1.312	-1.118	-0.7706
6	-1.881	-1.366	-1.170	-1.048	-0.7732
8	-2.063	-1.372	-1.171	-1.048	-0.7732
10	-2.077	-1.372	-1.171	-1.048	-0.7732
12	-2.079	-1.372	-1.171		
14	-2.079				
16	-2.079				

(b) b/a = 10

N	H/c 0.2	0.5	0.8	1.1	1.5	∞
4	-2.534	-1.006	-0.9103	-0.8311	-0.7737	-0.6166
6	-1.910	-1.096	-0.9132	-0.8324	-0.7749	-0.6174
8	-1.927	-1.096	-0.9132	-0.8324	-0.7749	-0.6174
10	-1.928	-1.096				
12	-1.928					

Table 3 Convergence of the coefficient $F_1^{t,}$ for a torus with its symmetry axis perpendicular to the wall.

(a) b/a = 2

N	H/c 0.5	0.8	1.1	1.5	∞
4	-2.943	-0.9314	-0.7724	-0.6734	-0.5810
6	-1.774	-0.8890	-0.6997	-0.6228	-0.5584
8	-2.262	-0.9175	-0.7071	-0.6230	-0.5590
10	-2.319	-0.9176	-0.7071	-0.6230	-0.5590
12	-2.323	-0.9176	-0.7071	-0.6230	
14	-2.324	-0.9176			
16	-2.324				

(b) b/a = 10

N	H/c 0.2	0.5	0.8	1.1	1.5	∞
4	-2.847	-0.8657	-0.6231	-0.5320	-0.4915	-0.4408
6	-2.226	-0.8223	-0.6044	-0.5219	-0.4748	-0.4304
8	-2.227	-0.8224	-0.6044	-0.5219	-0.4748	-0.4304
10	-2.229	-0.8224	-0.6044			
12	-2.229					

Table 4 Convergence of the coefficient T_3^r for a torus with its symmetry axis perpendicular to the wall.

(a) b/a = 2. H/c = 1.5

N \ M	4	6	8	10
4	2.295	2.296	2.297	2.297
6	2.295	2.296	2.297	2.297
8	2.295	2.296	2.297	2.297
10	2.295	2.296	2.296	2.296

(b) b/a = 2. H/c = 1.1

N \ M	4	6	8	10
4	4.55	4.46	4.44	4.44
6	4.29	4.24	4.21	4.21
8	4.14	4.20	4.24	4.23
10	4.11	4.21	4.23	4.23

Table 5 Convergence tests of $F_s^{\uparrow_s}/F_{s,\infty}^{\uparrow_s}$ for a torus inclined at 30° relative to the planar wall.
N ___ Number of rings (constant values of γ)
M ___ Number of points at each ring (constant values of θ)

(c) b/a = 10, H/c = 1.5

N \ M	4	6	8
4	1.828	1.829	1.829
6	1.828	1.829	1.829
8	1.828	1.828	1.828
10	1.828	1.828	1.828

(d) b/a = 10, H/c = 1.1

N \ M	4	6	8	10
4	2.504	2.508	2.519	2.523
6	2.502	2.524	2.525	2.525
8	2.501	2.517	2.522	2.522
10	2.501	2.519	2.521	2.521

Table 5 Convergence tests of $F_3^{t_3}/F_{3,\infty}^{t_3}$ for a torus inclined at 30° relative to the planar wall.
N ___ Number of rings (constant values of γ)
M ___ Number of points at each ring (constant values of θ)

(a) b/a = 2, H/c = 1.5

N \ M	4	6	8
4	1.096	1.096	1.097
6	1.094	1.094	1.094
8	1.094	1.094	1.094
10	1.093	1.093	1.093

(b) b/a = 2, H/c = 1.1

N \ M	4	6	8	10
4	1.43	1.42	1.40	1.40
6	1.26	1.28	1.28	1.28
8	1.33	1.34	1.37	1.37
10	1.35	1.36	1.37	1.37

Table 6 Convergence tests of $T_2^r / T_{2,\infty}^r$ for a torus inclined at 30° relative to the planar wall.
N ___ Number of rings (constant values of γ)
M ___ Number of points at each ring (constant values of θ)

(c) b/a = 10, H/c = 1.5

N \ M	4	6	8
4	1.096	1.097	1.097
6	1.096	1.097	1.097
8	1.096	1.097	1.097
10	1.096	1.097	1.097

(d) b/a = 10, H/c = 1.1

N \ M	4	6	8	10
4	1.298	1.301	1.305	1.305
6	1.296	1.302	1.305	1.305
8	1.296	1.303	1.304	1.304
10	1.296	1.303	1.304	1.304

Table 6 Convergence tests of $T_2^r / T_{2,\infty}^r$ for a torus inclined at 30° relative to the planar wall.
N ___ Number of rings (constant values of γ)
M ___ Number of points at each ring (constant values of θ)

(a) b/a = 2, H/c = 1.5

N \ M	4	6	8
4	-0.0476	-0.0475	-0.0476
6	-0.0470	-0.0464	-0.0464
8	-0.0468	-0.0468	-0.0467
10	-0.0468	-0.0467	-0.0467

(b) b/a = 2, H/c = 1.1

N \ M	4	6	8	10
4	-0.143	-0.143	-0.143	-0.143
6	-0.142	-0.142	-0.142	-0.142
8	-0.139	-0.139	-0.137	-0.137
10	-0.137	-0.137	-0.137	-0.137

Table 7 Convergence tests of $T_3^{\uparrow_1}$ for a torus inclined at 30 relative to the planar wall.
N ___ Number of rings (constant values of γ)
M ___ Number of points at each ring (constant values of θ)

(c) B/A = 10, H/C = 1.5

N \ M	4	6	8
4	-0.0399	-0.0399	-0.0399
6	-0.0400	-0.0400	-0.0400
8	-0.0400	-0.0400	-0.0400
10	-0.0400	-0.0400	-0.0400

(d) B/A = 10, H/C = 1.1

N \ M	4	6	8	10
4	-0.105	-0.104	-0.104	-0.104
6	-0.104	-0.103	-0.103	-0.103
8	-0.104	-0.104	-0.103	-0.103
10	-0.103	-0.103	-0.103	-0.103

Table 7 Convergence tests of $T_1^{\dagger}$ for a torus inclined at 30 relative to the planar wall.
N ___ Number of rings (constant values of γ)
M ___ Number of points at each ring (constant values of θ)

force coefficient for motion parallel to symmetry axis	-0.9062
force coefficient for motion perpendicular to symmetry axis	-0.7724
torque coefficient for the body rigidly held in a shear flow parallel to the symmetry axis	-0.9460
torque coefficient for the body rigidly held in a shear flow perpendicular to the symmetry axis	-0.1676
torque coefficient for rotation	-0.5568

Table 8 force and torque coefficients for the biconcave shaped disc in an infinite fluid.

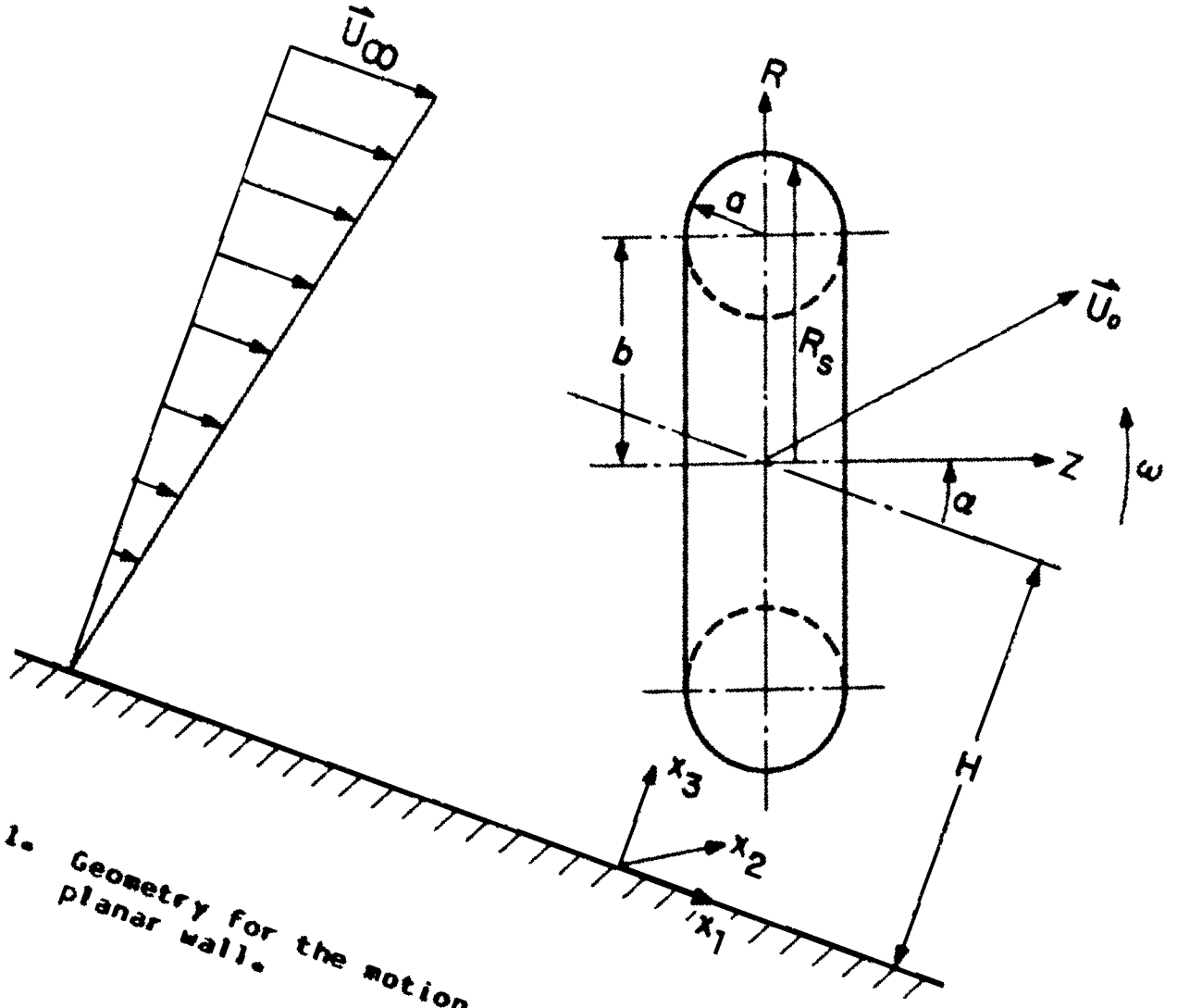

Figure 1. Geometry for the motion of a torus near a planar wall.

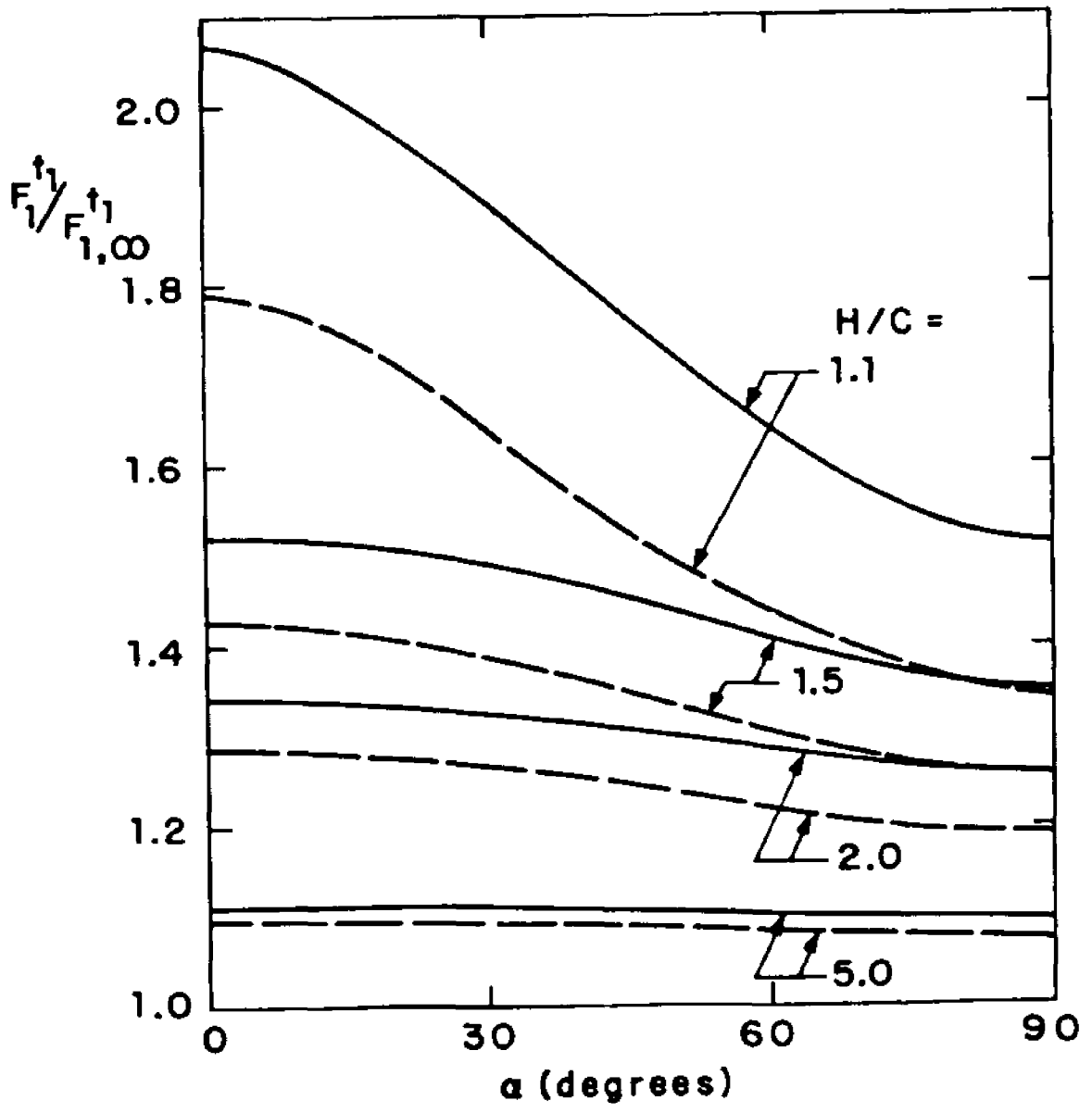

Figure 2. The ratio of resistance coefficients $F_1^{t_1}/F_{1,\infty}^{t_1}$ for a torus as a function of orientation angle and separation distance.
(_____ b/a = 2, _ _ _ b/a = 10)

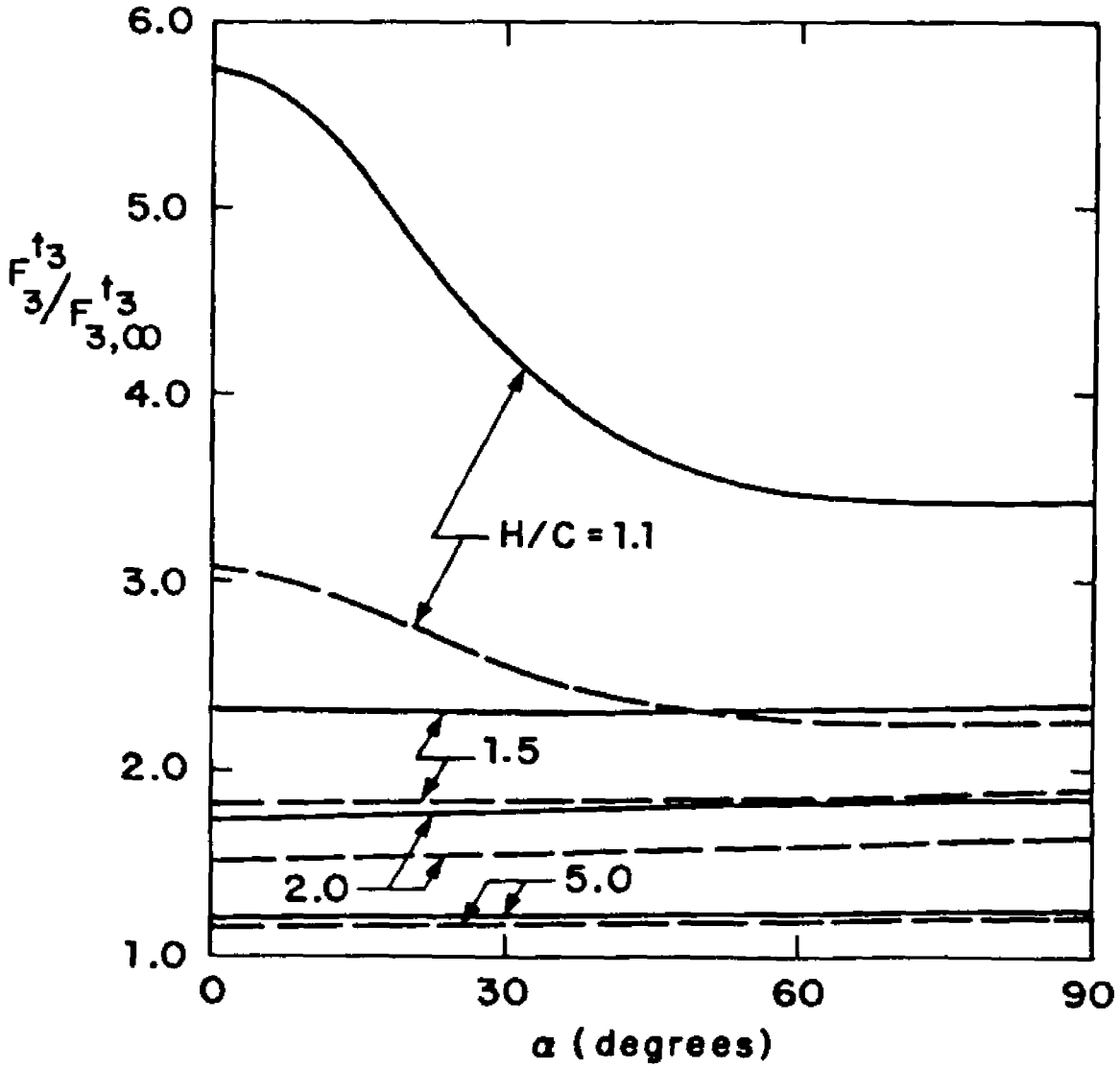

Figure 3. The ratio of resistance coefficients $F_3^{t_3}/F_{3,\infty}^{t_3}$ for a torus as a function of orientation angle and separation distance. (_____ b/a = 2, _ _ _ b/a = 10)

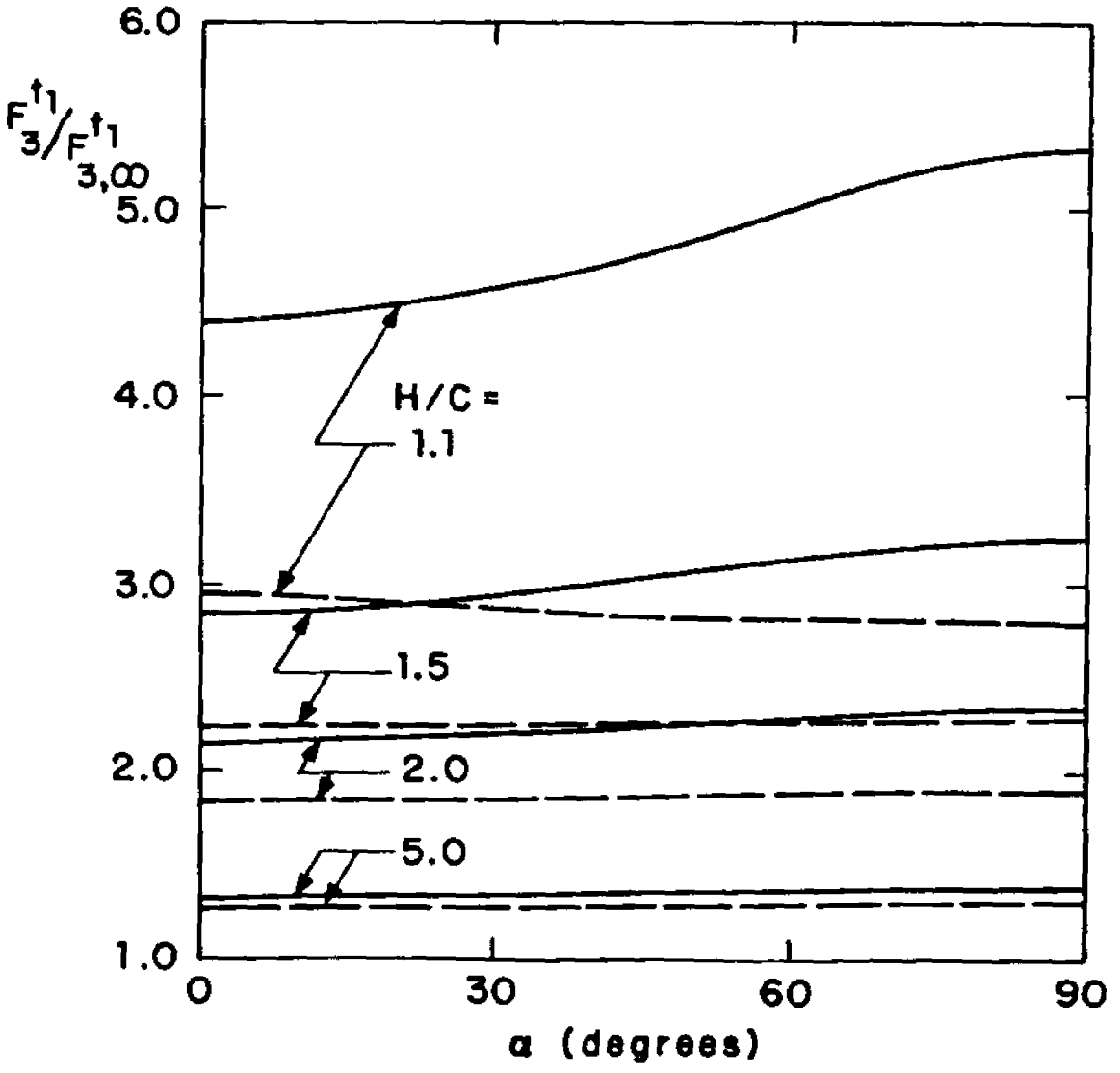

Figure 4. The ratio of resistance coefficients $F_3^{t_1}/F_{3,\infty}^{t_1}$ for a torus as a function of orientation angle and separation distance.
(_____ b/a = 2, _ _ _ b/a = 10)

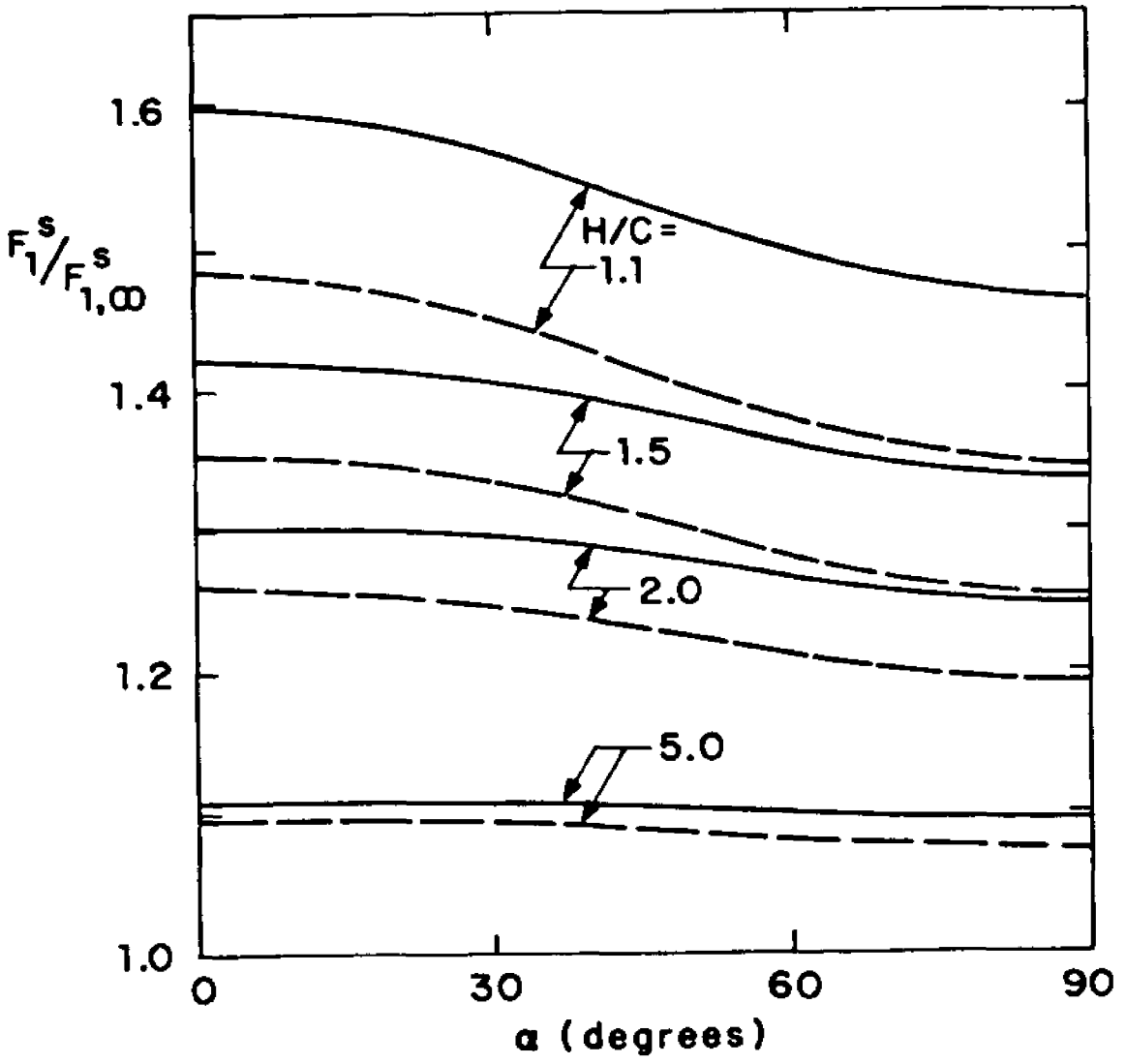

Figure 5. The ratio of resistance coefficients $F_1^s/F_{1,\infty}^s$ for a torus as a function of orientation angle and separation distance.
(_____ b/a = 2, _ _ _ b/a = 10)

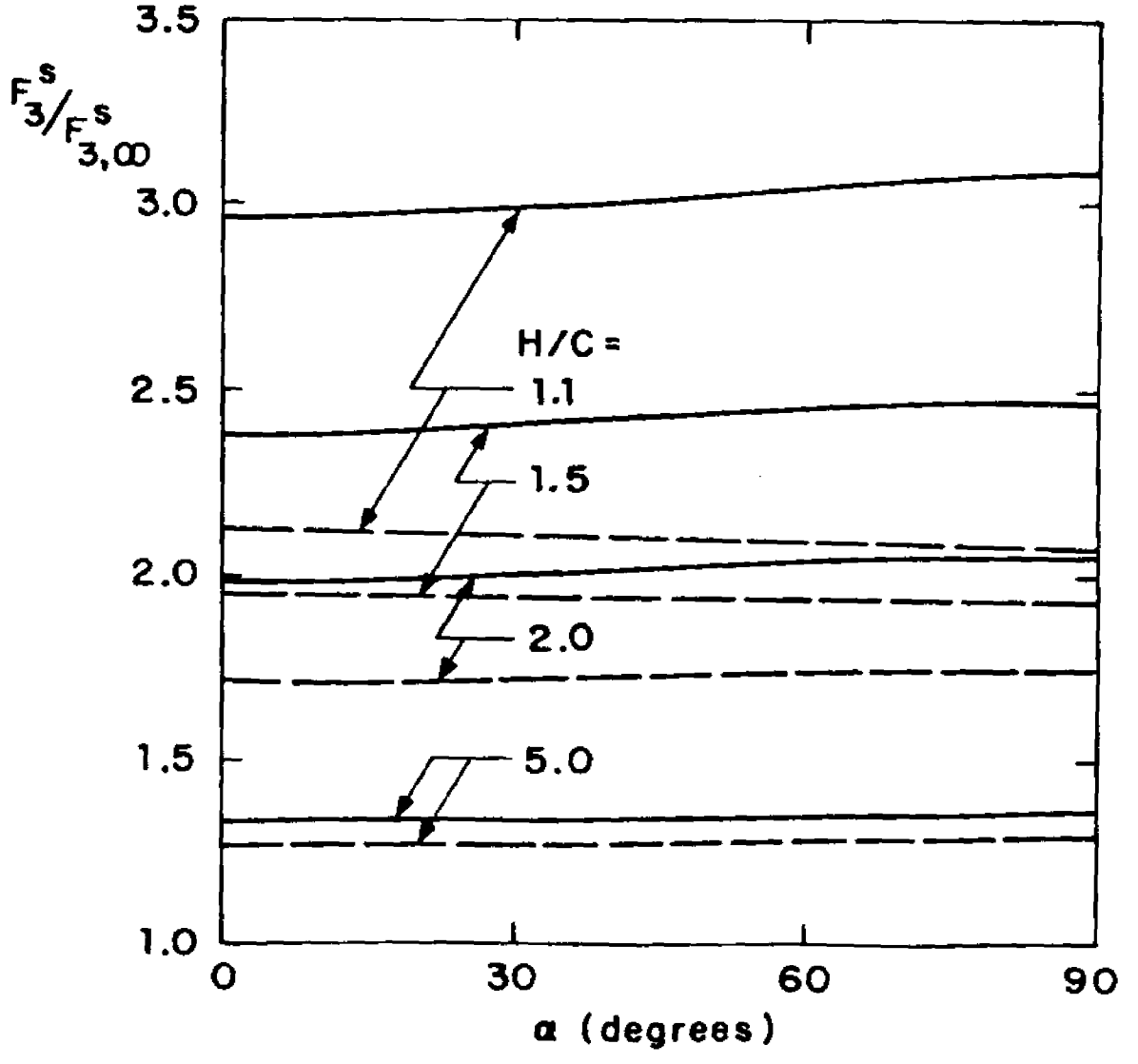

Figure 6. The ratio of resistance coefficients $F^s_3/F^s_{3,\infty}$ for a torus as a function of orientation angle and separation distance.
(_____ b/a = 2, _ _ _ b/a = 10)

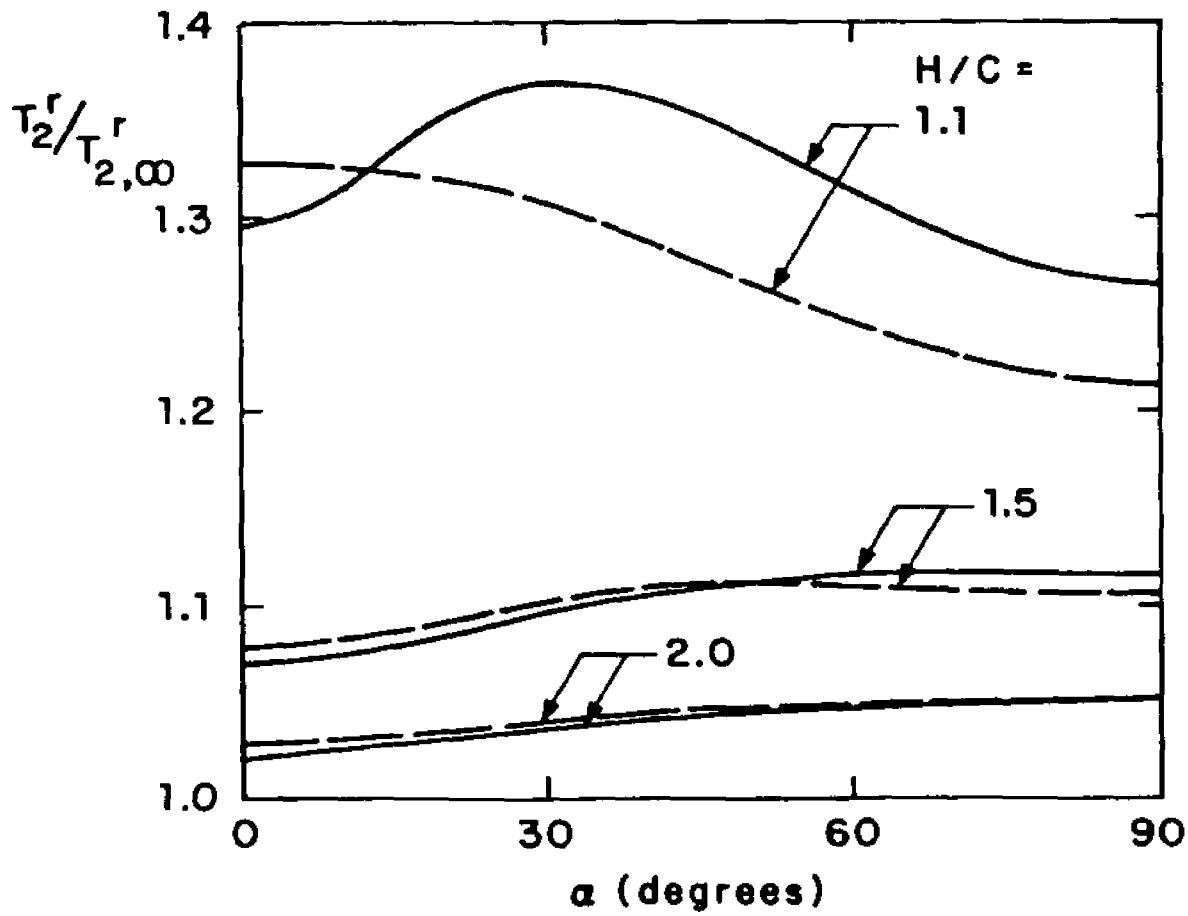

Figure 7. The ratio of resistance coefficients $T_2^r/T_{2,\infty}^r$ for a torus as a function of orientation angle and separation distance.
(_____ b/a = 2. _ _ _ b/a = 10)

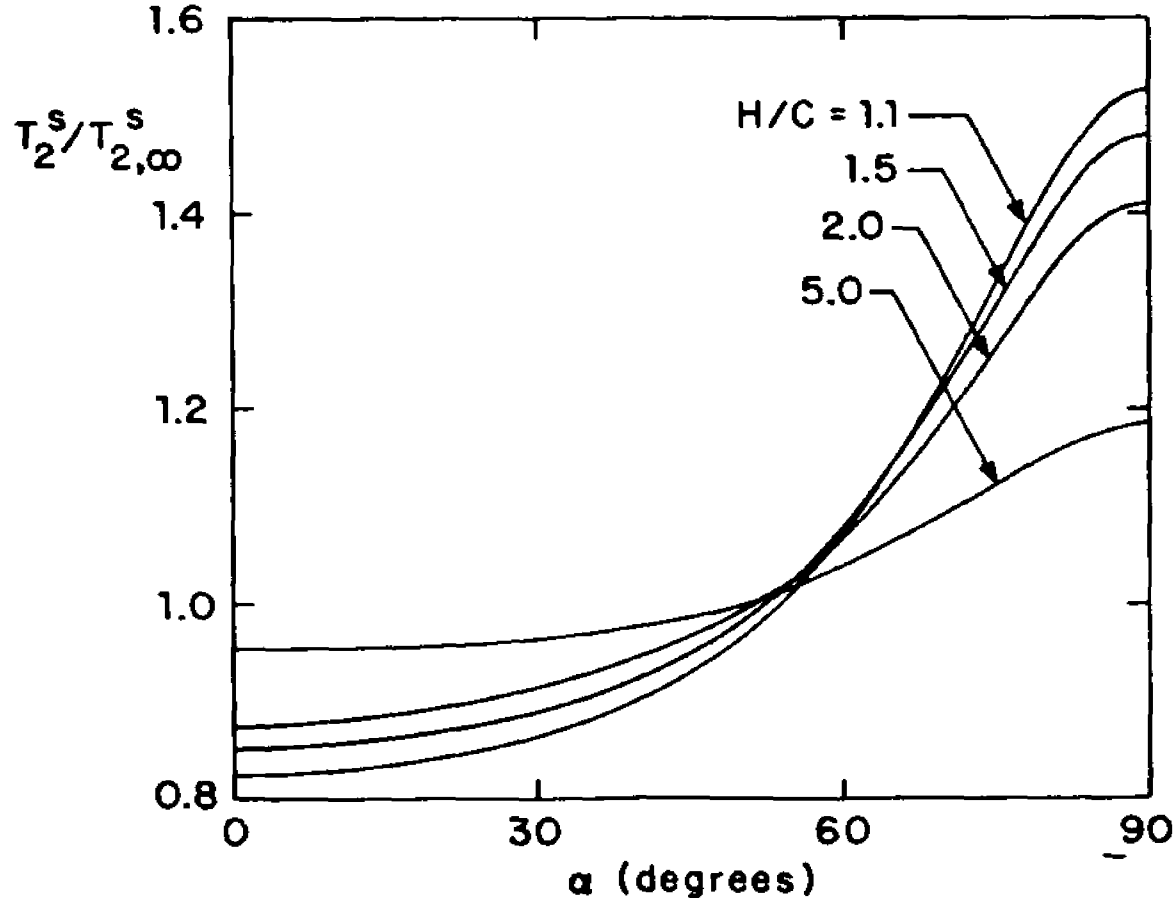

Figure 8a. The ratio of resistance coefficients $T_2^s/T_{2,\infty}^s$ for a torus with b/a = 2 as a function of orientation angle and separation distance.

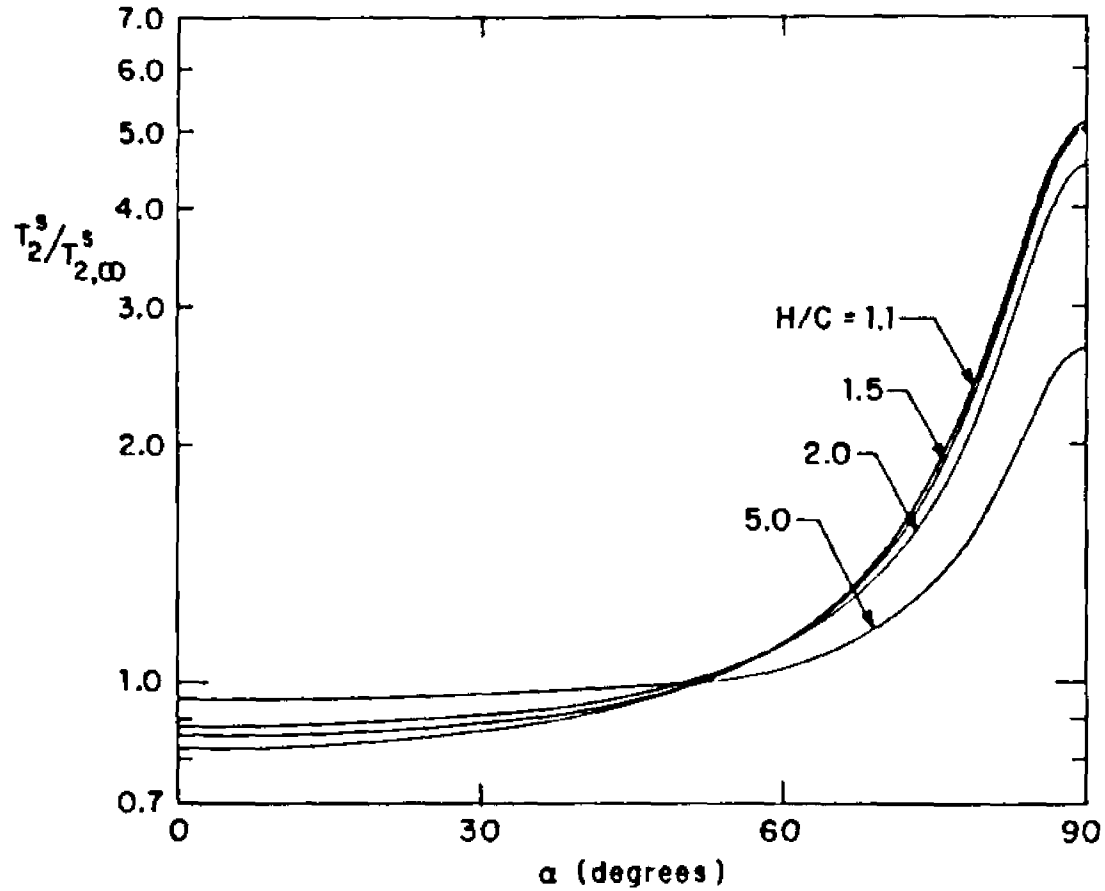

Figure 8b. The ratio of resistance coefficients $T_2^s/T_{2,\infty}^s$ for a torus with b/a = 10 as a function of orientation angle and separation distance.

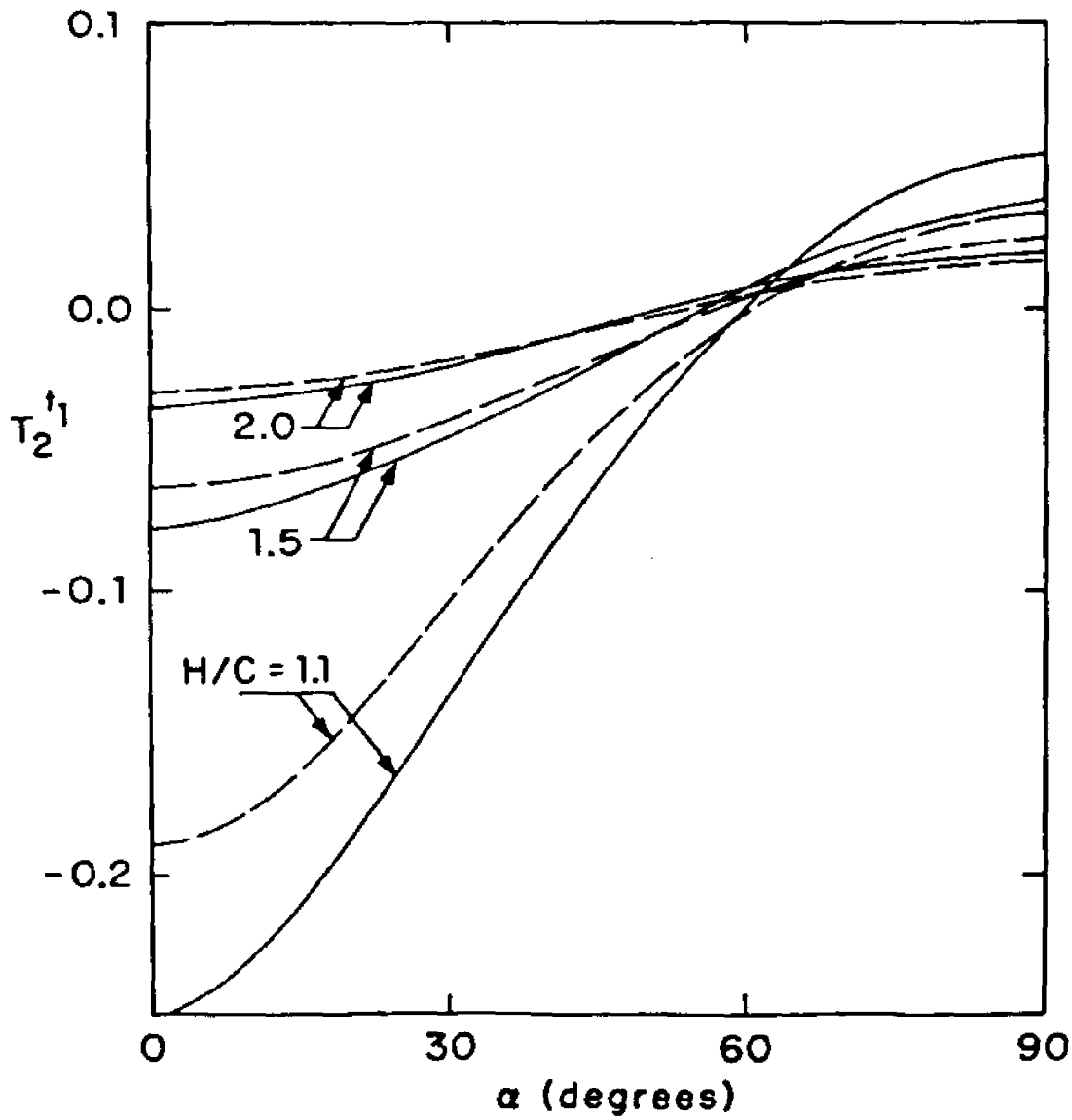

Figure 9. The resistance coefficient $T_2^{\dagger 1}$ for a torus as a function of orientation angle and separation distance.
(_____ b/a = 2, _ _ _ b/a = 10)

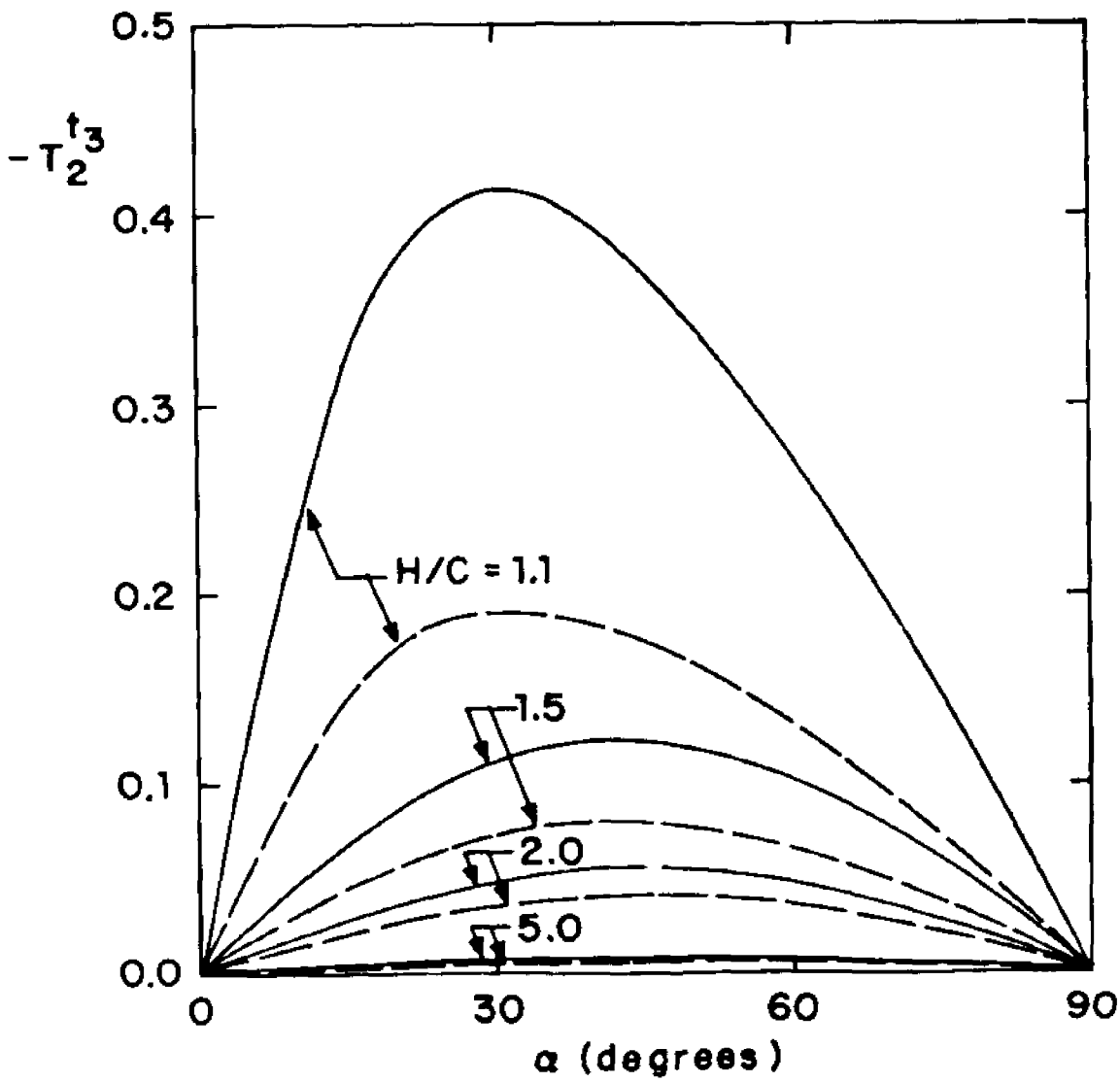

Figure 10. The resistance coefficient $T_2^{t_3}$ for a torus as a function of orientation angle and separation distance.
(_____ b/a = 2, _ _ _ b/a = 10)

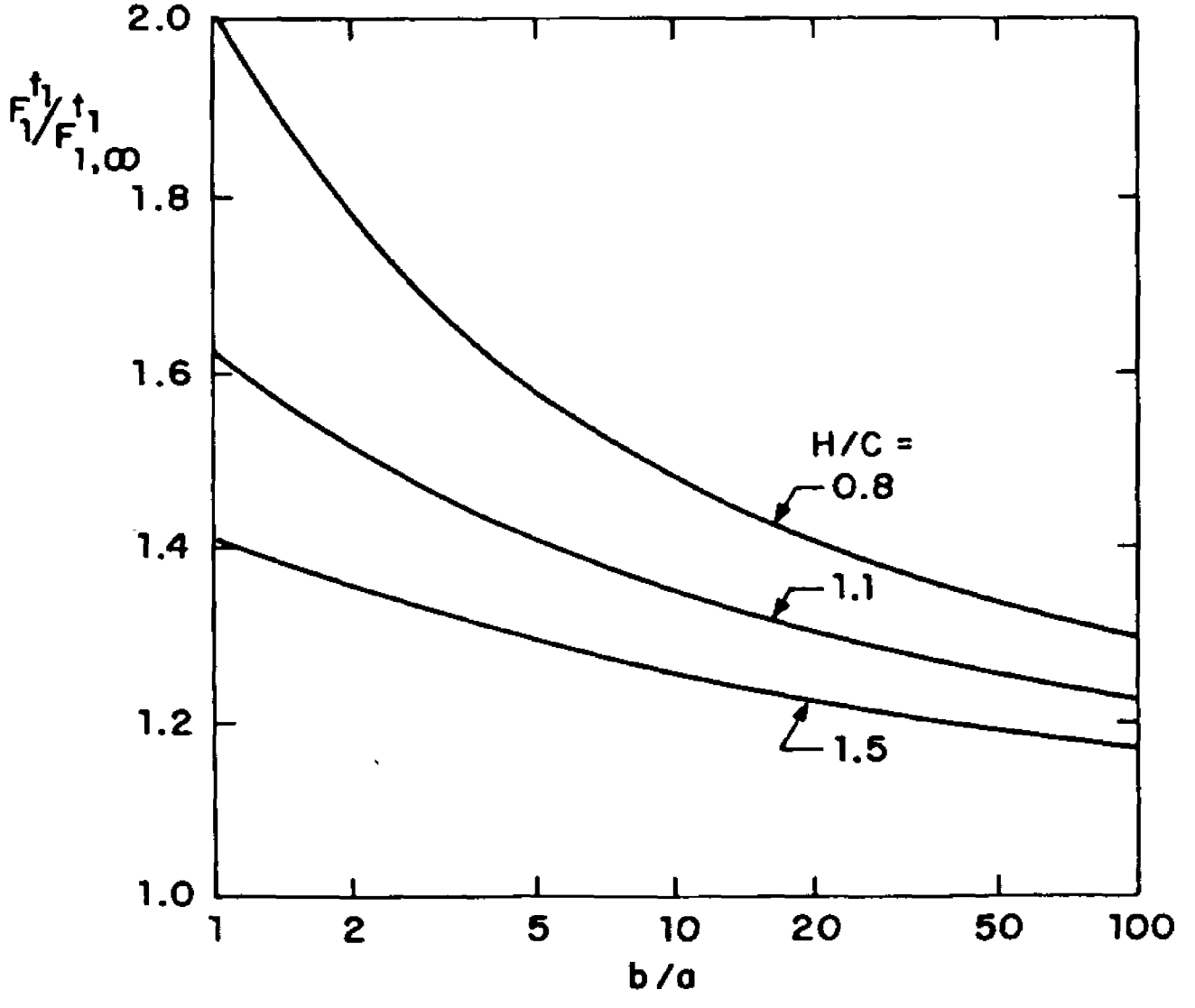

Figure 11a The ratio of resistance coefficients $F_1^{t_1}/F_{1,\infty}^{t_1}$ for a torus with its symmetry axis perpendicular to the wall as a function of b/a.

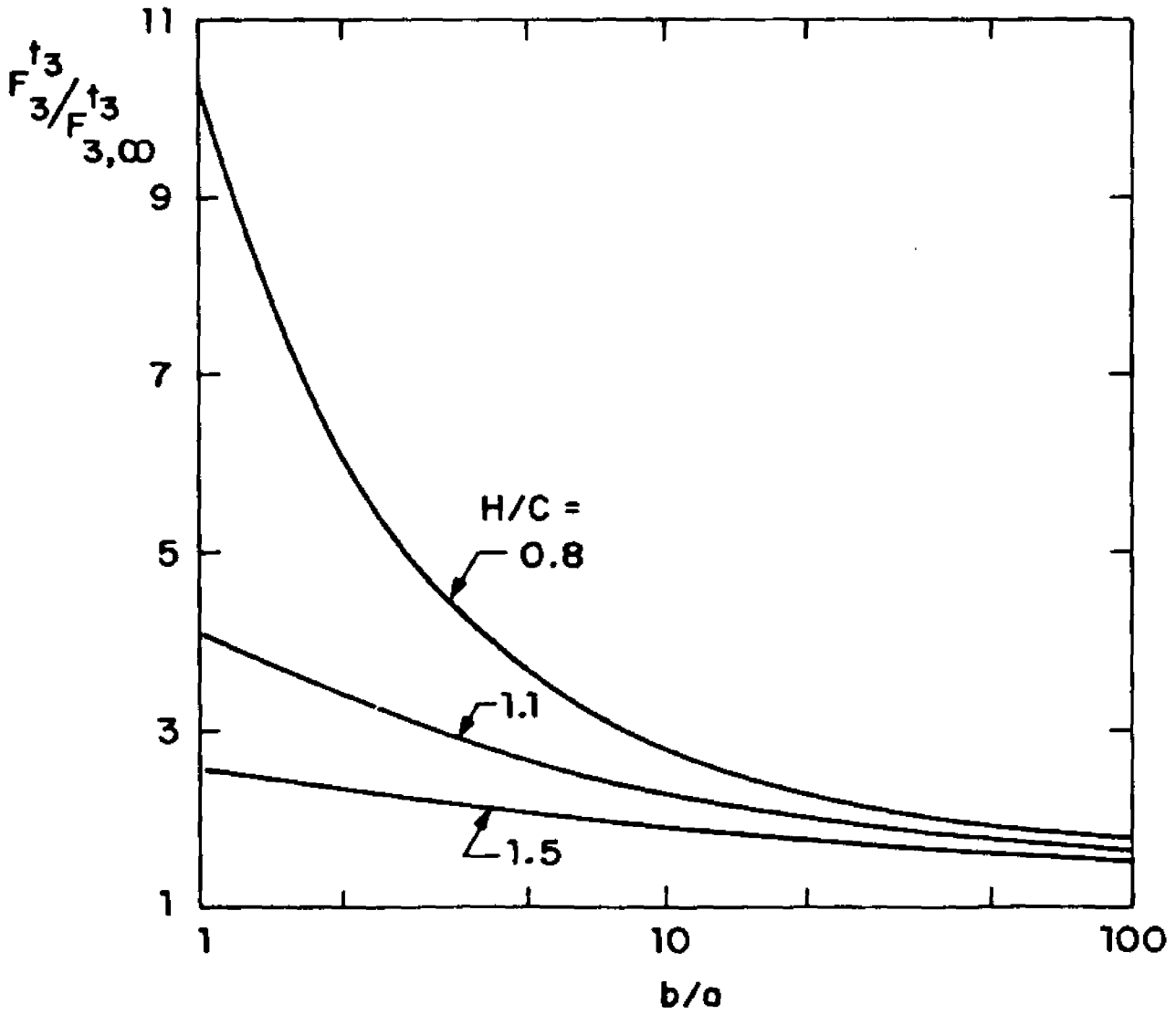

Figure 11b. The ratio of resistance coefficients $F_3^{t_3}/F_{1,\infty}^{t_3}$ for a torus with its symmetry axis perpendicular to the wall as a function of b/a.

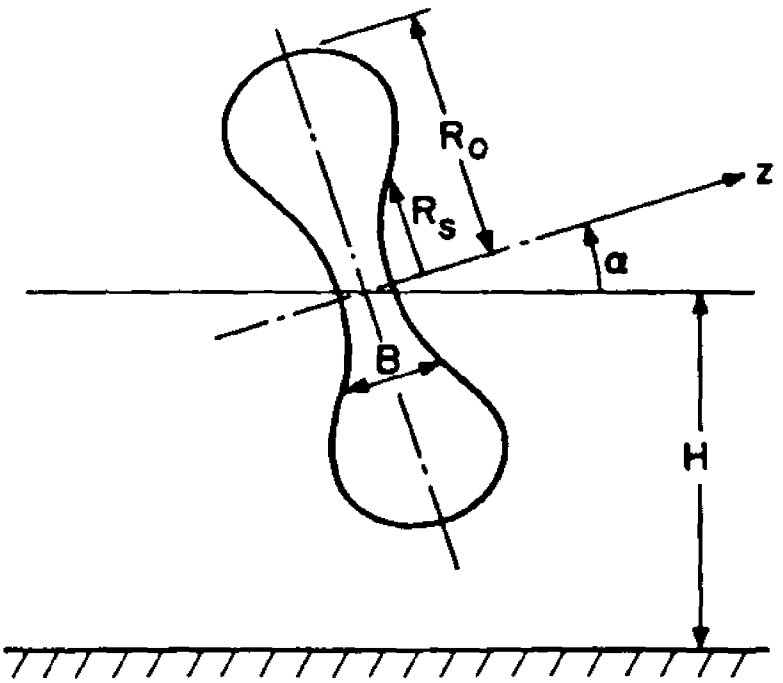

Figure 12. Geometry for a biconcave shaped disc.

CHAPTER 3

GRAVITATIONAL AND ZERO-DRAG MOTION OF AN OBLATE SPHEROID ADJACENT TO AN INCLINED PLANE AT LOW REYNOLDS NUMBER

Abstract

The theory developed in chapter 1 for the planar motion of an arbitrary body of revolution near a planar wall is applied to treat several specific problems. The first highly accurate solutions for the resistance tensor of an oblate spheroid moving near a planar wall are used to compute the translational and angular velocities and trajectories of a neutrally buoyant spheroid in a shear flow and the gravitational settling motion of a non-neutrally buoyant spheroid adjacent to an inclined plane. The neutrally buoyant spheroid in a shear flow undergoes a periodical motion toward and away from the wall as it continuously tumbles forward. For certain inclinations a spheroid setting under gravity near an inclined plane will finally reach an equilibrium position, after which it will translate parallel to the wall without rotation.

1. Introduction

The creeping motion of a non-spherical particle in three dimensional Stokes flow in the presence of a planar wall is of long-standing interest. Wakiya (1959) considered the motion of a spheroid parallel to a planar wall using the method of reflections. More recently Yang & Leal (1983, 1984) studied the arbitrary motion of a slender body near a flat fluid-fluid interface using a singularity method and slender body theory.

In chapter I the boundary integral technique was used to obtain solutions for the resistance tensor for a body of revolution tumbling adjacent to a planar wall at low Reynolds number. The force and torque were accurately computed for a spheroid translating parallel or perpendicular to the wall, rotating about an axis parallel to the wall, or which is rigidly held in place in a shear flow. The accuracy of the solutions has been tested for the special case of a sphere with the exact bipolar coordinate solutions of Brenner (1961) for the motion of a sphere perpendicular to a wall and Goldman, Cox & Brenner (1967a,b) for a sphere translating parallel to a wall, rotating adjacent to a wall or in the presence of a shear flow. The solutions of the boundary integral method were in good agreement with the exact solution up to a gap width of a tenth of the sphere radius. On the other hand, it was found that the solutions obtained by the method of reflections of

Wakiya (1959) are good only when the spheroid is far away from the wall (the spheroid-wall distance at least five times the spheroid semi-major axis).

For the motion of a sphere near a planar wall some of the elements of the resistance tensor are identically zero, such as the coefficients which give the force perpendicular to the wall due to the parallel motion or rotation about an axis parallel to the wall. But these forces are not zero for a spheroid. The hydrodynamic force and torque on a spheroid depend strongly on its orientation relative to the wall. This characteristic feature complicates the motion of a spheroid adjacent to a plane.

In this thesis we only consider the motion with planar symmetry. Jeffery (1922) has shown that a prolate spheroid is not stable with the axis of symmetry in the plane of symmetry of an unbounded fluid. We therefore will only consider the motion of an oblate spheroid which is stable in the plane of symmetry.

In the present chapter the resistance tensor for an oblate spheroid computed in chapter 1 is used to compute the translational and rotational velocities and trajectories for zero-drag motion in a shear flow and gravitational motion adjacent to an inclined plane.

2. General motion of an oblate spheroid adjacent to a planar wall

Consider the motion of a spheroid adjacent to a planar wall as shown as in figure 1. The spheroid has a half-length a and radius b. It is spaced at a distance H from the wall and has an orientation angle α relative to the wall. The spheroid is moving in the $x_1 x_3$ plane with velocity $\vec{U}_0$ which has components U_1 and U_3, and rotating along the x_2 axis with angular velocity ω. A shear flow $U_\infty = S \cdot x_3$ may be present in the x_1 direction.

In the zero Reynolds number flow limit the fluid velocity V must satisfy the creeping flow equations

$$\mu \nabla^2 \vec{V} = \nabla P \tag{1a}$$

$$\nabla \cdot \vec{V} = 0 \tag{1b}$$

subject to the boundary conditions

$$\vec{V} = \vec{\omega} \times \vec{\rho} + \vec{U}_0 \qquad \text{at the particle surface} \tag{2a}$$

$$\vec{V} = 0 \qquad \text{at the wall} \tag{2b}$$

$$\vec{V} = \vec{U}_\infty \ , \ P = 0 \qquad \text{at infinity} \tag{2c}$$

where $\vec{\rho}$ is the position vector whose origin is at the particle center.

The force and torque acting on the spheroid resulting from the planar motion may be expressed using 12 resistance coefficients as follows:

$$F_1 = 6\pi\mu b \left[F_1^{t_1} U_1 + F_1^{t_3} U_3 + b F_1^{r} \omega + H F_1^{s} S \right] \tag{3a}$$

$$F_3 = 6\pi\mu b \left[F_3^{t_1} U_1 + F_3^{t_3} U_3 + b F_3^{r} \omega + H F_3^{s} S \right] \tag{3b}$$

$$T_2 = 8\pi\mu b^2 \left[T_2^{t_1} U_1 + T_2^{t_3} U_3 + b T_2^{r} \omega + \tfrac{1}{2} b T_2^{s} S \right] \tag{3c}$$

The twelve resistance coefficients depend on the aspect ratio a/b, the separation distance H/b and the orientation angle relative to the wall α. Of the 12 resistance coefficients three pairs are related according to the reciprocity relations.

$$F_1^{t_3} = F_3^{t_1} \tag{4a}$$

$$F_1^{r} = \tfrac{3}{4} T_2^{t_1} \tag{4b}$$

$$F_3^{r} = \tfrac{3}{4} T_2^{t_3} \tag{4c}$$

The nine independent force and torque coefficients have been computed to a high degree of accuracy in Chapter 1. Therefore if the force and torque acting on the spheroid are known, the system of linear equations (3a)-(3c) can be solved for the unknown velocities U_1, U_3 and ω. We now consider some special cases.

3. Zero-drag motion of an oblate spheroid in shear flow

We consider the motion of a neutrally buoyant spheroid in shear flow adjacent to a planar wall. The condition of zero drag and zero torque require

$$F_1^{t_1} U_1 + F_1^{t_3} U_3 + bF_1^r \omega + HF_1^S S = 0 \tag{5a}$$

$$F_3^{t_1} U_1 + F_3^{t_3} U_3 + bF_3^r \omega + HF_3^S S = 0 \tag{5b}$$

$$T_2^{t_1} U_1 + T_2^{t_3} U_3 + bT_2^r \omega + \tfrac{1}{2} bT_2^S S = 0 \tag{5c}$$

Simultaneous solution of these three equations gives the values of the velocities U_1, U_3 and ω. For an oblate spheroid with $a/b=0.5$ the values of U_1, U_3 and ω are presented as functions of α at constant H/b in figures 2-4. The velocity U_1 and the angular velocity ω are even functions of α, while the velocity U_3 is an odd function of α. As expected from symmetry, all velocity components have a periodicity of 180°. Therefore they are plotted only in the range between 0° to 90°.

For the velocity component U_1 of greatest interest is the local slip velocity U_S of the spheroid center relative to the incoming velocity profile:

$$U_S = U_1 - U_\infty \tag{6}$$

Figure 2 shows the slip velocity as a function of α at constant H/b for an oblate spheroid with $a/b=0.5$. The slip velocity is negative for all orientation angles and separation distances, indicating that the spheroid always

lags the fluid in shear flow. For a given separation distance the spheroid experiences minimum slip at an orientation angle $\alpha = 90^{\circ}$.

Figure 3 shows the perpendicular velocity U_3 as a function of the orientation angle at constant H/b for an oblate spheroid with a/b=0.5. A peculiar feature is that the lateral velocity component U_3 changes sign and vanishes not only for α equat to 0° and 90° as expected from symmetry but also at a particular angle between them.

The angular velocity ω is shown in figure 4. The angular velocity is maximum at $\alpha = 0^{\circ}$ and monotonically decreases to its minimum value at $\alpha = 90^{\circ}$. Unlike the velocity components U and U , which are strong functions of the separation distance, the angular velocity ω changes little with separation distance, especially when α is close to 0°.

We next consider the trajectory of the particle in shear flow. The equations of motion of the particle in dimensionless form are:

$$\frac{dx_1^*}{dt^*} = \frac{U_1}{U_\infty} \cdot x_3^* \tag{7a}$$

$$\frac{dx_3^*}{dt^*} = \frac{U_3}{U_\infty} \cdot x_3^* \tag{7b}$$

$$\frac{d\alpha}{dt} = \frac{\omega}{S} \tag{7c}$$

where $x_1^* = x_1/b$, $x_3^* = x_3/b$ and $t^* = t \cdot S$.

To compute the three velocity components using equations

(5a)-(5c) for a single separation distance and orientation angle requires approximately 1 to 10 minutes CPU time on an IBM 3081 computer, depending on the particle-wall distance. Therefore it is impossible that all velocities needed to solve the differential equations (5a)-(5c) at each instant time be computed by solving equations (5a)-(5c) directly. We therefore assume interpolating functions in the form of a truncated Fourier series:

$$U_S = -U_\infty (a_0 + a_2 \cos 2\alpha + a_4 \cos 4\alpha + a_6 \cos 6\alpha) \quad (8)$$

$$U_3 = -U_\infty (b_0 \sin 2\alpha + b_4 \sin 4\alpha + b_6 \sin 6\alpha + b_8 \sin 8\alpha) \quad (9)$$

$$W = -S (C_0 + C_2 \cos 2\alpha + C_4 \cos 4\alpha + C_6 \cos 6\alpha) \quad (10)$$

where a_n, b_n and c_n are unknown functions of the aspect ratio and the particle-wall spacing H/b. For a given H/b the velocity components are obtained by solving equations (5a)-(5c) at seven orientation angles and the coefficients a_n, b_n and c_n are calculated using a least squares fit. Tables 1 - 3 list these coefficients for an oblate spheroid with a/b=0.5 and selected values of H/b. Intermediate values at arbitrary H/b are obtained by interpolation using cubic splines in a log-log scale. By comparison with the values obtained directly by solving equations (5a)-(5c) the velocities calculated by equations (8)-(10) have an error of less than 2% . The differential equations (7a)-(7b) are solved numerically using a fourth-order Runge-kutta method.

Figure 5 shows the trajectories of an oblate spheroid having an aspect ratio a/b=0.5 in shear flow, which begins its quasi-steady motion at the point x =0, x =1.25 with initial orientation angle α_0. For clarity, the scale in the x_3^* direction has been expanded by a factor of 40. Figure 6 gives the corresponding orientation angle for the trajectories shown in figure 5. The angular velocity ω is never zero as shown in figure 4, so the particle continuously rotates in one direction. Although the velocity perpendicular to the wall is zero when the spheroid axis is parallel or perpendicular to the wall, these positions cannot be maintained owing to the rotation. Therefore when the particle is translating parallel to the plane, it also drifts toward and away from the plane periodically. The period of the motion is a strong function of the aspect ratio of the spheroid. For a spheroid in unbounded shear flow the orientation angle satisfies the differential equation:

$$\frac{d\alpha}{dt^*} = \frac{1}{2}\left(1 + \frac{b^2 - a^2}{b^2 + a^2}\right)\cos 2\alpha \qquad (11)$$

The solution of equation (11) is

$$\alpha = \tan^{-1}\left[\frac{a}{b}\tan\frac{ab}{b^2+a^2}\right]t^* \qquad (12)$$

Therefore the dimensionless period of an oblate spheroid with a/b=0.5 in unbounded shear flow is $T^* = T/S = 2.5\pi$. Figure 7 shows the variation of the period T^* for an oblate

spheroid with a/b=0.5 as a function of the initial separation distance χ_3^* and orientation angle α. The period is maximum when the particle is close to the wall and monotonically decreases to its asymptotic value as the initial particle-wall spacing is increased. The period decreases with increasing initial orientation from 0° to 90° and as expected becomes independent of α_0 with increasing distance from the wall.

4. Spheroid settling under gravity adjacent to an inclined plane

We now consider the motion of a spheroid setting under gravity adjacent to a plane wall which is inclined at an angle β with quiescent fluid at infinity as shown in figure 8. A force and torque balance on the particle yields

$$6\pi\mu b\left[F_1^{t_1}U_1 + F_1^{t_3}U_3 + bF_1^{r}\omega\right] + \frac{4}{3}\pi ab^2(\rho_s-\rho)g\sin\beta = 0 \qquad (13a)$$

$$6\pi\mu b\left[F_3^{t_1}U_1 + F_3^{t_3}U_3 + bF_3^{r}\omega - \frac{4}{3}\pi ab^2(\rho_s-\rho)g\cos\beta = 0 \qquad (13b)$$

$$T_2^{t_1}U_1 + T_2^{t_3}U_3 + bT_2^{r}\omega = 0 \qquad (13c)$$

where ρ_s and ρ are the density of the particle and the fluid, respectively, and g is the gravitational acceleration. These three equations may be solved simultaneously to yield the two translational components U_1 and U_3 and angular velocity ω of the particle. In the Stokes flow limit, the settling of a spheroid adjacent to a wall inclined of an arbitrary angle β may be completely described by a linear superposition of the solutions at $\beta = 0^\circ$ and 90°. Thus we need only consider these two special cases.

The velocity components of the particle for $\beta = 0^\circ$, in which the plane is perpendicular to the direction of gravity, will be expressed as U_1', U_3' and ω'. The velocity components for $\beta = 90^\circ$, where the plane is parallel to the direction of gravity, will be expressed as U_1^s, U_3^s and ω^s.

The velocities U_1^3 and U_3^1 are equal by the reciprocity relations (4).

The translational velocity components U_1^3, U_3^3 and U_3^1 for an oblate spheroid settling under gravity having aspect ratio a/b=0.5 are shown in figures 9 - 11 respectively as a function of orientation angle α and particle-wall spacing H/b. All three velocities are nondimensionalized by the terminal velocity, U_t, of an isolated oblate spheroid in an unbounded fluid with the force of gravity acting parallel to its major axis and is given by

$$U_t = \frac{16\,ab}{27\,\mu} \frac{(\rho_s - \rho)\,g}{\left[-\frac{\epsilon}{1-\epsilon^2} - \frac{2\epsilon^2-3}{(1-\epsilon^2)^{3/2}} \sin^{-1}\sqrt{1-\epsilon^2}\right]} \qquad (14)$$

where $\epsilon = a/b$ is the aspect ratio. The angular velocities ω^1 and ω^3 are nondimensionalized by U_t/b and plotted in figures 12 - 13. The translational velocities U_1^1, U_3^3 and rotational velocity ω^1 are even functions of α while U_3^1 and ω^3 are odd functions of α. Thus they are plotted only in the range between 0° to 90°.

We next consider the trajectory of a spheroidal particle settling under gravity adjacent to an inclined planar wall. The required values of the translational and rotational velocities at arbitrary separation distance and orientation are interpolated the same manner as in section 3 for the motion of a neutrally buoyant particle in shear flow. For an oblate spheroid having aspect ratio a/b=0.5, the

translational and rotational velocity components are approximated by the truncated fourier series:

$$U_1'/U_t = (0.933 - a_0) - (0.06215 + a_2)\cos 2\alpha \quad (15)$$

$$U_3^3/U_t = (0.933 - b_0) + (0.06215 - b_2)\cos 2\alpha + b_4 \cos 4\alpha + b_6 \cos 6\alpha \quad (16)$$

$$U_3'/U_t = (c_2 - 0.06215)\sin 2\alpha + c_4 \sin 4\alpha + c_6 \sin 6\alpha + c_8 \sin 8\alpha \quad (17)$$

$$\omega^1 b/U_t = d_0 + d_2 \cos 2\alpha + d_4 \cos 4\alpha + d_6 \cos 6\alpha \quad (18)$$

$$\omega^3 b/U_t = e_2 \sin 2\alpha + e_4 \sin 4\alpha + e_6 \sin 6\alpha + e_8 \sin 8\alpha \quad (19)$$

where a_n, b_n, c_n, d_n and e_n are functions of particle-wall spacing H/b and have the value of zero when H/b approaches infinity. These coefficients are listed in tables 4 - 8 for selected values of H/b. Unfortunately, an excessive amount of computation time would be required to determine the force and torque coefficients needed for calculating the translating and angular velocity components in equation 11 for H/b<1.1. Since there is no other solution yet available for calculating the force and torque on an oblate spheroid adjacent to a wall at very small gap widths, the translational and rotational velocities are unavailable for H/b<1.1.

The equation of motion of a particle settling under gravity adjacent to a planar wall inclined at an angle β (see figure 8) are given in dimensionless form:

$$\frac{dX_1^*}{dt^*} = \frac{U_1'}{U_t}\sin\beta + \frac{U_1^3}{U_t}\cos\beta \quad (20)$$

$$\frac{dx_3^*}{dt^*} = \frac{U_3^1}{U_t}\sin\beta + \frac{U_3^3}{U_t}\cos\beta \qquad (21)$$

$$\frac{d\alpha}{dt^*} = \frac{\omega^1 b}{U_t}\sin\beta + \frac{\omega^3 b}{U_t}\cos\beta \qquad (22)$$

where $x_1^* = x_1/b$, $x_3^* = x_3/b$ and $t^* = U_t \cdot t/b$. The system of differential equations was solved numerically using a fourth-order Runge-Kutta method.

Figure 14 shows the trajectory of an oblate spheroid having aspect ratio a/b=0.5 falling adjacent to a planar wall inclined at $\beta = 85°$. Solutions are presented for an initial particle-to-wall spacing $x_3^*=6$ and various values of initial orientation angle α_o. For the sake of clarity the scale in the x_3^* direction has been expanded by a factor of 50. A curious feature is that the spheroid eventually reaches the same equilibrium position from the wall regardless the starting position. For some initial orientations the particle moves monotonically toward the equilibrium position while for others the particle oscillates toward and away from the wall until it reaches the final position. To give a full picture of the motion the same trajectories described in figure 14 are plotted in terms of the separation distance and the orientation angle relative to the wall in figure 15. Figure 15 shows that all the curves (solid lines) coalesce to the same point indicating that both the final equilibrium separation distance and the orientation angle are independent of the

initial position. For an oblate spheroid having a/b=0.5 the equilibrium position is given by $x_3^* = 3.70$, $\alpha = 130.5$. The dotted lines in figure 15 represent the positions for which the particle would take the same time to reach if it were released at $x_3^* = 6$ but with different initial orientations. When the particle has reached the equilibrium position it translates parallel to the wall without rotation at a constant velocity. In this position the gravitational component perpendicular to the wall is exactly balanced by the lift force due to the parallel motion and simultaneously the torque due to the parallel motion just vanishes at the equilibrium orientation. If the particle is slightly displaced perpendicular to the wall from the equilibrium position , a restoring force acts to return the particle to the equilibrium position. Moreover , if the equilibrium orientation of the particle is slightly disturbed, a restoring torque acts to return the particle to its equilibrium orientation. Thus the particle is in stable equilibrium.

The equilibrium position depends on the aspect ratio and the inclination angle of the wall. If the inclination angle β of the wall is decreased, the component of gravity perpendicular to the wall increases and thus the equilibrium position moves closer to the wall where the lift force is greater. Table 9 shows the final separation distance and orientation angle for selected inclination angles β for an

oblate spheroid with a/b=0.5. As the inclination angle β approaches 90°, the equilibrium separation distance becomes infinite.

REFERENCES

Brenner, H. 1964 Chem. Eng. Sci. 19, 519.

Goldman, A.J., Cox, R.G. & Brenner, H. 1967A Chem. Eng. Sci. 22, 637

Goldman, A.J., Cox, R.G. & Brenner, H. 1967B Chem. Eng. Sci. 22, 653

Jeffery, G.B. 1922 Proc. Roy. Soc. A102, , 161.

Wakiya, S. 1959 Res. Rep. Fac. Eng. Niigate Univ. (Japan) 8, 17.

H/b	a_0	a_2	a_4	a_6
		(x 0.01)		
1.1	9.91	2.69	-1.05	-0.20
1.3	5.84	1.06	-0.69	-0.08
1.5	3.82	0.52	-0.45	-0.03
1.75	2.44	0.25	-0.29	0.0
2.0	1.66	0.13	-0.20	0.0
2.5	0.873	0.046	-0.104	0.0

Table 1 The coefficients of U_3/U_∞ in shear flow for an oblate spheroid with a/b=0.5.

H/b	b_2	b_4	b_6	b_8
		(x 0.01)		
1.1	3.692	2.821	0.553	0.102
1.3	1.790	1.356	0.154	0.018
1.5	1.007	0.792	0.057	0.005
1.75	0.559	0.468	0.021	0.001
2.0	0.348	0.309	0.010	0.0
2.5	0.161	0.157	0.003	0.0

Table 2 The coefficients of U_3/U_∞ in shear flow for an oblate spheroid with a/b=0.5.

H/b	c_0	c_2	c_4	c_6
1.1	0.460	0.345	0.021	0.004
1.3	0.475	0.332	0.011	0.002
1.5	0.482	0.323	0.006	0.001
1.75	0.489	0.316	0.004	0.0
2.0	0.492	0.311	0.003	0.0
2.5	0.496	0.306	0.001	0.0

Table 3 The coefficients of ω/S in shear flow for an oblate spheroid with a/b=0.5.

H/b	a_0	a_2
1.1	0.3912	0.0376
1.3	0.3267	0.0201
1.5	0.2824	0.0125
1.75	0.2424	0.0081
2.0	0.2124	0.0057
5.0	0.0837	0.0627
20.0	0.0174	0.0

Table 4 The coefficients of U_i'/U_t in equation (15) for an oblate spheroid with a/b=0.5

H/b	b_0	b_2	b_4	b_6
1.1	0.6993	0.0903	-0.0208	-0.0043
1.3	0.6044	0.0526	-0.0089	-0.0012
1.5	0.5329	0.0328	-0.0042	0.0
1.75	0.4656	0.0216	-0.0022	0.0
2.0	0.4131	0.0149	-0.0013	0.0
5.0	0.1713	0.0009	0.0	0.0
20.0	0.0396	0.0003	0.0	0.0

Table 5 The coefficients of U_3^3/U_T in equation (16) for an oblate spheroid with a/b=0.5.

H/b	c_2	c_4	c_6	c_8
		(x 0.01)		
1.1	1.998	1.031	0.263	0.065
1.3	1.084	0.446	0.068	0.011
1.5	0.651	0.222	0.002	0.002
1.75	0.404	0.121	0.001	0.001
2.0	0.266	0.071	0.0	0.0
5.0	0.015	0.005	0.0	0.0
20.0	0.0	0.0	0.0	0.0

Table 6 The coefficients of U_3^1/U_T in equation (17) for an oblate spheroid with a/b=0.5.

H/b	d_0	d_2	d_4	d_6
		(x 0.01)		
1.1	1.398	4.651	0.641	0.109
1.3	0.760	3.280	0.294	0.032
1.5	0.462	2.499	0.154	0.009
1.75	0.269	1.885	0.085	0.004
2.0	0.168	1.478	0.052	0.001
5.0	0.0054	0.2602	0.0013	0.0
20.0	0.0	0.0167	0.0	0.0

Table 7 The coefficients of $\omega' b/U$ in equation (18) for an oblate spheroid with a/b=0.5.

H/b	e_2	e_4	e_6
	(x 0.01)		
1.1	6.229	0.824	0.153
1.3	4.656	0.391	0.044
1.5	3.607	0.196	0.008
1.75	2.767	0.112	0.001
2.0	2.184	0.068	0.0
5.0	0.3900	0.0018	0.0
20.0	0.0250	0.0	0.0

Table 8 The coefficients of $\omega^2 b/U$ in equation (19) for an oblate spheroid with a/b=0.5.

β (degrees)	x_3^*	α (degrees)
80	1.13	122.7
81	1.27	124.0
82	1.45	125.4
83	1.77	127.1
84	2.34	128.8
85	3.70	130.5
86	18.70	132.0

Table 9 The separation distance x_3^* and orientation angle α of the equilibrium position for the motion of an oblate spheroid with a.b=0.5 settling under gravity adjacent to a plane inclined at angle β .

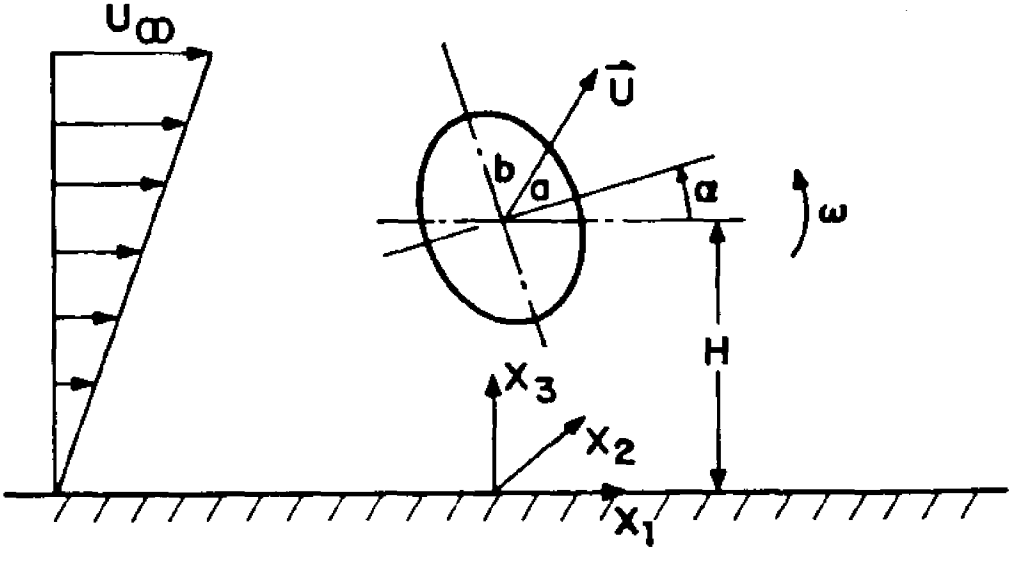

Figure 1. Geometry for the planar motion of a spheroid adjacent to a wall.

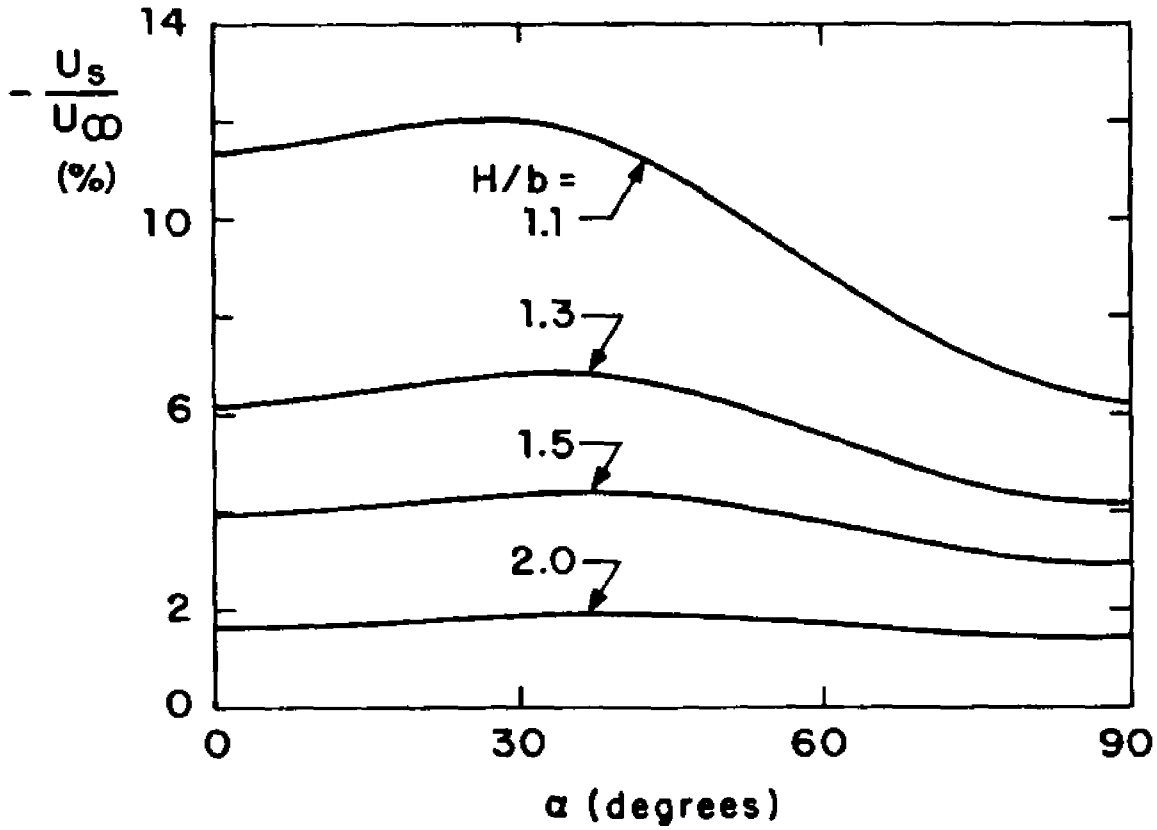

Figure 2. The slip velocity of a neutrally buoyant oblate spheroid with a/b=0.5 in shear flow.

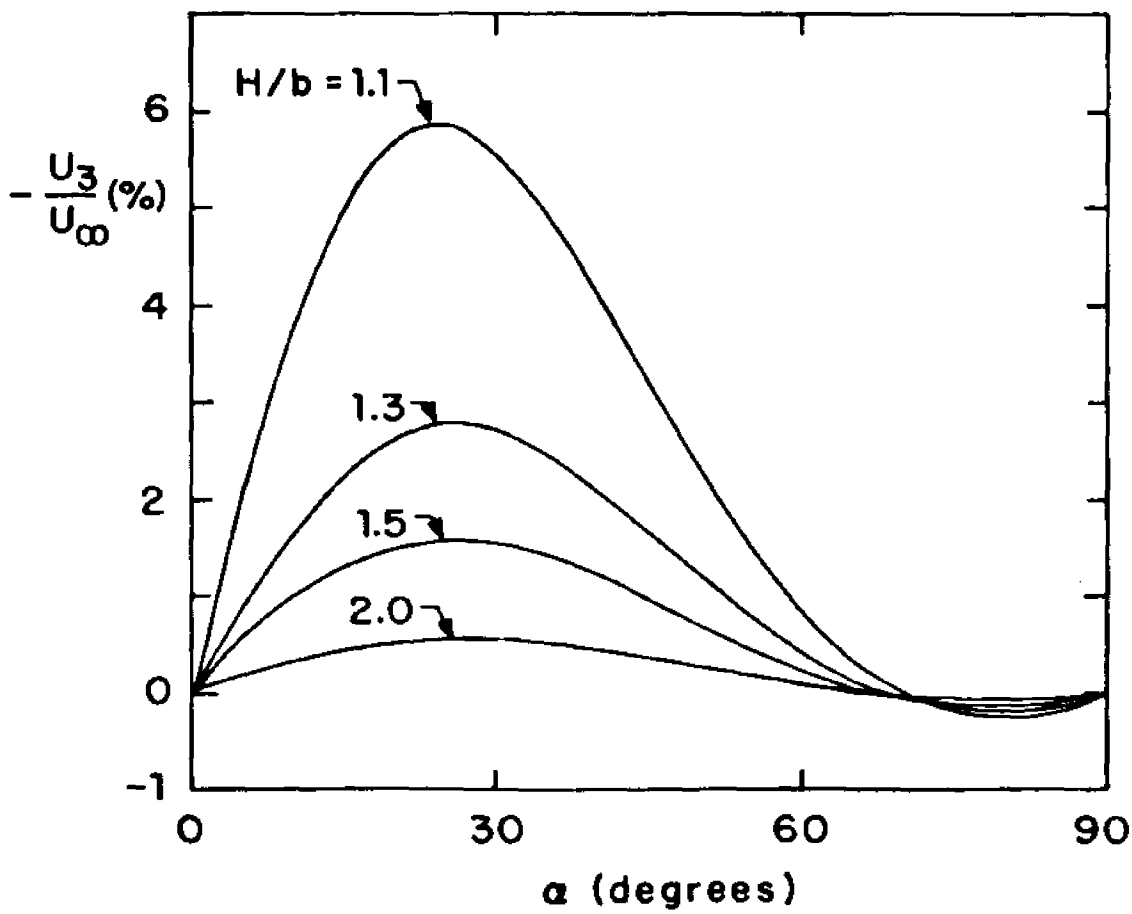

Figure 3. The velocity perpendicular to the wall of a neutrally buoyant oblate spheroid with a/b=0.5 in shear flow.

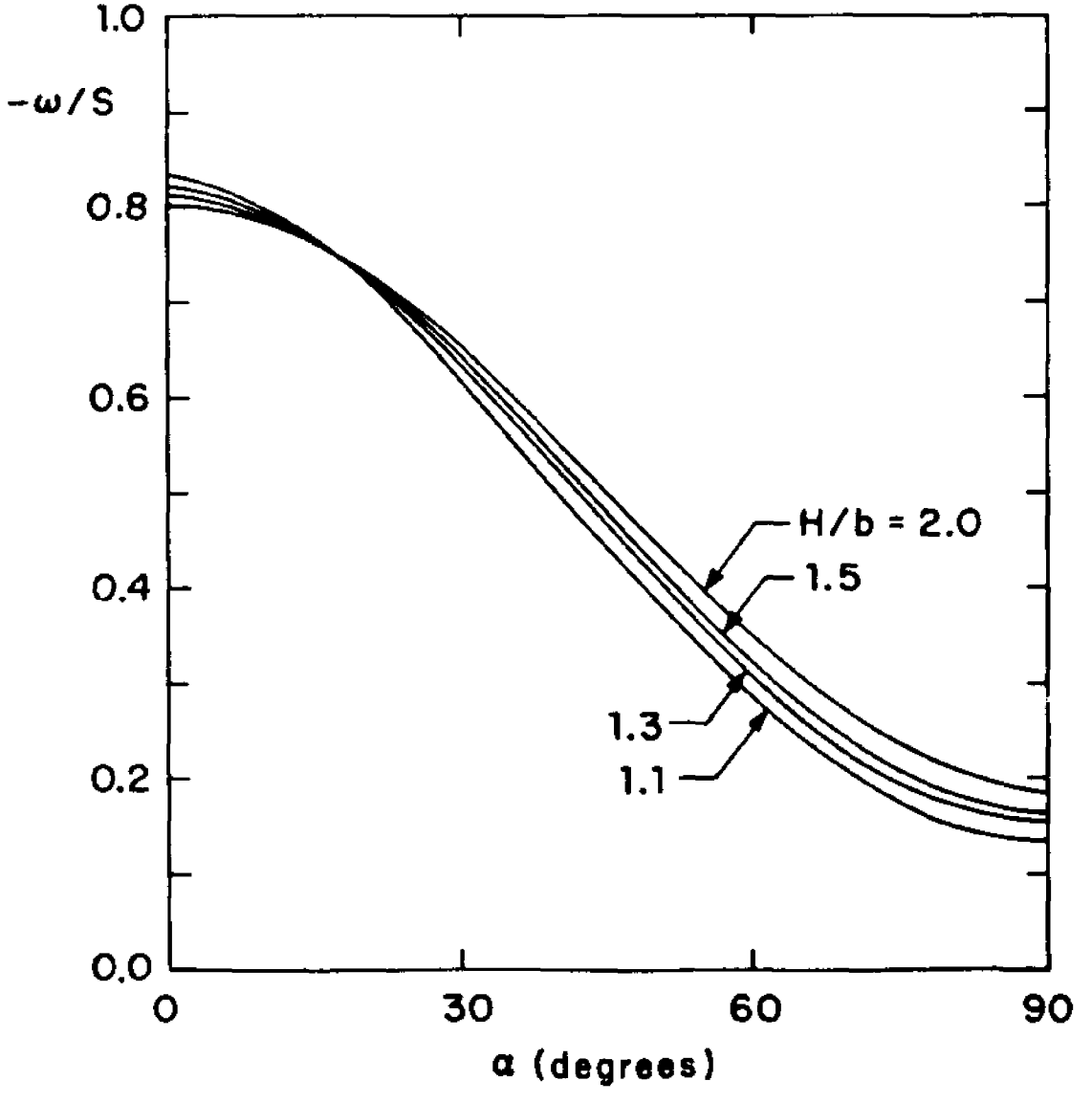

Figure 4. The angular velocity of a neutrally buoyant oblate spheroid with a/b=0.5 in shear flow.

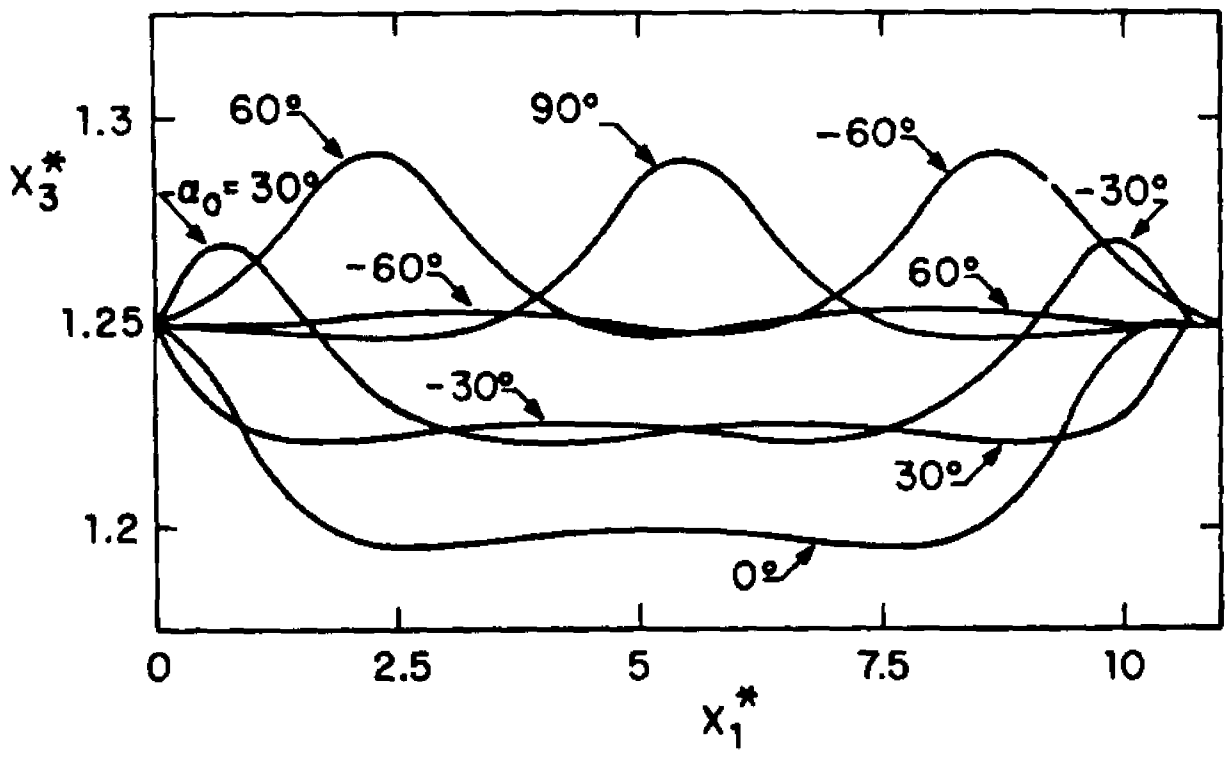

Figure 5. Trajectories of the center of a neutrally buoyant oblate spheroid with a/b=0.5 in shear flow.

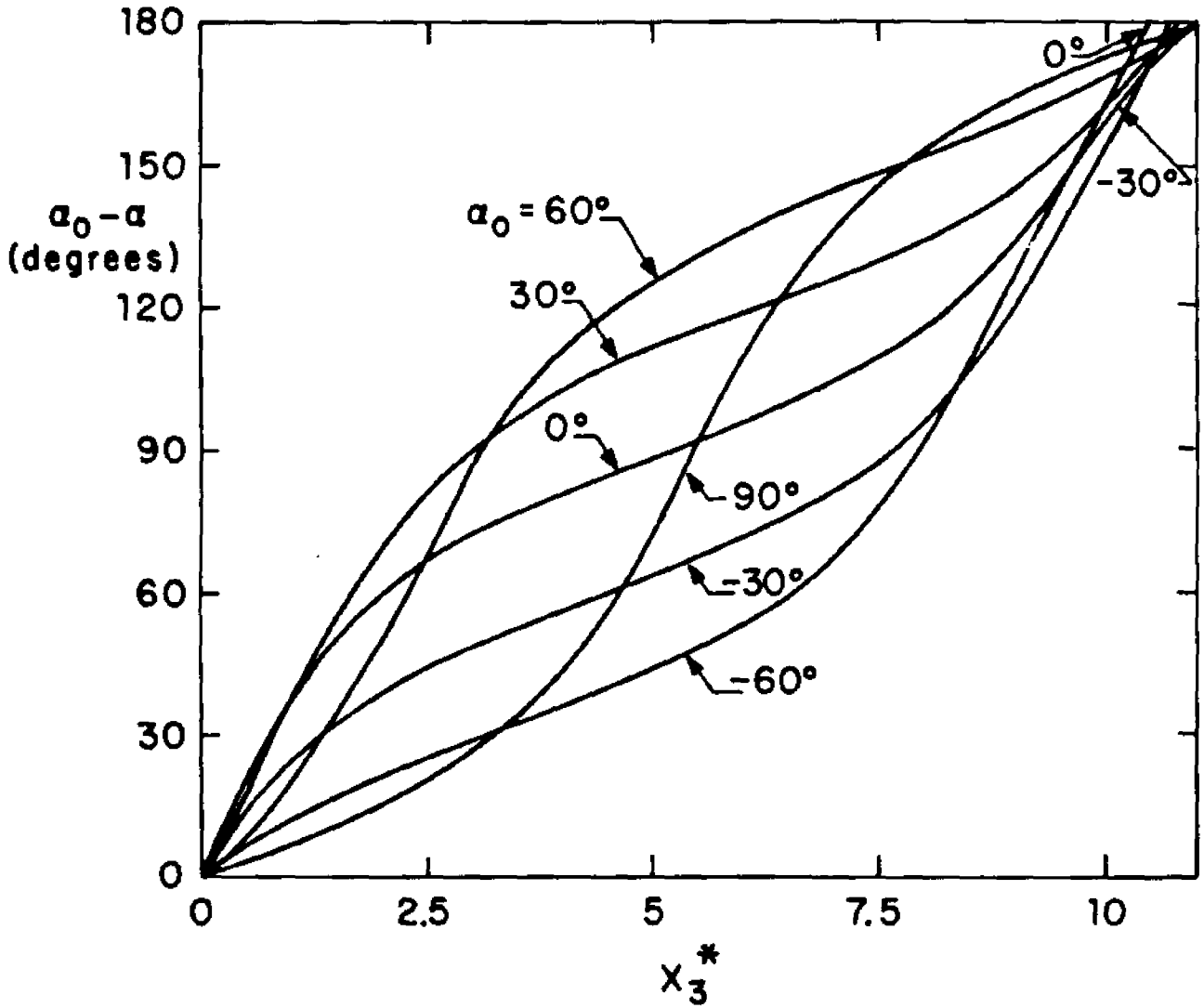

Figure 6. Variation of the orientation angle of a neutrally buoyant oblate spheroid with a/b=0.5 in shear flow.

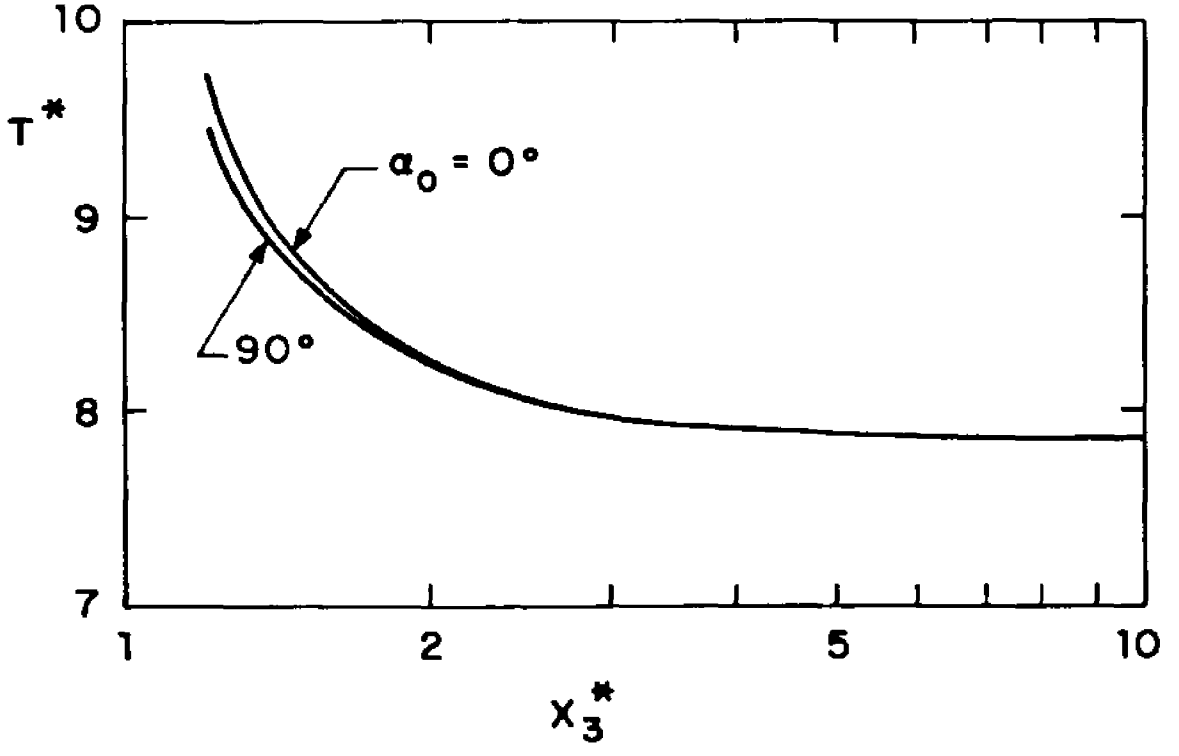

Figure 7. Variation of the period T^* for an oblate spheroid with a/b=0.5 as a function of the initial separation distance x_3^* and orientation angle

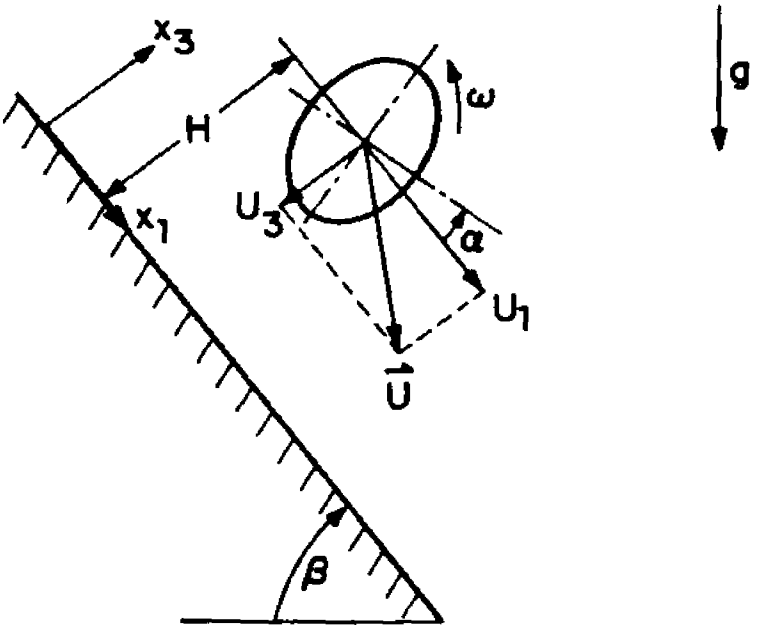

Figure 8. Schematic diagram of an oblate spheroid settling under gravity adjacent to a plane.

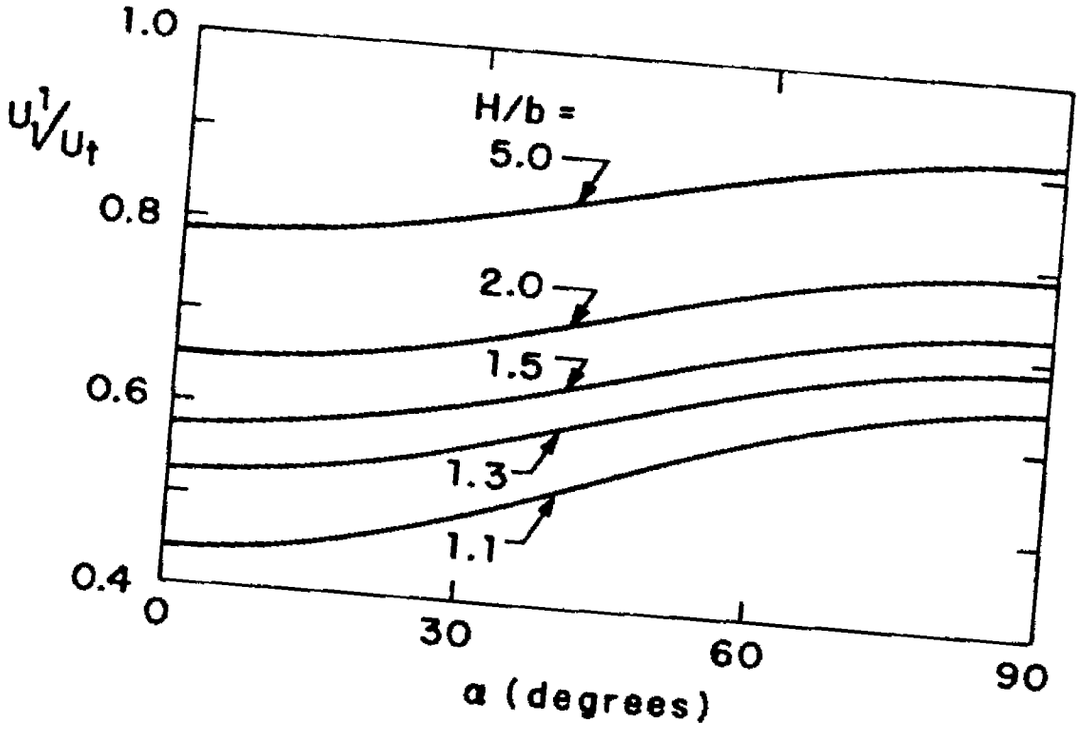

Figure 9. The velocity parallel to the wall of an oblate spheroid with a/b=0.5 moving under a gravitational force acting in the same direction.

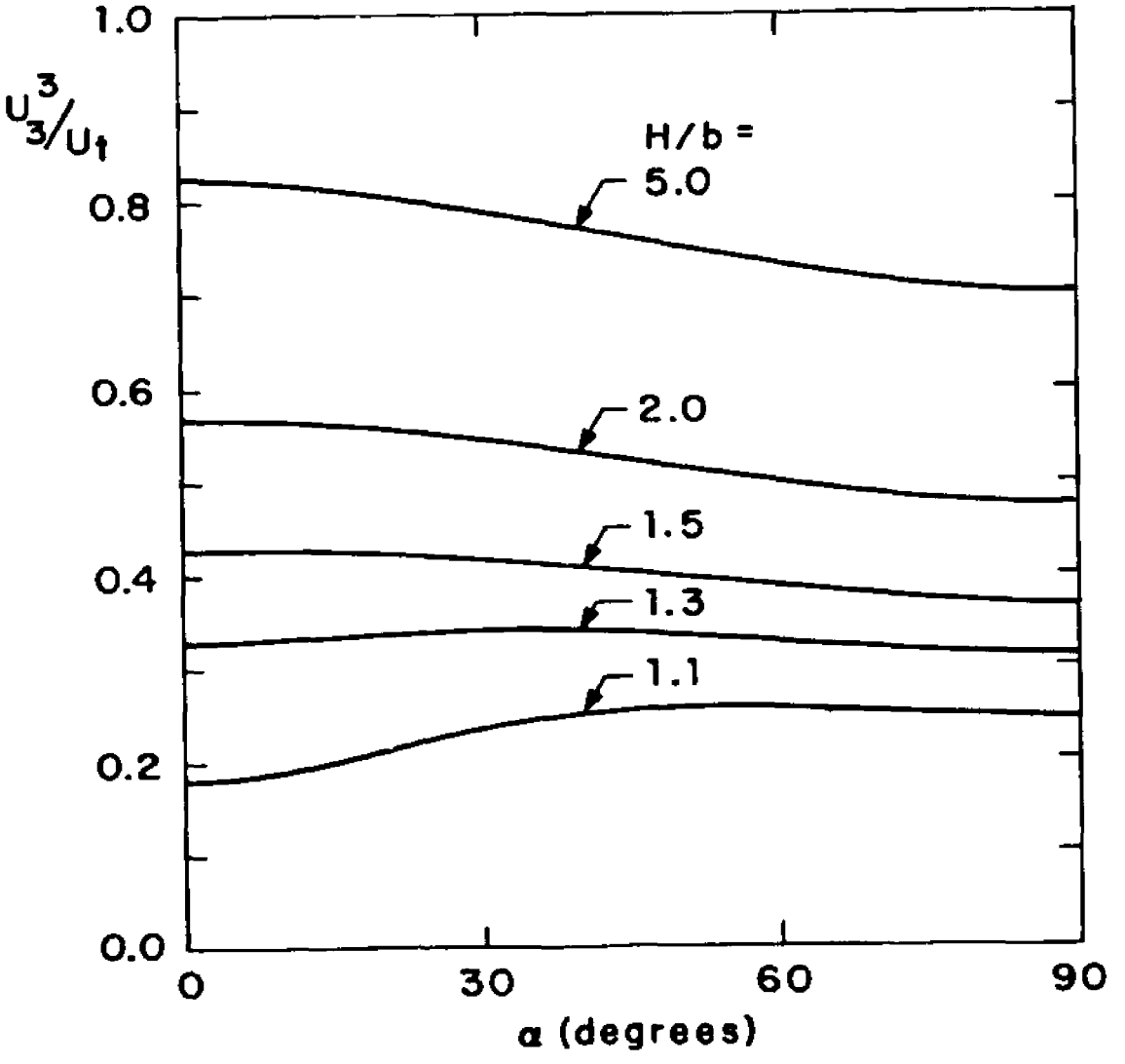

Figure 10. The velocity perpendicular to the wall of an oblate spheroid with a/b=0.5 moving under a gravitational force acting in the same direction

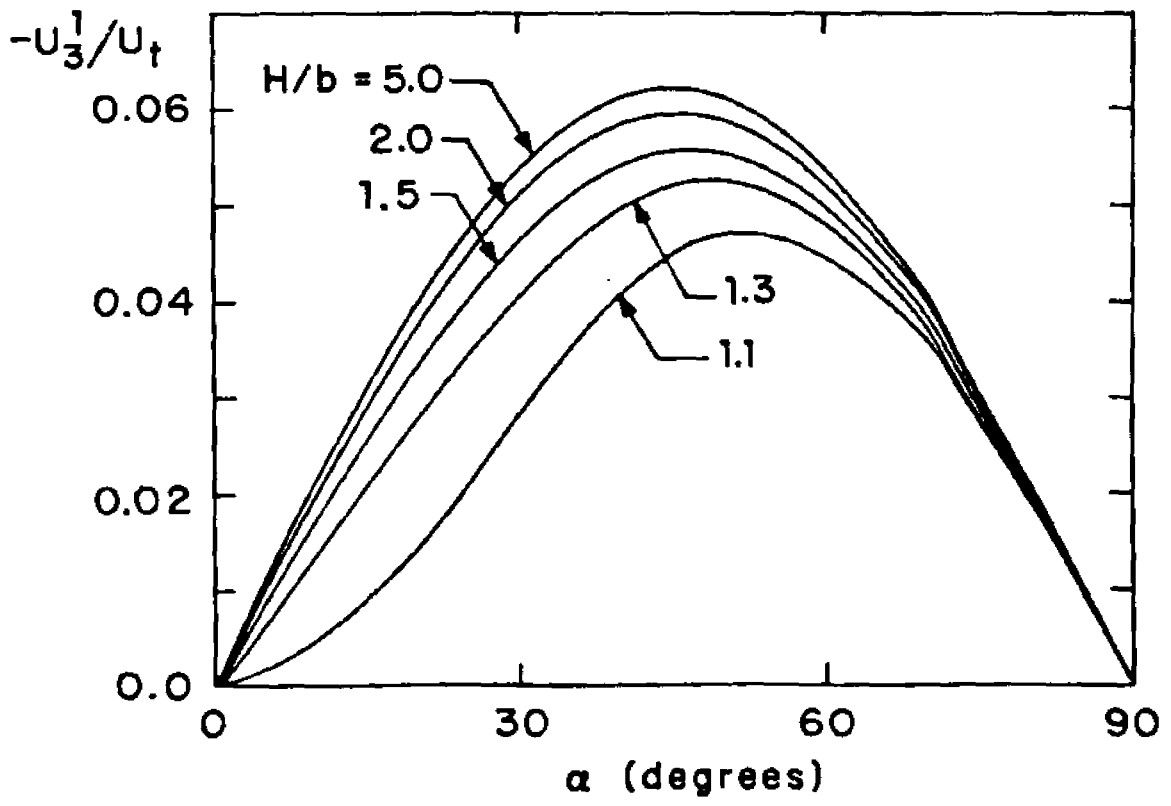

Figure 11. The velocity perpendicular to the wall of an oblate spheroid with a/b=0.5 moving under a gravitational force acting parallel to the wall.

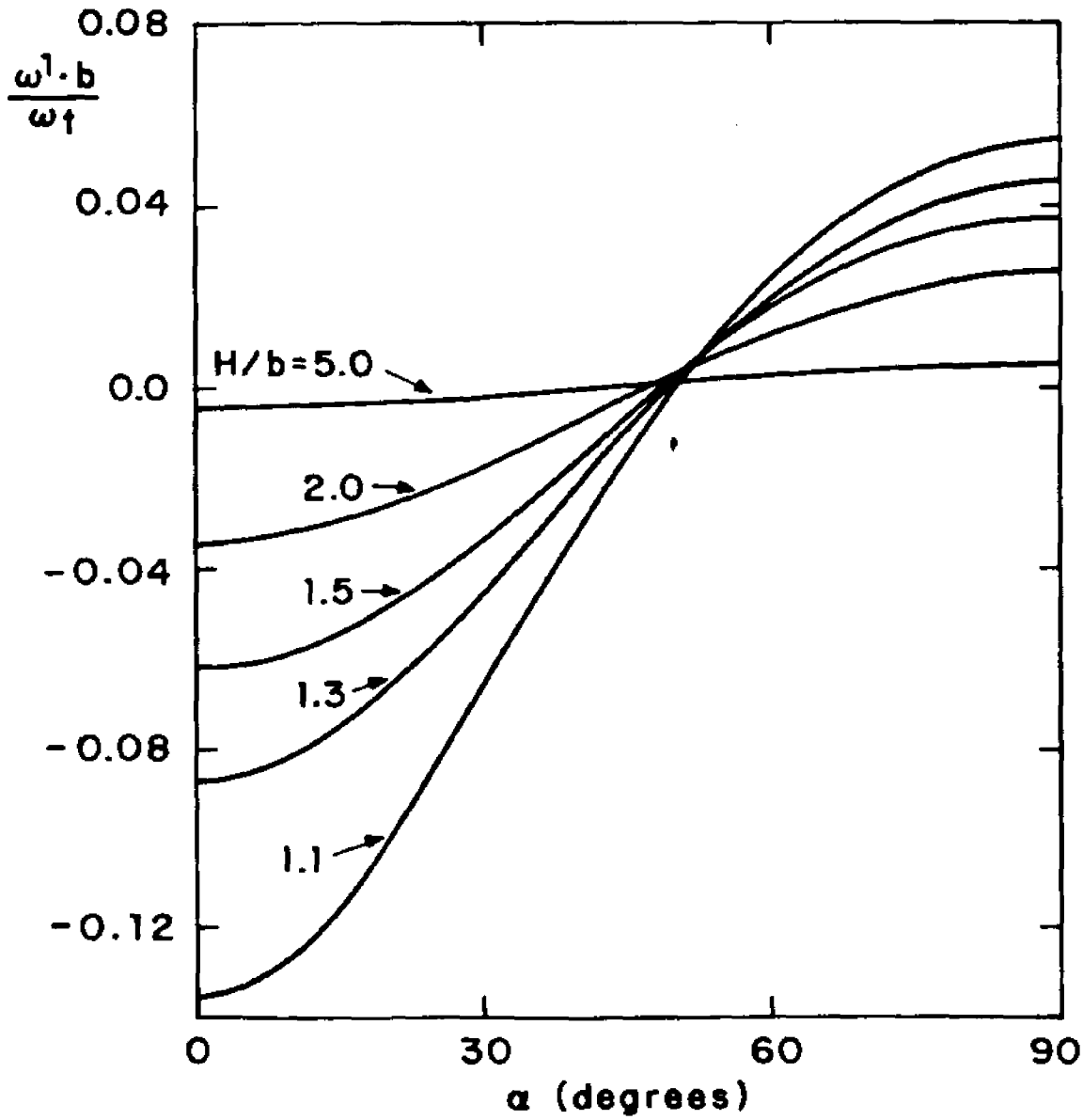

Figure 12. The angular velocity of an oblate spheroid with a/b=0.5 moving under a gravitational force acting parallel to the wall.

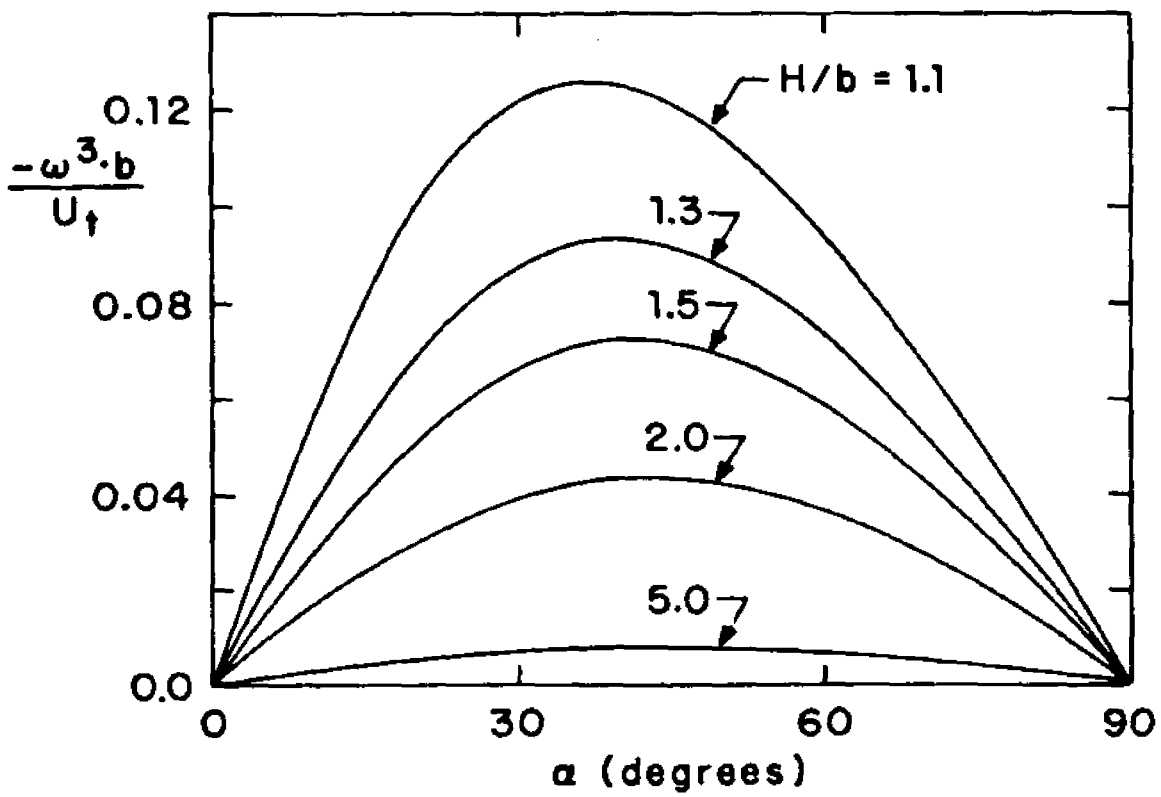

Figure 13. The angular velocity of an oblate spheroid with a/b=0.5 moving under a gravitational force acting perpendicular to the wall.

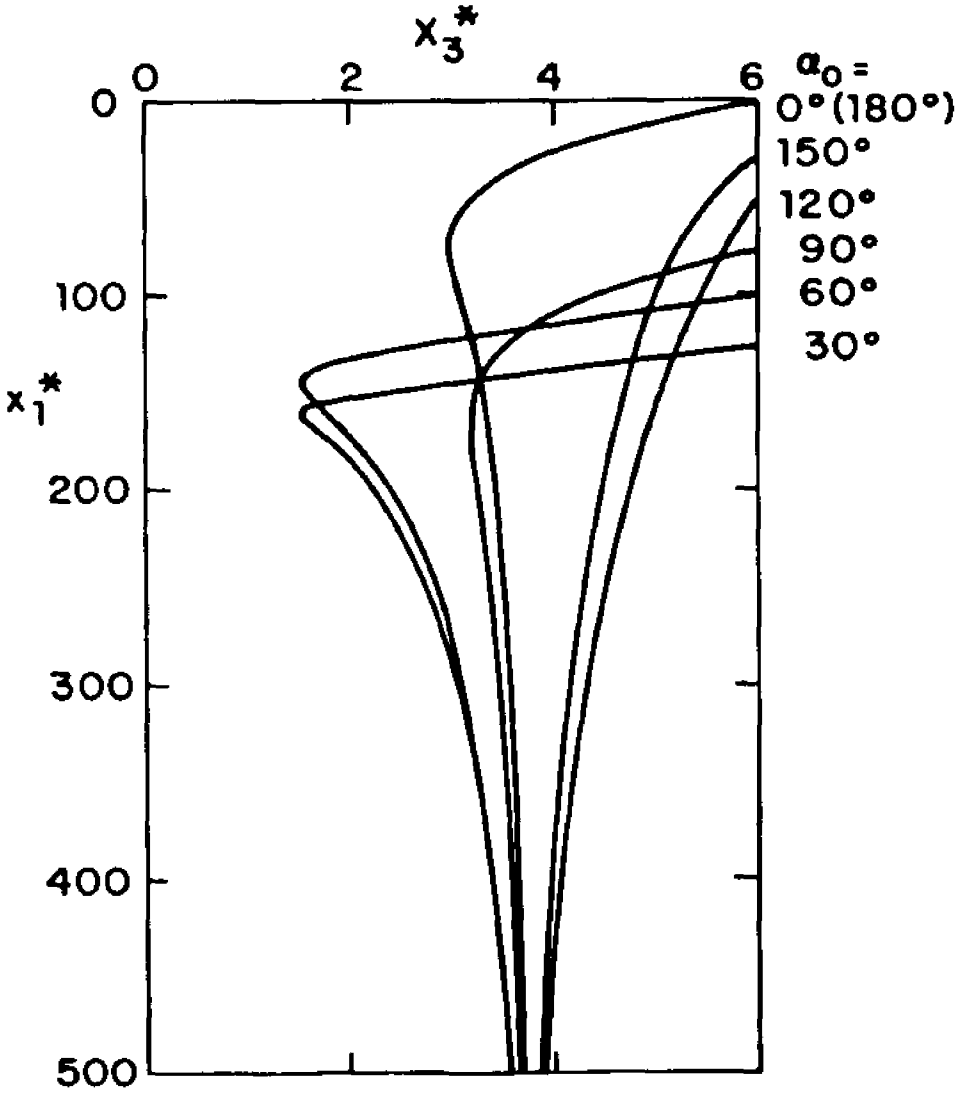

Figure 14. Trajectories traced by the center of an oblate spheroid with a/b=0.5 settling under gravity from the initial position $x_3^* = 6$ near a plane inclined at $\beta = 85°$.

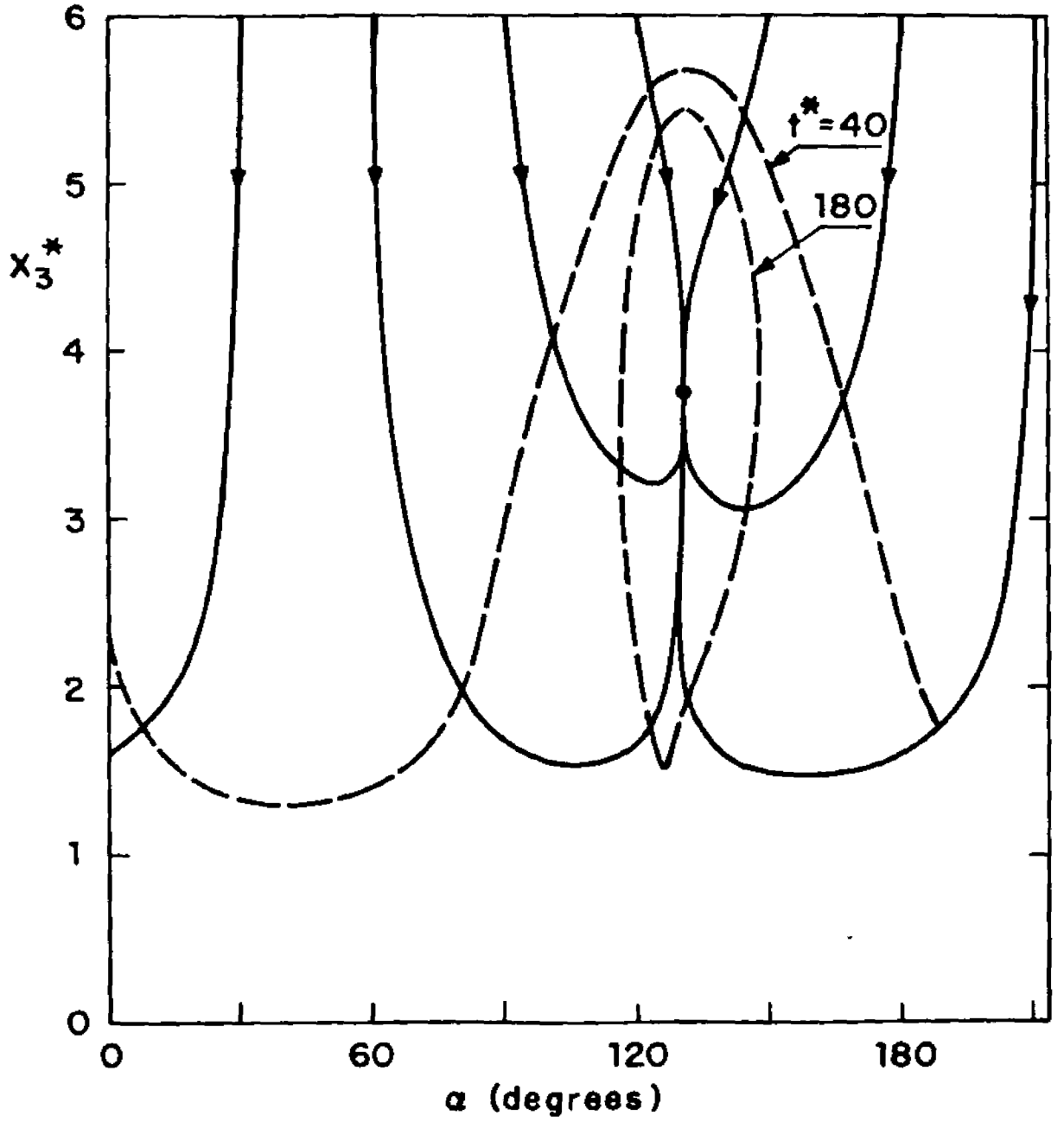

Figure 15. Trajectories of an oblate spheroid with a/b=0.5 settling under gravity from the initial position x_3^*= 6 near a plane inclined at ℓ = 85° in terms of the separation distance and the orientation angle relative to the wall.

CONCLUDING REMARKS

The successful application of the boundary integral method on the motion of a spheroid, a torus and a biconcave shaped disc near a planar wall in this study has shown that the method is effective and suitable for treating the motion of a body of arbitrary shape near boundaries. Examples of the types of problems which can be treated include the motion of a non-spherical particle between two walls or in circular cylinder. It has been shown that the accuracy of the method is much higher than the weak interaction theory of reflections. A limitation of the technique is the long computation time required to evaluate the double integrals in the integral equation. Therefore great effort has been taken in this study to evaluate the integral in the azimuthal direction analytically. In this way a tremendous amount of computational time has been saved and the accuracy of the solution is highly increased.

The last part of this study shows many interesting features of the motion of a non-spherical particle adjacent to a planar wall. The motion of a non-spherical particle is much more complicated than the motion of a sphere because of the dependence of the resistance force on the orientation and the fact that some coupling forces are not identically zero as in the case of a spherical particle.

As stated earlier, the resistance matrix of a particle moving adjacent to boundaries is essential in the study of the diffusive and convective transport of solute particles.

The author hopes that the accurate solution of the resistance matrix of a spheroid, a torus and a biconcave shaped disc adjacent to a planar wall, presented in this study, will be useful for solving the transport problems for particles of these shapes.